THE UNIVERSITY
of EDINBURGH

Evaluating the Way2Production SolFlex350 Digital Light Projection 3D Printer as a Fabrication Technology for Microfluidics.

MPhil Thesis by **Alexander Warne**

For submission to the College of Engineering at the University of Edinburgh

2020

Declaration of Originality

1. I declare that this thesis has been composed solely by myself and that it has not been submitted, in whole or in part, in any previous application for a degree. Unless stated otherwise by reference or acknowledgment, the work presented is entirely my own.

2. I confirm that this thesis presented for the degree of MPhil, has

i) been composed entirely by myself

ii) been solely the result of my own work

iii) not been submitted for any other degree or professional qualification

3. I declare that this thesis was composed by myself, that the work contained herein is my own except where explicitly stated otherwise in the text, and that this work has not been submitted for any other degree or professional qualification except as specified.

Signed by ALEXANDER WARNE:

22/01/2020

Abstract

Development of microfluidic devices for automated cell culture and integrated experiments offers a valuable evolution of biological laboratory practice. The strengths of 3D printing – versatile fabrication, low-cost and ease of use – provide a solution to difficulties in the fabrication of complex single and multi-layer devices. This work assesses the ability of a desktop W2P SolFlex350 resin printer to produce sub-200μm features necessary to replicate device designs currently created using traditional photolithography and multi-layer soft lithography. It is shown that features required for sub-200μm channel production are not viable using this 3D printer, but there is scope for further development of micro and milli-fluidics using desktop 3D printing. 3D printing to remove the need for layer-bonding in complex fluidic devices would enable increased complexity of device design. The possibility of using this to incorporate Raman spectroscopy as a non-invasive, label-free cell sorting mechanism in a continuous microfluidic cell culture device (chemostat) is explored both by assessing the capabilities of the 3D printer, and by evaluating the signal strength of fluorine-carbon bonds as a potential natural marker for Raman-based directed evolution. Organofluorine compounds were shown to produce detectable signals in aqueous solution but further research is necessary to enable detection at rates suitable for this type of device.

Lay Summary

Microfluidics refers to handling of small volumes of liquid. It is a simple but powerful method of minimising and automating biological cell culture, reducing waste and manual labour in the laboratory. It is not widely used in biological research because device fabrication is difficult and expensive. 3D printing could offer the solution to these difficulties. This research investigates the capabilities of a desktop W2P SolFlex350 3D printer in relation to the requirements for microfluidic fabrication.

Table of Contents

List of Figures

Page

Acknowledgements:

The author would like to acknowledge the contributions from Professor David O'Hagan of the University of St Andrews for providing samples and culture instructions for both Streptomyces MA37 and cattleya, Professor Maggie Smith of the University of York for providing Escherichia coli strain ET12567, and Professor Alistair Elfick of the University of Edinburgh for providing funding, facilities and materials for the project.

List of Abbreviations:

3D	Three-Dimensional
2PP	Two-Photon Polymerisation
ABS	Acrylonitrile Butadiene Styrene
CARS	Coherent anti-Stokes Raman Spectroscopy
DLP	Digital Light Processing
FFF	Fused-Filament Fabrication
PCR	Polymerase Chain Reaction
PDMS	Polydimethylsiloxane
RORSD420	Rinse-Out-Resin SD420
SERS	Surface-Enhanced Raman Spectroscopy
SLA	Stereolithography Apparatus
SRS	Stimulated Raman Scattering
UV	Ultraviolet
W2P	Way2Production

Chapter 1: Project Background

1.1: Introduction

Engineering of biology to perform tasks beneficial to humans is a consistently evolving field which already has a profound effect on our everyday lives. Bioengineering is responsible for antibiotic production in modern medicine, and naturally occurring enzymes are often extremely efficient catalysts of chemical reactions. Biological detergent offers an example of this technology, using bioengineered enzymes enable efficient clothes washing at 30°C, which compared to 40°C, uses approximately 12% less energy and could reduce carbon dioxide emissions by up to 220000 tons annually in the UK[1]. As our ability to harness natural organisms and processes improves, the potential application of bioengineering to solve many of the world's most pressing issues like food and fuel shortages are likely to be just as common in the future.

Understanding of genetics and cell metabolism has benefitted from several key technological advances. The rapid development of enabling technologies based on DNA amplification using polymerase chain reaction (PCR)[2] and Sanger sequencing[3] means genetic information can now be produced orders of magnitude cheaper and faster than ever before. The rate at which development and adoption of these techniques is illustrated by the fact that, according to the US National Human Genome Research Institute, the cost of sequencing has tumbled from almost $10000 per megabase in 2001 to under $0.1 in 2017[4]. CRISPR-Cas9 is perhaps the most recent example of such an enabling technology in the field of genetics, promising to vastly reduce the difficulty of targeted genetic alteration[5].

To handle the accelerated rate of data production achieved by modern biological technology, interdisciplinary collaborations between computer scientists and molecular biologists have given rise to the field of bioinformatics. This field aims to collate and process vast quantities of data to interpret results and guide further research. Coupled with the capability to more easily target DNA modification with CRISPR-Cas9, this interdisciplinary approach provides a powerful tool to perform research more efficiently and effectively than ever before.

While some aspects of biological research have rapidly improved over recent years, many ubiquitous practices in cell culture rely on outdated technology. Cellular manipulation is labour intensive, time consuming and uses volumes and quantities of cells which are disproportionate at the biological scale. Update of these practices is

long overdue, and interdisciplinary research is required to provide a solution. Microfluidic devices consist of micro-channels for manipulation of sub millilitre volumes and offer an efficient solution for handling cells in the laboratory. There are example of microfluidic cell culture devices but their uptake and indeed that of microfluidics in general is limited in biology. This reluctance is partly because complex devices are difficult to produce reliably, and fabrication is beyond the capability of most biological laboratories. Versatile microfluidic device fabrication would be an important step towards its incorporation into general laboratory practices, enabling automation of current techniques at appropriate scale and expanding the ability of many others.

The recent and ongoing revolution in the capabilities of additive manufacturing (3D printing) bears resemblance to that of PCR and DNA sequencing in genetics. In particular the rise of affordable desktop 3D printers, which are well within the budget of most laboratories (typically under £5000) and, if applied to microfluidic fabrication, could reduce the entry barriers for non-specialised labs and expand the current capabilities of microfluidic devices. The ultimate aim of this avenue of research is to develop 3D printed microfluidics as a widespread platform for experimental design in biological research. The first step towards this target is to evaluate the ability of desktop 3D printers, which are well within the budget of most labs, to recreate current microfluidic devices and expand the capability of microfluidic manufacture.

A promising example candidate of a powerful device enabled by the combination of 3D printing and microfluidics would be a microfluidic directed-evolution device, based around Raman spectroscopy. Raman spectroscopy is unusual as it can detect many chemical compounds *in vivo* without the need for engineering markers into target cells[6]. This characteristic is important because it offers the potential for cells to be cultured and monitored simultaneously, where the majority of detection methods are destructive to the cells they are testing, often requiring chemical fixation for analysis. In order to facilitate this application of Raman as a selective technology, the speed of Raman sorting must have a significant impact on the cell culture as a whole. Cell cultures on this small scale can only be provided by microfluidics. Integration of 3D printed microfluidics into general practices could revolutionise biological research with versatile, cost effective in-house fabrication of complex, custom experimental devices such as the one described.

1.2: **Microfluidics**

1.2.1: *Microfluidics*

Originally developed using photolithography techniques borrowed from the electronics industry, microfluidic devices consist of sub-millimetre diameter channels moulded into polymers such as Poly-Dimethyl-Siloxane (PDMS) or etched into materials such as glass. They are used to manipulate the flow of small volumes of liquid (typically sub-millilitre scale). Potential applications for this seemingly simple technology range from membraneless batteries[7] to sample preparation for Mass Spectrometry[8] and it is of significant interest in the manipulation of biological cells in small volumes.

Early microfluidic devices using photolithography and glass etching could produce precise, simple, single layer devices in glass or silicon. While these devices provide small volumes and simple flow, they are not suitable for complex systems requiring components such as pumps, valves and mixers, which are necessary for expanding the capability of microfluidics in biological research. Research using flexible elastomer PDMS by Professor George Whitesides[9, 10] demonstrated complex devices could be made using the elastomer and that it was well-suited to producing multi-layer, reproducible devices. The adoption of PDMS as the material of choice for microfluidics was due to both its physical properties (flexible, biocompatible, air-tight, optically transparent) and the ability to produce multiple replica devices at low cost from a master mould, using soft-lithography[11].

Using PDMS as a material for microfluidics, researchers such as Professor Howard Stone utilised the behaviour of laminar flow to develop methods of controlling[12] and manipulating liquids in multi-functional devices. Research by Professor Stephen Quake led to the development of valve systems and demonstrated functional nanolitre-scale devices[13]. One device resulting from this research is the microchemostat discussed below, illustrated in *figure 1.5*, which represents a highly capable, steady state culture device for bacteria. The combination of this research and contributions from others expanded the capability of microfluidics in relation to biological research, demonstrating the revolutionary potential for this technology.

Microfluidics has been adopted as a research vessel in many laboratories, yet despite the benefits of microfluidics, it is currently not widely used outside of specialist research groups.

In recent years there has been an explosion in new fabrication techniques for microfluidic devices for specific purposes, this is largely due to the specialist equipment and expertise required for construction and operation. The most difficult part of creating a microfluidic device using soft lithography is manufacturing a master mould. Traditionally this has been using photolithography, where masks are commonly generated using glass or quartz coated in opaque chromium. They can be designed using computer aided design (CAD) and laser etched to produce holes through which UV will pass to the photoresist. Expensive techniques including X-rays, electron beams or ion beams can be applied in the photolithographic process to increase the resolution of the master mould for smaller, more precise microfluidic channels and features. The accuracy of devices can range from 250μm to 600nm resolution depending on materials and methods used[14,15]. This mask is placed over a photoresist layer, which is spread thinly and evenly onto a silicon wafer by spin-coating and baked to solidify and remove solvent. When exposed to UV light, the photoresist changes in chemical properties so that it is soluble in a 'developer solution' in areas where the mask has allowed light passage. This photoresist is then washed off, leaving a negative mould for PDMS to be cast, shown in *figure 1.1 (A-D).*

A limiting factor for this process is that the equipment for generating a photoresist film, including a silicon wafer and spin-coater, is only available in specialised laboratories. Furthermore, once created these masks are impossible to alter, and modification of the device design requires complete *de novo* fabrication of a master mould. This is a major drawback as devices cannot be easily adapted or created for different purposes, and any small changes are as expensive as creating an entirely new master mould.

The material of choice for soft-lithography based devices is PDMS, which is a transparent silicone rubber, which offers biocompatibility for culture of cells, low cost and the ability to cold cast around a master mould. Addition of PDMS and cross-linker to the master mould is ideally performed in a clean room under a vacuum to avoid contaminants and bubbles respectively. Layer depth is determined by the depth of PDMS mixture applied to the mask and curing is performed at 80°C for several hours

or 65°C for 24 hours. After removing the PDMS cast, it can be bonded to a flat surface such as a glass slide or used as a layer if a more complex, multi-layer device is the intended application.

The main advantage of soft-lithography based manufacture is that devices can be incredibly detailed, and the manufacturing of simple, single layer devices is well-established. Master moulds can be re-used to generate the same device many times over. Making a complex, multi-layer device with in-built control systems is possible but is far is far more complicated. Microfluidic valves are made possible because of the physical characteristics of cured PDMS. Flexibility enables the creation of valves by aligning control layers above or below the sample layer. The control layers are controlled via pneumatic or hydraulic pressure and as they are pressurised, they expand to form a block in the sample layer, thus forming a valve system[16]. Though the theory is simple, the assembly of these layers must be incredibly precise, and adhesion must be perfect to prevent leakage between layers. The significance of the difficulty and unreliability of this particular process is demonstrated by a number of publications attempting to overcome the issue [17, 18, 19].

The difficulty in design and production of new microfluidic devices is such that unspecialised laboratories generally continue with traditional methods of culture, despite their labour and consumable intensiveness. Even in laboratories with the ability to utilise a microfluidic device, an entire laboratory group will often perform research using a single device design from one master mould because while making copies of a device is cheap and straightforward, fabricating a new master is expensive. This limitation simply isn't conducive to a fast paced, efficient research environment.

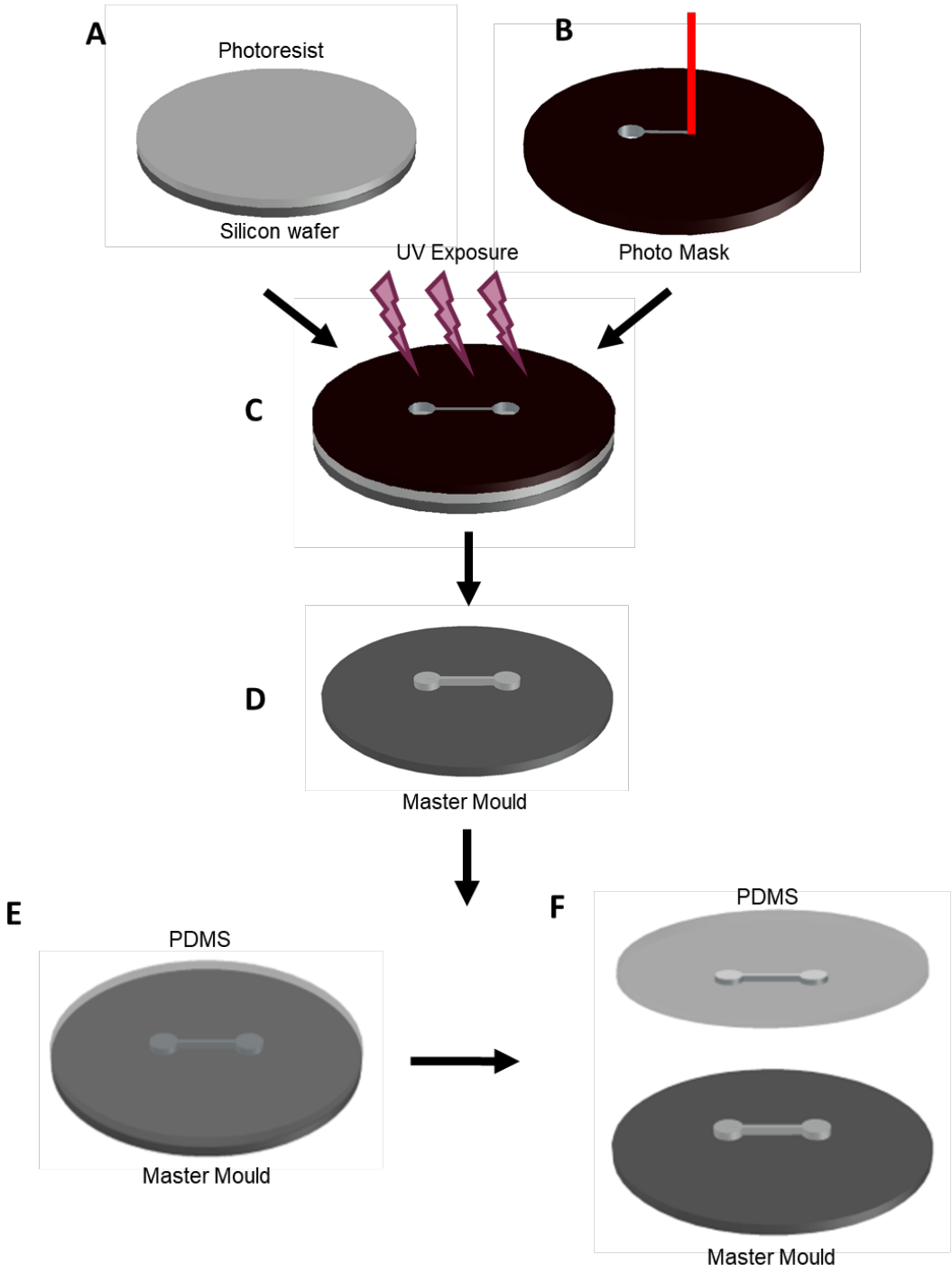

Figure 1.1 – Fabrication of a PDMS Microfluidics Device using Photolithography and Soft-Lithography. (A) A silicon wafer with spin-coated photoresist layer. (B) Laser etching of photomask. (C) UV light exposure of photoresist through photomask. (D) Finished master mould post wash. (E) Soft-lithography with PDMS cast onto master mould. (F) Removal of PDMS device from mould. PDMS is then attached to substrate such as glass slide.

1.2.2: *Experiments on a Chip*

The majority of molecular biological research is performed on *in vitro* cell cultures and is still manipulated by hand, using Gilson pipettes or equivalent. Standard sizes for single channel pipettes in most laboratories are P2, P10, P20, P200, P1000 and P5000, the nomenclature indicates the maximum volume in µl the pipette can transfer, with the smallest volume typically 10% of the maximum (www.gilsonuk.com). In practice, transferring 0.2µl by hand with a P2 pipette is subject to an extreme margin of error and should be avoided if the volume of the substance transferred is relevant to the results of the experiment (e.g. adding DNA to PCR reactions).

The most common reaction vessels for liquids in molecular biology are microcentrifuge tubes (commonly referred to by the brand name Eppendorf), these tubes come in several sizes, with 0.5ml the smallest and 1.5ml the most common. The use of vessels of these volumes is so deeply ingrained in biological research that many standard pieces of laboratory equipment are designed specifically to use them, examples of this can be easily found on the website of Fisher Scientific, one of the leading providers of laboratory equipment in the UK (www.fishersci.co.uk). In mammalian research, 96-well plates are the vessel of choice for high throughput analysis. The reaction volume recommended by offerings from Corning (www.fishersci.co.uk) are 75-200µl. To put the sizes into the perspective of the biological cells they are intended to explore, *Escherichia coli*, one of the best characterised and most widely used bacteria in microbiological research have cellular volumes of just 0.4-3 femtolitres[20]. Mammalian cells are substantially larger in size, with the most commonly used immortal cell line HeLa averaging roughly 2000 femtolitres (bionumbers ID100434). As previously mentioned, the smallest volume technically transferrable by Gilson pipette is 0.2µl, equivalent to 200000000 femtolitres. A standard 1.5ml microcentrifuge tube is 1.5e+12 or 1500000000000 femtolitres, equivalent to the volume of 750 million HeLa cells or 5 trillion *E.coli* cells.

It is abundantly clear that ubiquitous practices in molecular biology use vastly disproportionate volumes for the research they are undertaking. A fundamental flaw of this traditional approach is that almost all historical and current research into cellular

behaviour is based on averaging the characteristics of millions of cells, with no possibility of understanding these characteristics at a single cell resolution. RNA analysis for determining gene expression using the 'Gold Standard' Qiagen RNeasy Mini Kit for extraction for achieves 15-25µg RNA in an elution volume of 30-100µl. DNA is even harder to extract, requiring 2 million cells with the Qiagen DNeasy Mini Kit for 15µg in elution volume of 100-200µl (www.qiagen.com). To perform a single 50µl PCR amplification using MyTaq polymerase by Bioline (www.bioline.com) it is recommended that 200ng of Eukaryotic DNA is used. One experiment with no reserve sample would require at minimum, a negative control, positive control and experimental, meaning two samples with DNA. This means that the theoretical minimal number of cells for this experiment would require over 50000 cells. There are several factors which amplify this number in practice, firstly it is highly undesirable to perform an experiment with no reserve sample. Secondly, the extracted DNA will be in a minimum volume of 100µl with this kit. In a 50µl MyTaq reaction, 13µl are taken up by reactant so the theoretical maximum volume containing the 200ng DNA is 37µl. This requires at least 75000 cells to acquire this concentration in the 100µl elution volume of the kit. As stated, it would be ill-advised to have no reserve sample and in addition, it is best to minimise the reaction volume in which the DNA is contained to minimise the possibility of reactants from the kit interfering with the polymerase enzyme. This means that in practice, the number of required cells is several times greater than this theoretical minimum.

Population averaging is a powerful method for investigating the prevailing characteristics and interactions of a group of cells. It has produced reliable data and insights which have built the foundations of modern molecular biological knowledge, but the lack of information on the heterogeneity of populations means there is a complete lack of key data about the behaviour of sub-populations of cells and the effect they have on this average[21]. The presence of heterogeneity is more important in some research than it is in others, as sub-populations of cells may not affect the normal activity of a population. Research by Balaban et al[22] highlights a sub-population of *E.coli* 'persistent' cells which are resistant to antibiotic exposure, but re-grow a population which is still sensitive to the antibiotic when the selection is removed. What is important about this study, is that the phenomenon of 'bacterial persistence' was observed much earlier, in 1944[23], but the precise mechanisms by which it takes place had been a mystery prior to this research. Balaban et al utilised

microfluidics to grow and directly observe the behaviour of single cells when exposed to antibiotics using light microscopy. This direct analysis of different cells is perhaps one of the most reliable means by which data can be obtained. It is not as susceptible to experimental errors such as contamination and it is able to provide data of individual cells, rather than just averaging the output of a population. The potential for microfluidics to enable more reliable, higher resolution data in molecular biology is significant, coupled with other technologies like bioinformatics and single-cell analysis, it provides a versatile tool for biological laboratory research.

Aside from the limitations imposed by the nature of population averaging, this approach to molecular biology leads to vast quantities of waste. In order to save time and reduce potential contamination, laboratories have increasingly switched from re-usable, autoclavable glassware to disposable plasticware. A nature correspondence article from 2015 from the University of Exeter estimates that worldwide laboratory plastic waste from research laboratories totalled some 5.5 million tonnes in 2014, roughly equivalent to 83% of recycled plastic worldwide in 2012[24]. While actively reducing plastic waste using these techniques can go some way to mitigating this [25] a fundamental change of approach is the only way to properly address the issue. Wasted culture medium, biological material and energy are further examples of areas in which techniques can and should improve. Reducing the size of reaction vessels and reducing the requirement for manual pipetting would reduce the cost of running a lab by reducing all these forms of waste, meaning more money could be spent on research and the environmental impact of laboratory research would be drastically improved.

Cell culture in molecular biology is labour intensive. Researchers are often required to plan multiple-day experiments which require manual input at specific points in a cell culture's cycle. It is normal for PhD or Post-Doctoral researchers to work odd hours and weekends in order to maintain cell cultures and perform experiments at specific time points, time which could be far more appropriately spent if this process was reliably automated. Different cell types require vastly different conditions for growth and while different labs use different protocols, most growth media is made up in batches of 500ml to litre scales[26]. Some media must be used before its components expire and so must be made up in these batches as and when it is required, with excess or contaminated reagents going to waste. Miniaturising cell culture would mean only a fraction of these reagents would be required for the same experiment.

This would prevent waste, increase experimental efficiency and reduce manual input, enabling the potential for multiple experiments of the same or different types to occur in parallel.

The concept of microfluidic devices is simple. Reducing the total volume of an experiment to microlitre or sub-microlitre scale comes with a range of advantages, from increased control of fluids with laminar flow to vastly reduced costs compared with traditional millilitre scale experiments. The increased resolution provided by microfluidic channels also enables an array of experimental techniques which can significantly enhance the capabilities of laboratory research, particularly in a molecular biological setting. An umbrella term for miniaturising and performing experiments in this way is 'Lab-on-a-Chip'.

Adapting microfluidics to improve experimental techniques is a fruitful and well populated field, sometimes using it as part of an experiment and sometimes to replace an experimental technique entirely. Lab-on-a-Chip Mass Spectrometry (LOC-MS) is one current, commercial application for this technology. Ionisation of analytes is a core component of Mass Spectrometry, as it measures mass to charge ratios. This ionisation can be achieved using a process called Electrospray Ionisation to ionise liquid droplets containing samples and when used together with Mass Spectrometry, is known as ESI-MS. In general, lower flow rates of electrospray mean increased sensitivity of ESI-MS, this is because lower flow rates lead to smaller droplets and increased ionisation efficiency. Scaling down capillaries and sample droplets to 'micro-electrosprays'[27] or more recently 'nano-electrosprays' enables increased sensitivity and decreased sample size for ESI-MS. Nano-electrospray ionisation is particularly beneficial for protein and peptide analysis, as more data can be acquired from the small samples this type of research produces[28]. The ability to reduce the quantity of material required for analysis is paramount if cell culture and laboratory protocols are to be minimised.

Electrophoresis is a staple of classic and current molecular biology. Electrophoresis gels are used to separate charged biological molecules, including RNA, DNA and proteins, based on their molecular weight. Separation can be analysed by viewing with intercalating dyes (e.g. SybrSafe for nucleotides) or stained using specific targeting compounds such as antibodies in protein gels. Protein analysis using Western Blotting, commonly requires 50µg or more of total cellular protein per well in

an electrophoresis gel[29]. To put this into perspective, a common and highly cited method for extracting astroglial and oligodendroglial cells from rat brains[30] can extract 20-40mg of cell protein in 1-2x10^7 viable cells, from sample material of 10 rat brains. This means that on average, approximately 2ng of protein can be extracted from each cell. Under ideal conditions, at least 25000 of these cells are required to provide 50ug of cellular protein to fill a single lane in a Western Blot. Microchip Capillary Electrophoresis (MCE) is significantly more efficient than the current common electrophoresis methods loaded using manual pipetting and optical visualisation. Adopting MCE instead of large electrophoresis gels would reduce sample volume requirements, increase control of sample loading (which with current manual pipetting can result in a large error margin between gel lanes)[31].

The ability to process and analyse smaller samples is essential for the adaptation of experiments to run in microfluidic devices. If smaller samples cannot be successfully analysed, the advantages of replacing current lab practices with microfluidics won't translate into useful experimental data. This means that while many procedures can be improved in both sensitivity and complexity for the user (such as MCE instead of electrophoresis), experiments requiring larger samples for analysis would not be a natural fit for minimisation.

A benefit of miniaturisation is the ability to run more experiments in parallel. The development of DNA and RNA sequencing technologies has been rapidly improving in terms of cost, capability and speed. While the methods outlined above remain by far the predominant method of investigating gene expression in molecular biology, the development of high throughput single-cell RNA or DNA sequencing offers insights into previously unseen sub-populations of cells[32]. Simultaneous analysis of thousands of individual cells by coupling microfluidics with single cell sequencing produces vast amounts of high-quality data for analysis. The need to store and process all this information has resulted in the field of bioinformatics. This has rapidly grown since its inception and its integration into modern research cannot be understated. A combination of bioinformatically directed hypotheses with experimental evaluation provides a powerful partnership when appropriately applied. Many databases are free to access and there are various online tools to predict and model biological processes from gene function to protein interactions. This interdisciplinary approach to identifying useful research targets can streamline the process of investigation to produce informed hypotheses for wet lab evaluation.

Sequencing of cells and most data about individual cells has been acquired by fixing or isolating cell contents mid-process by cross-linking their proteins and amino acids with chemicals such a formaldehyde, and observing them when they are no longer alive. This is very effective for taking a snapshot of what an individual cell or group of cells were doing under specific conditions at a specific time, however, it removes the ability to see how these same individuals progress after this snapshot. A major potential advantage of microfluidic devices is that single cells can be monitored *in situ* while they are alive, meaning that multiple readings can be taken from a single cell to see how it develops. Simple microfluidic devices which trap cells in place during growth can do this[33], however, more complex microfluidics which require multi-layer control mechanisms are less common.

A fundamental advance in the processes of molecular biological laboratory research provided by microfluidics is not just minimising reaction sizes and increasing sensitivity. It is the ability to string together what are currently separate, sequential procedural steps into a single experimental chip. This serves to eliminate transfer stages between different procedures, increasing efficiency, reducing sample loss and drastically reducing the risk of contamination resulting from numerous transfers between numerous vessels. Each vessel and each pipette transfer carries the risk of contamination, which can result in an entire experiment being wasted, along with the reagents and time it consumed. An example of this integration was provided in a recent publication by Yang et al. [34], who demonstrated a microfluidic chip with the ability to extract DNA, perform PCR and analyse the result using MCE and fluorescent detection. This publication utilises computer aided design (CAD) software and computer numerical control (CNC) milling to fabricate a microfluidic cartridge. This has the advantage of rapid in-house fabrication of a two-dimensional chip, with the ability to fabricate changed designs with relative ease. In addition, Yang et al. employed a modular system design, meaning different experimental elements can easily be added and removed from a particular cartridge, in contrast to microfluidic chips fabricated through soft lithography.

The ability to combine multiple processes in a single chip opens an array of potential experimental advances. One of these would be minimising and automating a chemostat for continuous cell culture. The chemostat is an attractive option because it would enable continuous cell culture with reduced manual input, reduced waste and more controllable growth conditions.

1.2.3: *Miniaturising the Chemostat*

The basic concept of a chemostat is to dilute a cellular culture at a rate equal to that of cellular multiplication. The establishment of equilibrium - where removal of old cells and media equals input of fresh media - enables constant cell growth at a controlled concentration, under specified environmental conditions. This enables continuous culture, as opposed to the batch culture techniques which are prevalent in biological research. This technology can be utilised in the form of continuous bioreactors for production of industrial compounds such as ethanol [35] or for research on cellular characteristics such as gene expression, by removing environmental variables in a controlled system. The method and term 'chemostat' was documented in 1950 by Novick and Szilard, with the principle still much the same in full sized chemostats today (*Figure 1.2)* [3637].

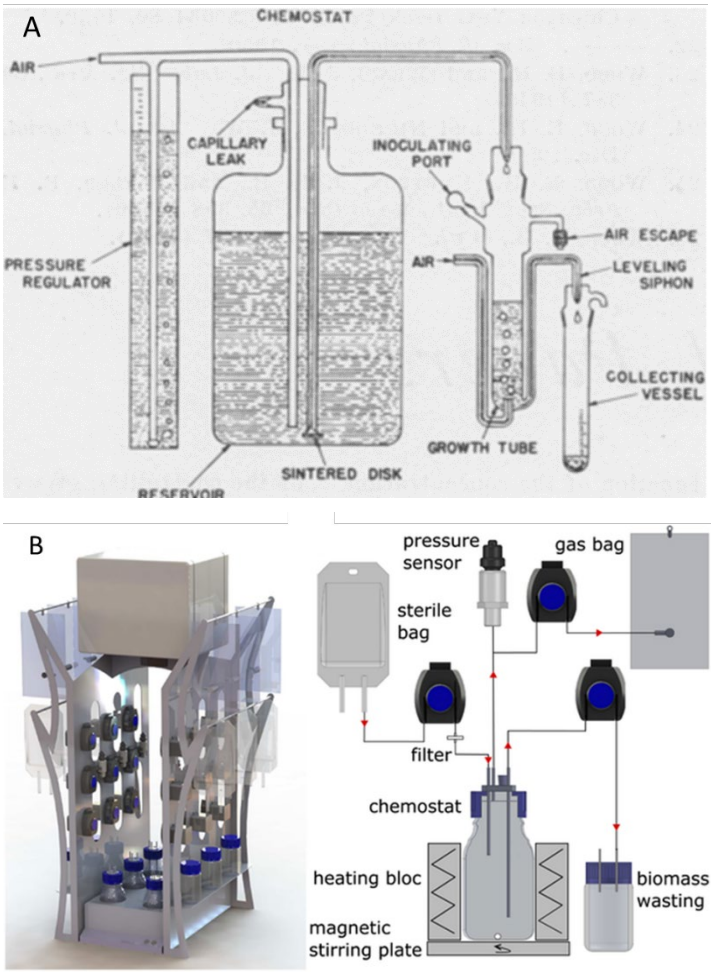

Figure 1.2 – The Chemostat. (A) Diagram of original chemostat, taken from[36]. (B) General view of a modern LAMAC chemostat system and diagram of components of one chemostat in the LAMACs module. Taken from[37].

The ability to control the environment and growth state of a cellular population offers a novel method of observing evolutionary adaptation, the process responsible for every functional gene in present day life, from the efficiency of individual proteins to the interaction of complex multi-gene networks. Observing the response of a population to a known, consistent or changing selection pressure depending on the experiment and evaluating changes in genetic characteristics in a chemostat is a powerful technique for demonstrating this process in a controlled environment [38]. While observing genetic changes in genetic properties of organism in response to an engineered selection pressure is highly useful for characterising the cellular mechanisms responsible, the potential of chemostats as a tool for directed evolution could be extremely important to developing novel products for specified tasks.

Adapting organisms to develop proteins such as enzymes suitable for industrial use is vital for producing products such as biological detergent. Many industrial chemical processes are financially and environmentally disastrous, requiring hazardous chemicals, consuming vast amounts of energy and producing significant waste. Halogenation of chemical compounds is a prime example of this. The addition of a carbon-halogen bond, particularly carbon-fluorine, in the place of a carbon-hydrogen has been shown to reliably improve the efficacy of various lead compounds[39]. While other halogens can often show improvements, fluorine is the most sought after in pharmaceuticals as it exhibits reliable, predictable improvements including: increased metabolic stability, increased bioavailability and more recently suggested, binding affinity and selectivity. These effects are such that approximately 20% of all new pharmaceutical compounds contain fluorine[40]. The addition of fluorine to a lead compound is also widespread in agrochemistry, with around 14% of current compounds containing fluorine (up from just 4% in 1977)[41].

Current techniques of fluorination include electrophilic fluorination, nucleophilic fluorination and deoxofluorination. These techniques are expensive, non-specific and deoxofluorination in particular requires extremely hazardous reagents such as sulphur tetrafluoride. Production in biological systems offers the ability to produce highly complex proteins and molecules with a comparatively miniscule amount of energy. Sophisticated networks of enzymes work to produce almost every compound found in living organisms from the basic building blocks we acquire through food. In addition, they are often self-regulating, producing different elements in response to appropriate stimuli. Harnessing the extensive potential of these cellular networks as production

factories, replacing chemically and energetically expensive chemical production with efficient, safe and highly specific biological production would be of enormous advantage for the environment and manufacturers alike. Though natural fluorination is scarce, mostly due to the insolubility and extreme electronegativity of fluoride ions, there are examples of the process. The first fluorinase was discovered by Professor David O'Hagan's lab in St. Andrews in the soil dwelling bacterium *Streptomyces cattleya*[42] and until recently, when genome mining provided evidence of a further three fluorinating organisms[43], was the only known source of natural fluorination. Utilising technology to adapt and harness biological production in place of current practices would be a huge step forward.

Creation of proteins and compounds with totally unique properties from scratch is extremely difficult. Many in the field of synthetic biology aim to produce novel gene networks and organisms with specific purposes, some with success, such as E.*coli* biosensors for arsenic detection[44]. These however are all based on naturally occurring proteins, or at least active regions within them. The reason it is so difficult to generate totally novel proteins is that their function is dictated by their 3D structure, which is generated by folding of chains into highly specific shapes, based on the interaction of properties of individual amino acids within the chain. Altering just one amino acid within a chain can totally disrupt the function of the entire protein, or it can have little to no effect. Protein folding is extremely complex, influenced by a vast array of factors in addition to the properties of amino acids, often relying on organism specific 'chaperones' – small proteins which aid in correctly folding a protein as it is synthesised [45]. With the continuous improvement of computational modelling tools [46], it is possible that future research into completely unique protein properties will be a reliable method of production. The most advanced current techniques, however, involve biological optimisation of numerous potential or lead structures, which are predicted by computational analysis of naturally occurring compounds. In short, nature is better at producing functional proteins after millennia of optimising the technique than we are.

While the advantages of chemostats are clear for research on steady state culture, chemostats have not been widely adopted in general biological research, where batch cultures are still generally preferred. Many factors are responsible for the lack of significant uptake of chemostats. One major issue is that of aggregation, which occurs in approximately 35% of populations in yeast[47] for example. They are cumbersome to

set up, susceptible to contamination due to the length of run time and large number of potential vulnerabilities and they waste significant volumes of reagent if only small samples are needed. Chemostats are excellent at providing a selection pressure by modifying the nutrient content in supplied media, this has been used effectively to study and optimise organisms for survival in a nutrient starved environment [48]. They are not capable however of differentiating between individual cells within a population and they do not provide specific pressures to optimise cellular processes for a task other than nutrient limitation. It is here that microfluidics can have a significant impact on the future of chemostat and general wet lab technology.

Several examples exist of microfluidic devices as a means of establishing steady state microbial culture in a small volume. A simple microfluidic chemostat which does not dilute cells but maintains their media nutrient supply to study cellular growth without nutrient depletion is demonstrated by Groisman et al.[49] (*Figure 1.3)*. The feeding channels of the device are 150μm in width and growth chambers are 100μm by 70-200μm. Capillaries of 0.6μm height and 20μm width connect the growth chambers with fresh culture medium in the feeding channels while preventing yeast or bacteria from passing through. This is achieved by the 0.6μm height of the capillaries, as *E.coli* cells are approximately 1μm at their narrowest diameter and yeast cells far larger. This design does not require valves or complex components to replenish culture medium, and is characteristic of many microfluidic devices. As previously discussed the tendency for yeasts and bacteria to form biofilms is an issue for growth on this scale. Biofilms were readily formed in this device, which is described as a positive aspect as their formation can be studied, however, it limits the longevity of cultures grown in suspension using a device of this format.

A similar simple device created by Long et al.[50] (*Figure 1.4)* operates in a different manner. In this device, *E.coli* are trapped within small channels of 0.6-0.9μm width and 1.1μm depth. The size of the cells dictates that they are unable to escape these channels. Larger nutrient rich channels flow on either end of the growth channels, delivering fresh growth media and serving to wash away excess cells which grow at the ends of the channels. This device was designed and used to monitor growth and single cell expression of common detection marker Green Fluorescent Protein (GFP) for 50 generations of bacterial division. Trapping cells in microchannels is a useful method for single cell analysis in microfluidics.

One of the more complex devices published to date is that of Jason Kelly's PhD project[51] (*Figure 1.5)*. This device incorporates a growth loop of 16 individual segments, a peristaltic pump of three valves and ports for inlet and waste. The reason for the complexity is that each individual segment can be flushed with lysis buffer to remove the issue of biofilms and aggregation while the rest of the growth chamber is isolated. This mechanism also serves as the dilution phase for chemostat growth equilibrium. The device was used to monitor long-term growth of *E.*coli bacteria with a synthetic gene circuit[52]. With a total volume of just 16nL, this is the smallest long-term microfluidic chemostat available in the literature to date. A chemostat of this size, depending on growth conditions and sorting speed, could comfortably offer a viable overall volume for single-cell sorting to have a selective effect on the culture as a whole. If instead of random discarding of one of the chambers, cells could be continuously monitored and selected for, this would be a suitable device design for a directed evolution device. This device utilised multi-layer soft lithography, which drastically increases the difficult in reliable fabrication.

Park et al.[53] (*Figure 1.6*) fabricated another microchemostat in 2013 using multi-layer soft lithography. The device design is innovative as it minimises the number of valves and multi-layer control channels, reducing the difficulties associates with valve leakage and alignment in multi-layer microfluidic devices. Decreasing the complexity of devices in order to make fabrication reliable without sacrificing functionality is a major limitation of devices generated with soft lithography.

3D printing offers the ability to incorporate increased functionality and complexity without making the fabrication process more difficult and with DLP printing in particular, without increasing build time.

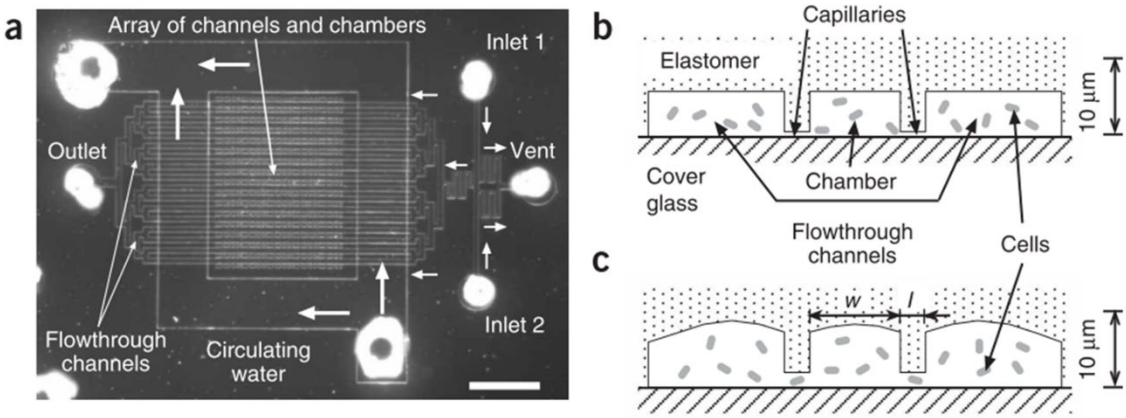

Figure 1.3 – Microfluidic device by Griosman et al.[49] (A) Labelled image of reactor. The feeding channels of the device are 150µm in width and growth chambers are 100µm by 70-200µm. Capillaries of 0.6µm height and 20µm width connect the growth chambers with fresh culture medium in the feeding channels while preventing yeast or bacteria from passing through. (B) Diagram of reactor function from the side, illustrating relative channel dimensions.

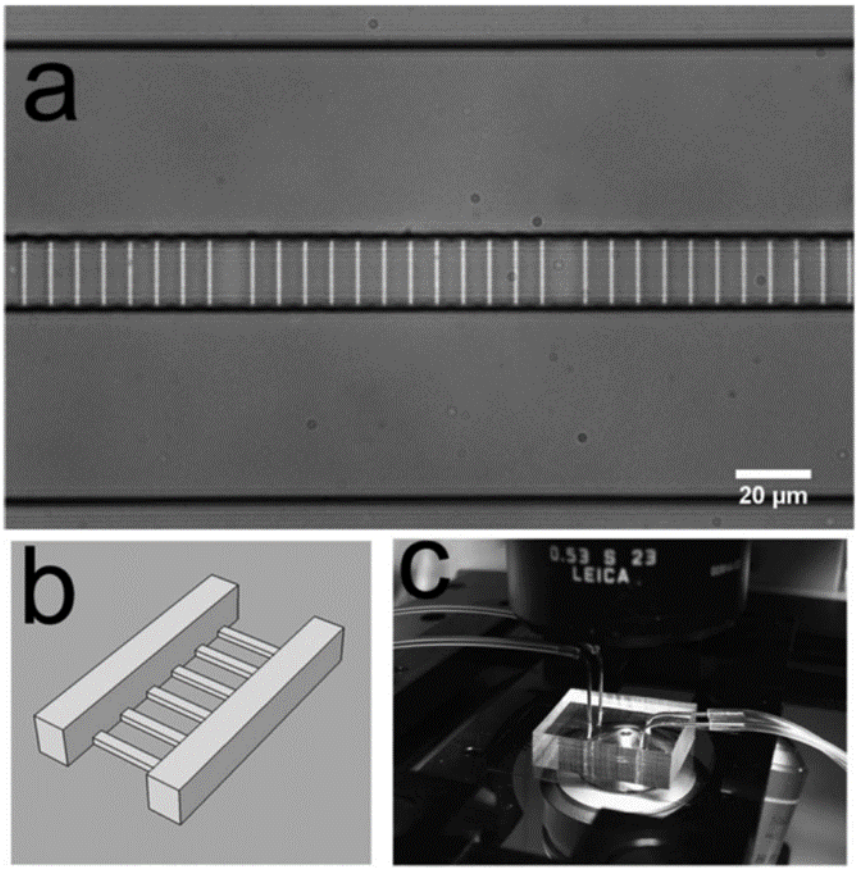

Figure 1.4 – Microfluidic device by Long et al.[50] (A) Image of reactor with scale bar. Smaller growth channels are 0.6-0.9µm in width, 1.1µm deep and 20µm in length. Feed channels are 50µm in width and 20µm in depth. (B) Illustration of 3D reactor design. (C) Operational reactor under microscope for imaging and monitoring.

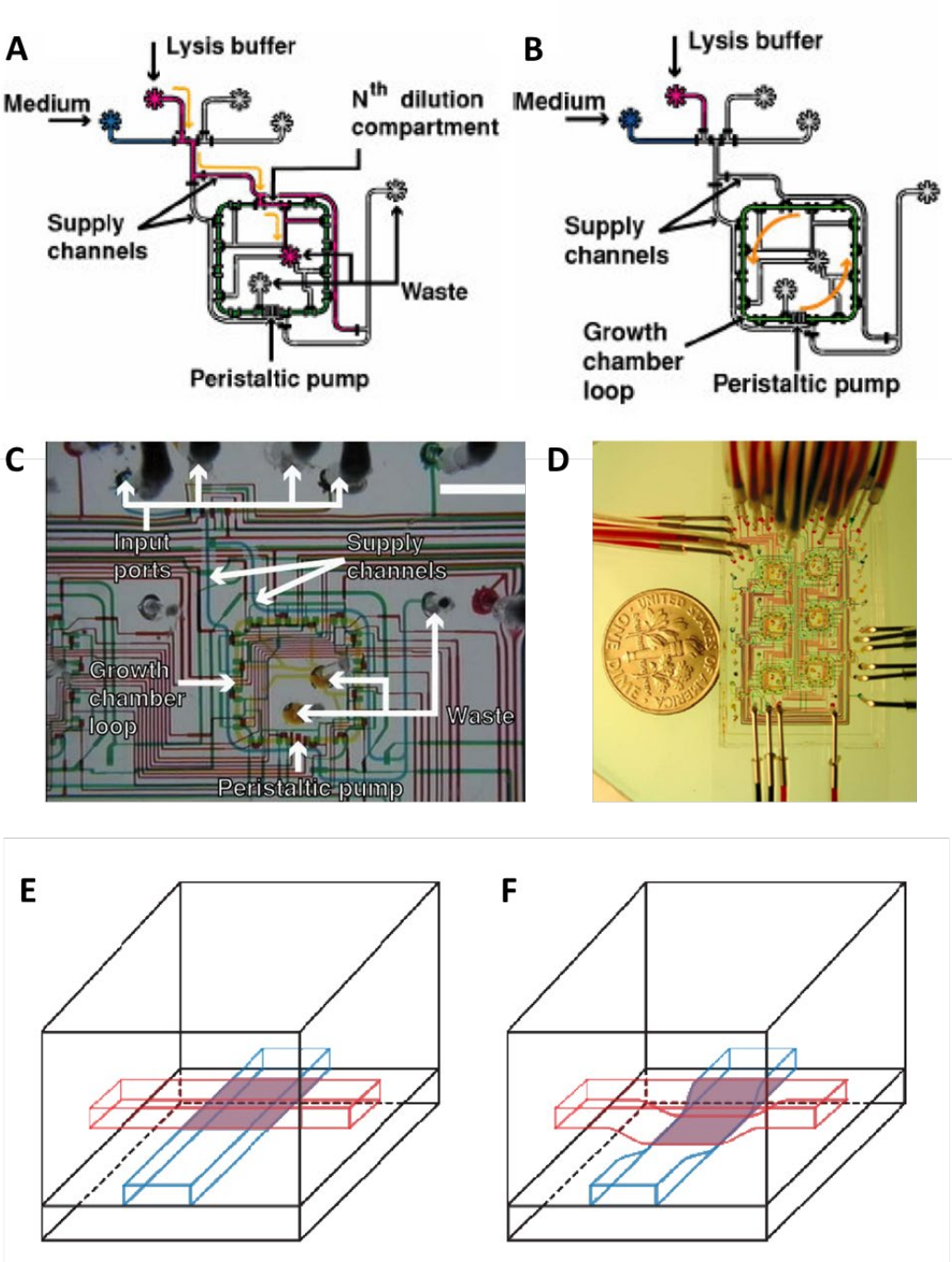

Figure 1.5 – Microfluidic device by Kelly, J[51] used in[52] (A) Cleaning phase of a segment of the reactor. (B) Growth phase of reactor. (C) Image of actual device, showing complexity of control valves and supply channels. (D) Image of chip with six reactors adjacent to a US Dime for scale. (E) Multi-layer pneumatic valve in the open position. (D) Multi-layer pneumatic valve in the closed position.

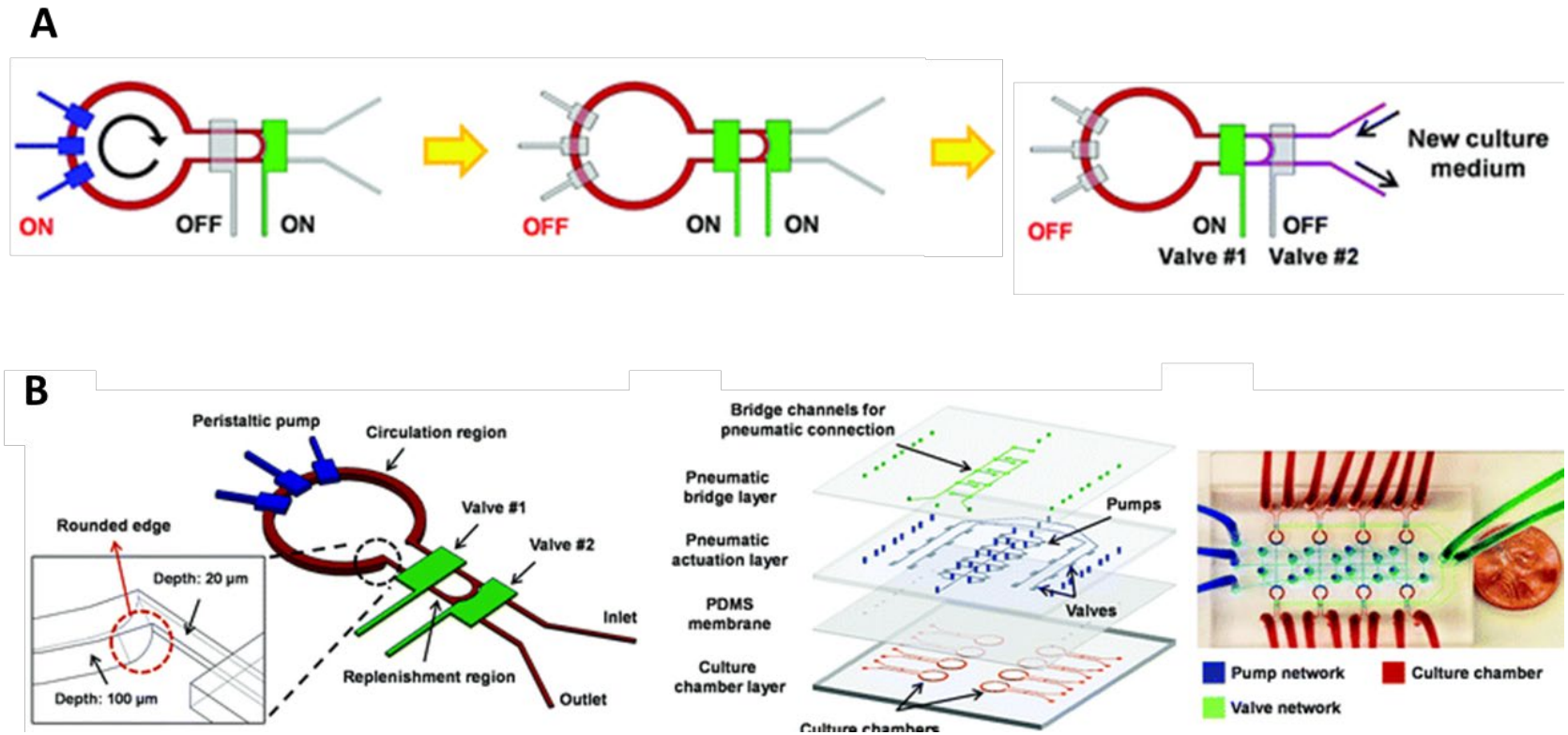

Figure 1.6 – Microfluidic device by Park et al.[46] (A) Reactor operation from growth phase (left), isolation of section of reactor for cleaning and media replenishment (centre), cleaning and media replenishment phase of operation. (B) Schematic view of reactor (left), illustration of multi-layer design of device (centre), chip with 8 reactors adjacent to a US Cent for scale.

1.2.4: *Device Control*

While many examples exist of microfluidic devices designed for growth of trapped and adherent cells, the ability to mix and manipulate cell culture volumes would be necessary for retrieval of desired cells. There are two prevailing methods currently used to manipulate culture volumes and cells within channels of a microfluidic device. One of these is to adhere multiple layers of channels together using multi-layer soft-lithography. This is the method used to fabricate complex devices with pneumatically controlled mechanical valves, including those mentioned here by Kelly, J[51] and Park et al.[53]. Taking the design by Jason Kelly, there are two separate layers of channels, separated by a thin membrane, these must be perfectly aligned and sealed to function. The first layer is the sample layer, the network of channels in which the bacteria grown and the experiment functions. The second layer consists of control channels, placed strategically over the first layer to provide a network of control valves. The valves are pneumatic, when pressurised they are designed such that they expand and compress the layer below, preventing flow in the sample layer (*Figure 1.5 E-F*). This is typical of multi-layer soft lithography devices.

The advantage of this design is that the culture is in a continuous suspension, meaning cells can interact with one another during growth as a normal population would. With bacteria, this means horizontal gene transfer can occur, which is an important component in bacterial evolution[54]. Where it is not essential to move cells from one place to another within a reactor, microfluidic devices will be designed to function without valves and without the need for multi-layer construction[50]. This is largely due to the difficulty of reliably bonding layers together, both in terms of alignment between layers and leakage between layers. As previously mentioned, there are many publications and reviews which attempt to provide solutions to bonding and sealing layers[55,19], demonstrating the difficulty in this fabrication method. The primary reason for this is that master moulds are essentially designed in a two-dimensional layout, other than the ability to alter the height of the channels. Features that do not directly contact the silicon wafer in the master mould cannot be included. This means that a multi-layer device consists of two single-layer devices adhered

together. The ability to incorporate both sets of control channels into a single master mould would be of great benefit for producing these kinds of devices, as soft lithography could mould an entire device in a single-step without the need for layer alignment and adherence. This is the area in which 3D printing could offer advantageous fabrication over traditional multi-layer devices.

The second option for control of microfluidic devices is digital droplet-based microfluidics. In these devices, the contents are not homogenous but contained in isolated microdroplets of sample, separated by a second immiscible liquid. The liquids are sandwiched between electrodes, which serve to control the movement of microdroplets via electrostatic charges[56]. These devices are often referred to as electrowetting-on-dielectric (EWOD), as the high surface area to volume ratio of microfluidic droplets facilitates the ability of electrowetting to move droplets. This has the advantage of avoiding complex and problematic mechanical valve systems and as the droplets are self-contained, they do not exert the same channel constraints as a continuous device. Droplets can be combined with relative ease, which can serve to add reagents or sample to a given droplet. Droplets can be formed consistently, and the technology could be used in combination with continuous cell culture. One disadvantage is that the control mechanism relies on the high surface area to volume ratio of microdroplets and suffers from limited scalability[57].

1.2.5: *Chemostats for Directed Evolution*

While publications related to microfluidics have become increasingly common[58], the creation of a novel microfluidic device has been restricted to the point that not many biological laboratories consider or are even aware of its potential applications. The time and expense of a master mould and the degree of specialisation required to generate and operate a complex, multi-faceted microfluidic chip is beyond most labs whose specialties lie elsewhere. This has limited the uptake of these devices as a versatile method of undertaking bespoke experiments, meaning the vast majority of labs still use decades old techniques. A standardised, reliable and accessible in-house fabrication technique for microfluidics in desktop 3D printing would provide the basis for the widespread adoption of the technology in field of molecular biology. If readily designed, prototyped and improved within a lab, it would offer all the

advantages of a chemostat and potential for far more, without the drawbacks of conventional systems. Because these devices would work with culture volumes which are orders of magnitude smaller than current chemostats, they are far more capable of monitoring small volumes of cells, with the potential to analyse single cells *in situ* [59].

1.3: Raman Spectroscopy

1.3.1: *Non-Invasive Spectroscopy*

Monitoring cells *in situ* without damaging them is possible with several techniques. A successfully adopted method is optical visualisation using fluorescent markers, including GFP described by Long et al. A promising alternative technology is Raman spectroscopy.

Raman spectra can be obtained for any compound which contains a chemical bond which emits Raman signal, which is any asymmetric chemical bond. All the bonds within a given molecule can affect the overall spectrum, meaning molecules have a specific 'fingerprint'. This means that unlike fluorescence markers, cells can be monitored for compounds they contain without altering them or requiring the development of marker systems[60]. Combining a microfluidic chemostat of similar scale to that developed by J.Kelly[51] with single or multi-cell, non-invasive monitoring technology such as Raman would vastly expand the potential of chemostats as a method of directed evolution. Being able to monitor and select individual cells for any property detectable by Raman, in a controlled population small enough that this selection pressure can influence the entire culture would be an extraordinarily powerful tool for optimising synthetic or naturally occurring proteins and enzymes for industrial use. A vital step towards achieving this kind of system is a reliable, accessible fabrication technique. Desktop 3D printers capable of these resolutions would provide the answer. Part of this research is to determine whether creating a device such as this is currently feasible with commercial desktop 3D printing technology, and the potential for this to be possible in the future.

Raman spectroscopy is a type of spectroscopy which measures a molecule's change in vibrational energy when exposed to a photon. When a molecule is exposed to a

photon, the energy absorbed excites the electrons and nuclei. The electrical energy state transitions rapidly after photon absorption because electrons can quickly change conformation around the nuclei and absorb the photon energy. The nuclei of a molecule are far larger, meaning their conformation does not change with the electrons. Once the molecule has increased in electrical potential, the nuclei then reposition to form a new equilibrium. This repositioning results in a vibration of the chemical bonds between the atoms in a molecule. This is called the Franck-Condon principle and using this principle it can be predicted what vibrational state is most likely to occur (on average) after the transition for a given molecule. This is because a change from one vibrational state to another is more likely when the vibrational wave functions of both the electrical and vibrational transition.

Raman spectroscopy is based on the phenomenon that when chemical bonds are exposed to a light source, the interaction of photons and the vibrating bond emits photons of the same energy level (elastic or Rayleigh scattering) but on rare occasions (approximately 1 in every 10^{10} photons) results in a shift in energy level of the photon emitted relative to the original photons, this is called inelastic or Raman scattering[61]. Inelastic scattering results in two possible photons of changed state, one with a longer wavelength and lower energy level (Stokes) and one with a shorter wavelength and higher (anti-Stokes), in relation to the original wavelength. A Raman spectrometer shines a laser of specific wavelength onto a sample, filters out Rayleigh scattering, and detects the photons which are emitted at a longer wavelength (Stokes). The combination of photon wavelength shifts from different bonds in a sample produces a Raman spectrum, and is indicative of the chemical bonds, along with other aspects of the state of the sample compound.

1.3.2: *Factors Affecting Raman Spectra*

A Raman spectrometer typically consists of a light source (usually a laser), a sample, an objective lens to focus on the sample, a notch or edge filter to remove the original laser wavelength, a detector and a grating to disperse the signal onto the detector, increasing the resolution at particular ranges of wavenumber (*Figure 1.7*). As Raman signal is proportional to intensity of light, it is important to tightly focus the beam on the sample to produce the best results. Raman signal is affected by several factors

and it is particularly important to optimise the system to produce the best signal to noise ratio. The noise is the signal which is not produced by the target molecule, but by other factors such as sample fluorescence and the signal from cover slides or solution media.

The intensity of Raman signal is affected by the laser power (in mW) and wavelength. Higher power lasers will generate more Raman signal but will result in localised heating of the sample which can damage or destroy it. There are several commonly used laser wavelengths in Raman spectroscopy, which are affected by the availability of suitable lasers, the detection range of silicon detectors and the type of analyte. In general, a shorter wavelength will provide a much stronger Raman signal and a longer wavelength or lower energy laser will produce a weaker Raman signal. The increased Raman signal produced by shorter wavelength lasers means that shorter acquisition times are possible to produce the same results when compared with longer wavelengths. One drawback is that shorter wavelengths also tend to increase autofluorescence in biological samples when compared with longer wavelength lasers, which can overwhelm the Raman signal and make detection more difficult. 532nm, 633nm and 785nm wavelength lasers are the most common for Raman spectroscopy, with 532nm producing strong signals but higher autofluorescence in biological samples, particularly at higher wavelengths[62]. Lasers with shorter wavelengths than this are not commonly used to study biology, as they can cause cellular damage in a relatively short time period[63]. Longer wavelengths produce less Raman signal, meaning longer acquisition times are required to produce the same signal compared with shorter wavelengths. The benefit of longer wavelengths is that there is less fluorescence, meaning they can produce a better signal to noise ratio than lasers with shorter wavelengths. 785nm lasers are therefore the most common, as they are the most versatile laser source which can be detected by silicon-based charge-coupled device (CCD) detection systems. Longer wavelengths produce even less fluorescence but require different detections systems than CCDs, as their Raman signal detection decreases significantly above 800nm. In this research, a 785nm laser is used as the light source to enable increased signal to noise ratios.

In addition to the laser light source, the magnification and numerical aperture of the objective lens on the sample are important for the intensity of Raman signal. This is because the intensity of light on the sample is affected by the size of the laser spot and the amount of light in the spot. In general, a larger aperture will allow collection

of more light and therefore Raman signal, though it is not as straightforward as this in practice. Higher magnification will focus the laser on a smaller area, increasing the Raman signal due to the higher density of photons.

Raman spectra can be compared irrespective of the laser wavelength. This is due to the fact that Raman shift is directly dependent on the vibrational structure of the molecules in the sample. Spectra are reported in wavenumber (cm^{-1}), which the spatial frequency of the wave (waves per cm), it is the reciprocal of the wavelength of light in a vacuum. This is useful because it means Raman fingerprints acquired with one system can be directly compared with spectra acquired with a system using a different wavelength laser, as is done in chapter 3 of this thesis.

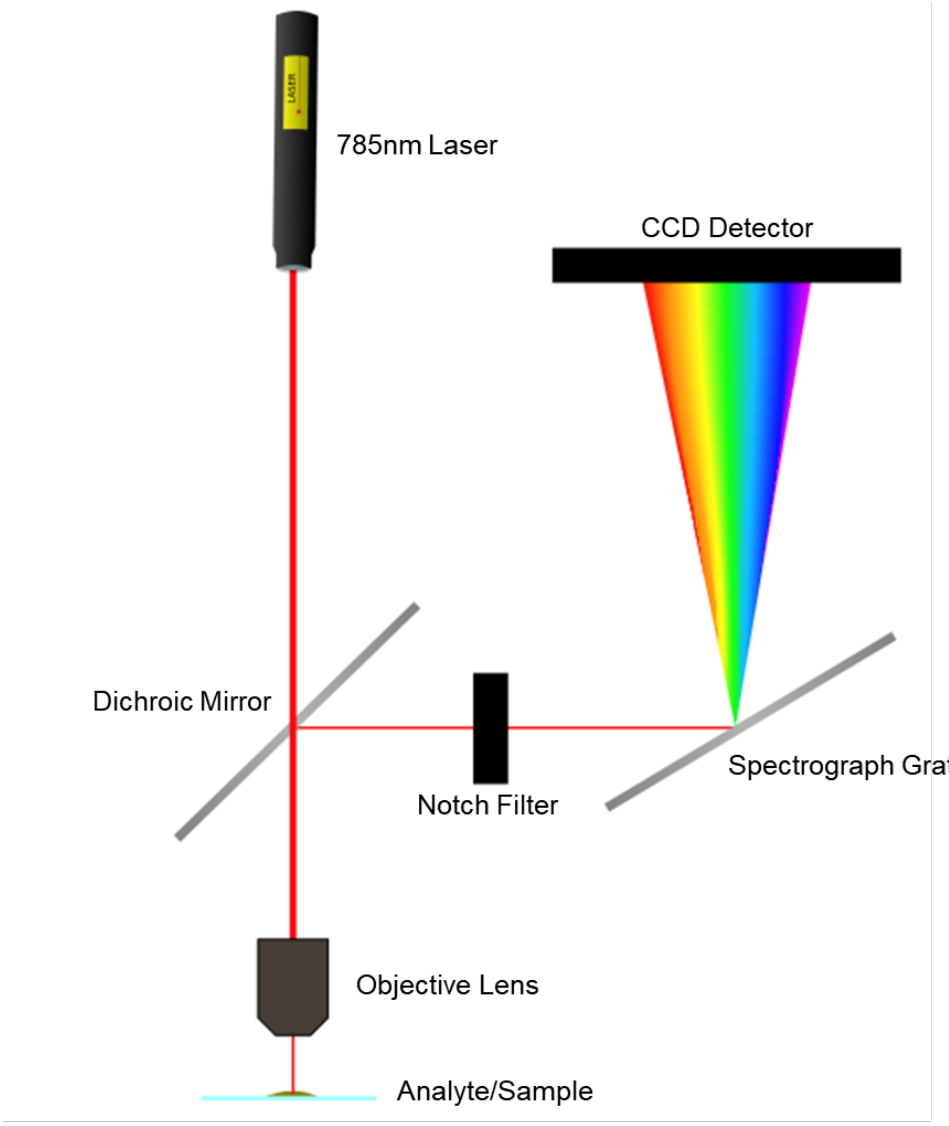

Figure 1.7 - Basic Raman Spectrometer Setup. The laser passes through the dichromic mirror to the objective lens where it is focused on the sample. Photons emitted and reflected from the sample pass back through the lens and are reflected through a notch filter to remove the original laser wavelength. The beam is separated by the grating and detected by a CCD to produce a Raman spectrum.

1.4: 3D Printing

1.4.1: *Additive Manufacture*

The recent revolution in desktop additive manufacturing (3D printing) technology provides a potential alternative to classic microfluidic manufacture. The ability to print 3D structures directly eradicates the requirement to adhere multiple layers of PDMS, it removes the necessity for a specific, expensive master mould and crucially, enables rapid production and testing of designs with reduced need for specialist expertise and equipment.

3D printers come in many forms, the three most common types for polymers are stereolithograpy (SLA), digital light processing (DLP), and extrusion printing/fused filament fabrication (FFF). Extrusion printers are by far the most common devices available to amateur hobbyists, offering low cost materials (~£40 per kg for ABS) and equipment (a moderate quality printer can be purchased under £1000). In extrusion printing, a polymer filament (commonly ABS) is fed into a melting chamber and deposited through a nozzle layer by layer in 3D space. Support material can be printed to enable more complex prints with overhanging edges. Depending on the quality of the printer, this is either made from the same print material to be manually removed afterward or is printed in a different, soluble material (usually PVA) from a second nozzle. While the low cost of this technology is an advantage, detailed printing has been shown to be inconsistent. Generally, FFF printers are incapable of reliably producing channels of under 500μm (compared with less than 10μm for soft lithography)[64].

SLA and DLP printers utilise laser and ultra-violet (UV) curable liquid resins to produce thin layers on a build platform. Most desktop resin printers utilise inverted printing, where build platforms are lowered into a tank of resin and the part is built upside-down relative to its design. When the build platform is submerged in resin and a specified distance from the lower surface of the resin tank, curing of the resin is facilitated by UV light, provided from beneath the tank from a light source. The key difference between SLA and DLP printing is the source of light. SLA printers use a laser and mirror array to ‘draw’ the desired layer, where DLP printers utilise UV projection to project an entire layer across the print area. This enables DLP printers to print an

entire layer at once, much faster than SLA printers which have to scan the entire area of a layer before moving on to the next. The resolution of these different printers depends on the laser spot size for SLA and pixel size for DLP, the most popular desktop SLA printer is the Formlabs Form 2, which has a spot size of approximately 140µm. DLP printers commonly have a pixel size of 50µm, such as the one utillised in this project. The market penetration of DLP printers is significantly lower than that of SLA and FFF, in part due to the lack of a reliable, mass market desktop system such as the Form 2, they will undoubtedly become more popular as new products are brought to market.

There are three ways in which these technologies can be used to manufacture microfluidic devices. A 'positive' print where the device is printed directly[65], a negative 'sacrificial template' for casting of PDMS[66, 67] (*Figure 1.8)* or replicating current negative master moulding. Previous negative structures have been printed with extrusion printers in ABS, before being dissolved in acetone post PDMS casting[67]. Because they use FFF extrusion printing they are generally capable only of producing channels in the millimetre range. Positive printing can be performed using light curable resins in SLA and DLP printing and can produce more detailed prints, however, the properties of the resins are a limiting factor for producing microfluidics. Most resins are rigid and cannot therefore be used for traditional valve systems, along with unproven biocompatibility and varying degrees of transparency. Resin prints also leave residual uncured resin on the printed model, which must be fully removed prior to use.

In this work, a DLP Way2Production SolFlex 350 printer with resolution of 50µm X/Y and 25µm Z axis is used in conjunction with a water-soluble 'rinse out resin', along with manufacturer's own resins, with the aim of providing both the benefits of negative printing with additional detail provided by DLP printers over extrusion.

1.4.2 *Soft Lithography*

As previously described, the most common technique for fabricating microfluidic devices is soft lithography. This technique utilises soft, flexible polymers such as PDMS to quickly and inexpensively produce copies of a master mould. The master mould, traditionally, has been fabricated using photolithography. The primary

limitations of this approach would be the inability to rapidly iterate device design and the need to outsource production of the master mould for the majority of laboratories. PDMS casting could easily be applied to a 3D printed master mould, enabling in-house production and rapid device fabrication and iteration at low cost. In addition, a truly 3D master mould would eradicate the issues associated with multi-layer soft lithography if the mould were removable post casting. 3D printing in soluble materials offers this function, removing many constraints put on device design by multi-layer soft lithography and enabling the embedding of functional components into devices.

1.4.3: *Fused Filament Fabrication*

Fused filament fabrication (FFF) or as it is more commonly referred to Fused Deposition Modelling (FDM) makes up the vast majority of desktop 3D printers on the market today. Made popular in desktop format by Makerbot (www.makerbot.com), the process uses reels of plastic filament as a base material for producing 3D shapes. The filament is fed through an extruder and in turn pushed through a nozzle, which is heated above the melting temperature of the plastic. The plastic melts in the nozzle and is deposited layer by layer onto a build platform in 3D space to form a print, becoming solid as it cools. The X/Y movement of the print is usually performed by the print head assembly, which contains the heaters and nozzles (and sometimes also extruders). Print heads are mounted on sliding rails and movement controlled via belts and stepper motors, though other mechanisms of controlling travel such as linear rails do exist. Z movement is controlled either by moving the build platform downward away from the nozzles on each layer, or less commonly by moving the print head assembly upward (*Figure 1.9).*

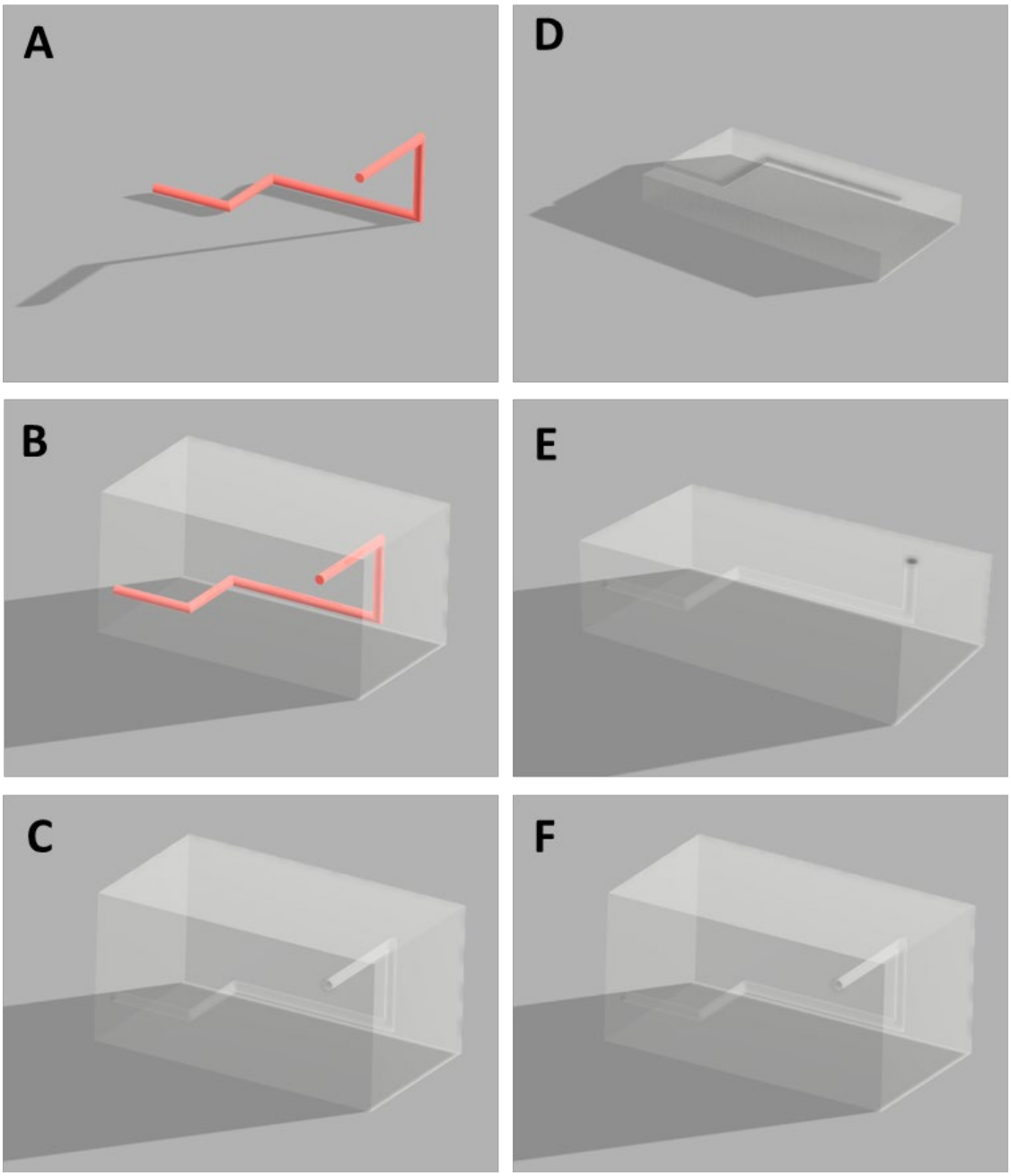

Figure 1.8 - Illustration of 3D Printing Approaches. (A) 3D printed scaffold structure made from soluble resin. (B) Scaffold with PDMS cast around to produce device. (C) Final device after dissolving sacrificial template with water. (D, E) Direct layer-by-layer 3D printing of device, leaving open tubes using a DLP printer. (F) The same device as C, using direct printing.

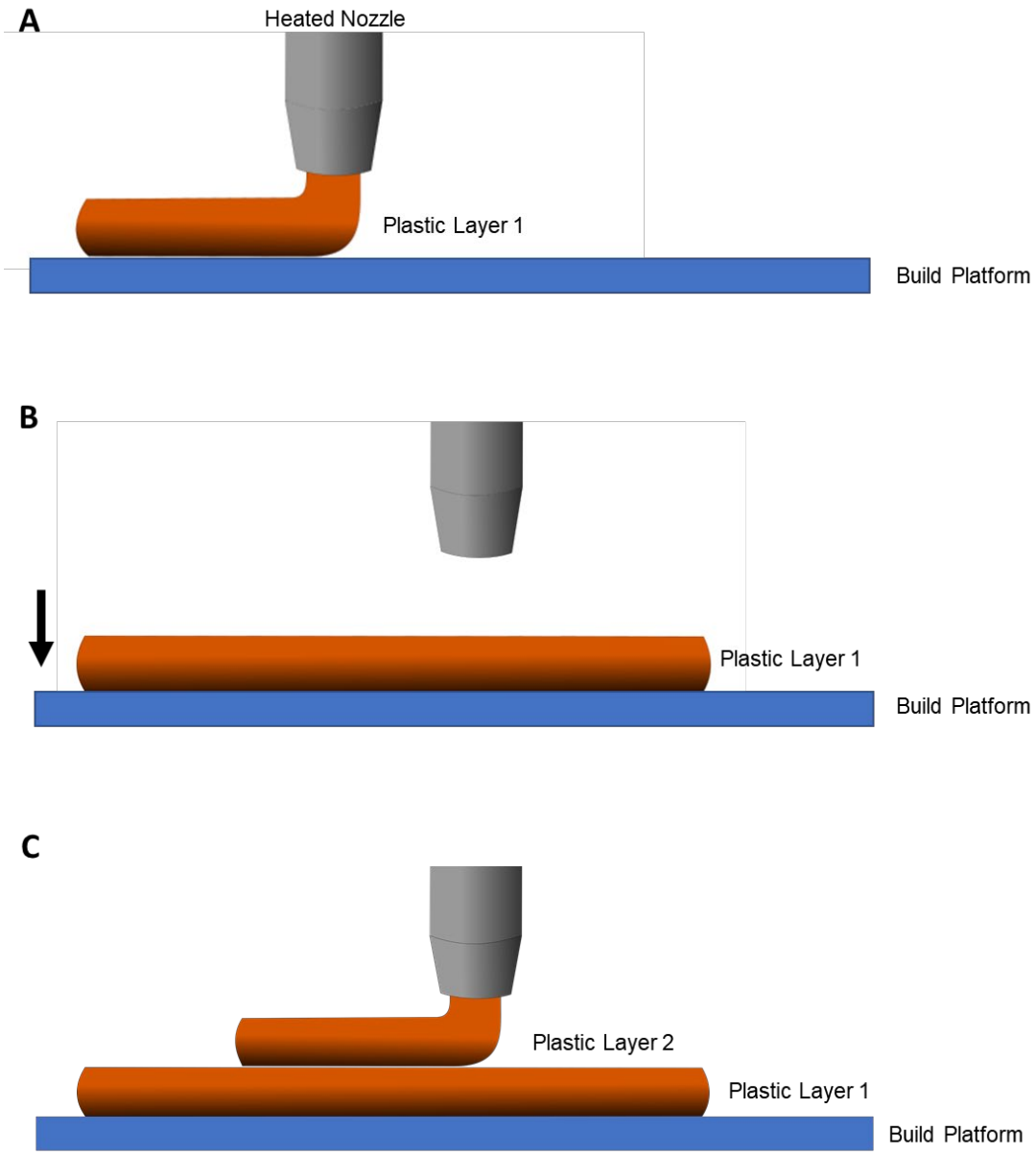

Figure 1.9 – Side view of Fused Filament Fabrication (FFF). A hot nozzle melts plastic and uses it to lay out shapes on a build platform. 3D models are built by laying plastic down in layers to form the printed part. (A) First layer is deposited on the build platform. (B) Material extrusion stops and build platform is lowered for next layer. (C) Layer 2 is deposited onto the first layer to form a 3D shape.

The advantages of FFF include range of material choices, low cost and ease of use, with plenty of community and manufacturer support available. ABS and PLA are the most common general-purpose materials, with PLA generally considered the cheapest and easiest to print. Different materials are available with different properties and are application dependant. Amazon have recently released their own Amazon Basics ABS filament for £14-18 per Kilogram (www.amazon.co.uk), demonstrating the mass market appeal of this technology.

Along with a wide range of material choice is a wide range of machine choice. Makerbot drove the push for this mass market technology but have been superseded by newer companies such as Ultimaker. Reliable machines such as the Flashforge Creator Pro (a Makerbot Replicator 2 copy) (www.flashforge.com) can be purchased for under £1000. In general, cheaper machines can print with one material at a time, are less positionally precise and lack features such as heated print beds, which are required to prevent warpage using certain materials. More expensive machines such as the Ultimaker S5 (www.ultimaker.com) are capable of printing with multiple materials simultaneously and can often print with soluble support materials such as PVA.

The width of a single extrusion in the X/Y plane is dictated largely by the nozzle diameter through which it extrudes. The majority of multi-purpose desktop 3D printers of this type, such as Ultimaker and Makerbot, use 0.4mm diameter nozzles, meaning the minimum width of this extrusion is theoretically 0.4mm. Precision is dictated by a variety of machine build factors, chiefly print head mass, printer structural rigidity and control of print head movement. Z dimensions are dictated by the height of the nozzle above the surface on which material is deposited. On the first layer of a print, this is the build platform, which must be true, level and adjusted to the correct height for the first layer of a print. The first layer of a print is essential for successful printing, if the first layer is not deposited in such a way that it sticks to the build platform, it does not form a stable base for subsequent layers and may become detached entirely. The Z-height of subsequent layers is determined by the distance between the previous layer and current layer in the Z-axis. Usually this is performed by moving the build plate using a Z-screw.

There are examples of both larger and smaller nozzles for different purposes. Larger nozzles can deposit more material and are generally used for large format printers, as the increased speed makes printing large parts feasible and surface finish is often less of an issue on these types of parts. Smaller nozzles can print smaller features, at the expense of speed and reliability. Many FFF machines offer the ability to interchange different nozzles for different diameters, or sometimes where materials require it. An Ultimaker 3, a popular sub-£3000 printer, has options of two nozzle types (Print Cores) for different materials, and three different nozzle diameters – 0.25mm, 0.4mm (standard) and 0.8mm. While layer height is determined primarily by the chosen Z-axis parameters, nozzle size plays a role in determining the upper and lower limits of this choice. For an Ultimaker 3, layer heights for a 0.25mm nozzle are 60-150µm, a 0.4mm nozzle is 20-200µm and a 0.8mm nozzle is 20-600µm.

As previously mentioned, the first layer of a print has different requirements and is controlled in a different way. To ensure print bed adhesion, the first layer is always printed so that the extruded plastic is 'squished' onto the bed. This means that the X/Y extrusion is wider than the other layers and the Z resolution is smaller than other layers. The significance of this effect in relation to printing with microfluidics is that a printed microfluidic channel derived from a 3D print of this type will likely be at the lower limit of X/Y and Z resolutions, requiring only one layer. If this layer is the first layer of a print, then it would be imprecise and not repeatable under standard setup procedures.

1.4.4 *Stereolithography Apparatus (SLA 3D Printing)*

SLA 3D printers differ substantially from FFF. The base material of an SLA printer is a photosensitive liquid resin, rather than a filament, which solidifies in when exposed to ultraviolet light. This process is called photopolymerisation and is known as curing the resin, illustrated in *Figure 1.12*. Resins used for this process typically consist of a mixture of monomers, oligomers and photoinitiators. The most common photopolymerisation process is radical mediated photopolymerisation. When exposed to UV light the photoinitiators release radicals which trigger cross-linking and polymerisation of monomers and oligomers. This cross-linking sets of a chain reaction of radical release and further chain-growth polymerisation. The reaction is typically

halted when two growing chains cross link together. The 3D solid is formed by curing multiple layers of resin on top of one another in a specific shape, which is similar to the method used for FFF. Liquid resin is contained in a tank, in which the build plate is submerged. The resin is cured onto the build plate using a scanning ultraviolet laser, the build plate is then moved away from the laser's curing surface by the distance of the specified layer height and the next layer is cured onto the previous one, so a 3D shape is formed.

The build platform of a resin-based printer can be either lowered deeper into a large resin tank on each layer, or 'inverted', so a build platform is raised from the bed of the tank and the print build suspended upside down in relation to the finished part. There are advantages and drawbacks to each approach. Traditional lowering of a build platform away from the print surface limits the height of a print in the Z axis to the depth the platform can be submerged, requiring a volume of resin equal to an entire potential full build volume in each of the X, Y and Z axes, regardless of the size of any given model. The Formlabs Form 2 (www.formlabs.com) is the most popular desktop SLA machine on the market, and utilises an inverted approach, meaning that only the depth required to reliably cure a single layer is required, where the X and Y axes still require the full build area. Practically, tanks for inverted printing will contain enough resin for either an entire print or at least numerous layers to avoid the need to constantly refill between layers. The drawback of inverted SLA is that resin is cured onto both the resin tank surface and the build platform simultaneously. The bond between the build tank surface and the rest of the printed part much be broken carefully, using a peel action, so as not to break small features from the printed part, or pull the entire printed part from the build platform. Non-inverted SLA does not have the issue of a peel action, as it cures at the top surface of the liquid tank. *Figure 1.10* shows a side-view illustration of inverted SLA printing.

There are several major advantages to using resin-based printers over filament, the first is that the minimum theoretical width of a feature within a print is only the width of a laser spot or pixel, which is generally far smaller than a standard diameter FFF nozzle. The Form 2 uses a 405nm wavelength laser with a 140µm spot diameter. The Form 2 has a minimum layer height of 25µm, comparable to other printers of its type and also to that of FFF technologies. This means that theoretically, 140µm x 25µm is the smallest printed dimension, compared with the 250µm x 60µm with a 0.25mm nozzle on an Ultimaker 3.

Another advantage of SLA, and resin-based printers in general is that the outer edges of a given layer are straighter than FFF. Layers in FFF are extruded in such a way that there is a ballooning of material in the X/Y plane either side of the printer nozzle, perpendicular to the direction of travel. This is because the rate of material extruded exceeds that which is required to fill the space between the nozzle and the print to ensure adhesion. As the laser in an SLA machine selectively cures material in place, rather than depositing new material in empty space, this ballooning effect does not take place. The result of this effect is that for equivalent layer height, surface quality from an SLA machine is generally more consistent than with FFF.

The first layer of an SLA print on a Form 2 has similar characteristics to an FFF machine, in that it is 'squished' onto the build platform to ensure proper adhesion to the build platform. Form 2 printers go further than this, with the first 5mm of a given print also 'squished' to ensure proper adhesion. To prevent affecting prints, parts are built on rafts and support structures so that they are at least 5mm away from the first layer of the build. Using rafts with FFF printers is also a common method of ensuring consistency on the first layer of a printed part, though the way in which they are used differs between the two technologies. FFF machines build directly on top of a printed raft, where in SLA on a Form 2, parts are connected to a raft only by thin support structures.

This smaller feature size is of great benefit here when attempting to produce microfluidics, however, 140µm x 25µm is still an order of magnitude larger than the smallest channels in microfluidic devices described previously – some of which are essential for operation. Microfluidics fabricated by a Form 2 would be unable to recreate these devices, which would instead need redesigning to suit the resolution an SLA printer like the Form 2 is capable of.

1.4.5: *Digital Light Processing (DLP)*

DLP 3D printing is similar in technology to SLA, in that it uses the same method of submerging a build plate into a liquid tank of photo-sensitive resin. The primary difference between the two technologies is the source of light used to cure the resin. Where SLA uses a scanning laser, DLP utilises a projector or screen to emit ultraviolet

light from pixels. Generally, the same resins can be used for SLA and for DLP, depending on the wavelength at which they are cured.

While similar to SLA in almost all respects, the key difference is that stationary pixels are used to cure an array of dots, rather than drawing a shape with a scanning laser. The volume cured by a given pixel is called a ‘voxel’ and has no standard parameters between manufacturers. The main advantage of this approach is speed, particularly when a larger area is cured on a given layer. The reason for this is that an SLA printer ‘draws’ the outline of a layer, then scans back and forth to fill in the shape, much like an FFF printer. This takes time, and the more area in a given layer that requires curing, the longer it takes to draw and fill in. In contrast, a DLP printer simply projects an entire layer at once, with the time to cure one voxel equal to that of curing an entire layer as they are cured in parallel.

Another advantage of desktop DLP vs desktop SLA in a Form 2, is that a DLP printer such as the W2P Solflex350 used in this research has a pixel area in X/Y of just 50µmx50µm, over 60% smaller than a Form 2 laser spot of 140µm. Theoretically then, this means that a desktop DLP printer can print a minimum feature that is 60% smaller than a desktop SLA machine like the Form 2. In practice there are several limits to this apparent advantage, relating to the fact that a pixelated projection cannot create a curve as well as a scanning laser, and the behaviour of a given printer when printing features at the smallest end of its capabilities.

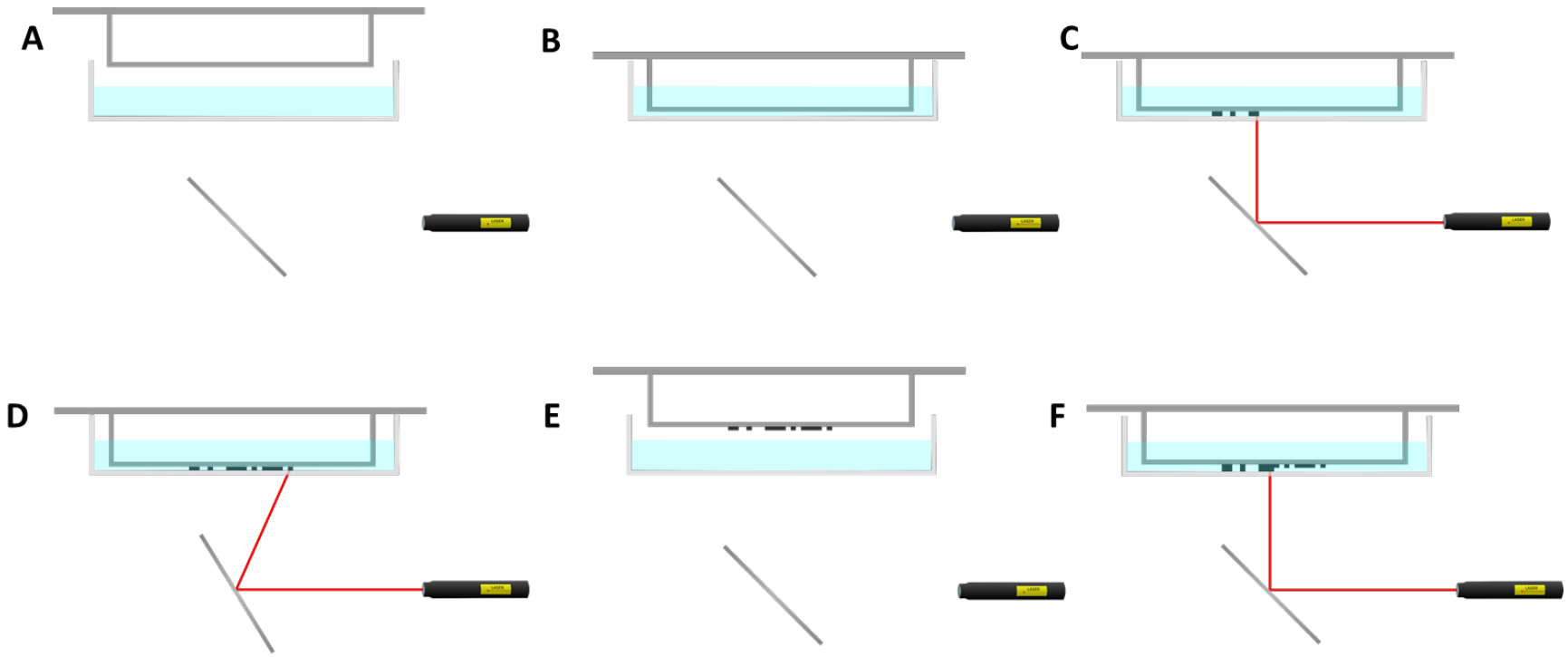

Figure 1.10 – Inverted SLA printing side-view. (A) When idle, the printer leaves the laser off, resin in the tank and build platform suspended out of the tank. (B) The build platform is lowered to the specified layer height above the lower surface of the resin tank. (C-D) A laser is guided in the X/Y by small mirrors, the laser beam passes through the resin tank floor window and cures resin to the tank and build platform. (E) The printed layer is peeled from the resin tank surface and the build platform raised out to enable flow of fresh resin into the void. (F) The build part is lowered back into the tank but the specified layer height above the previous layer, the laser cures the next layer onto the first.

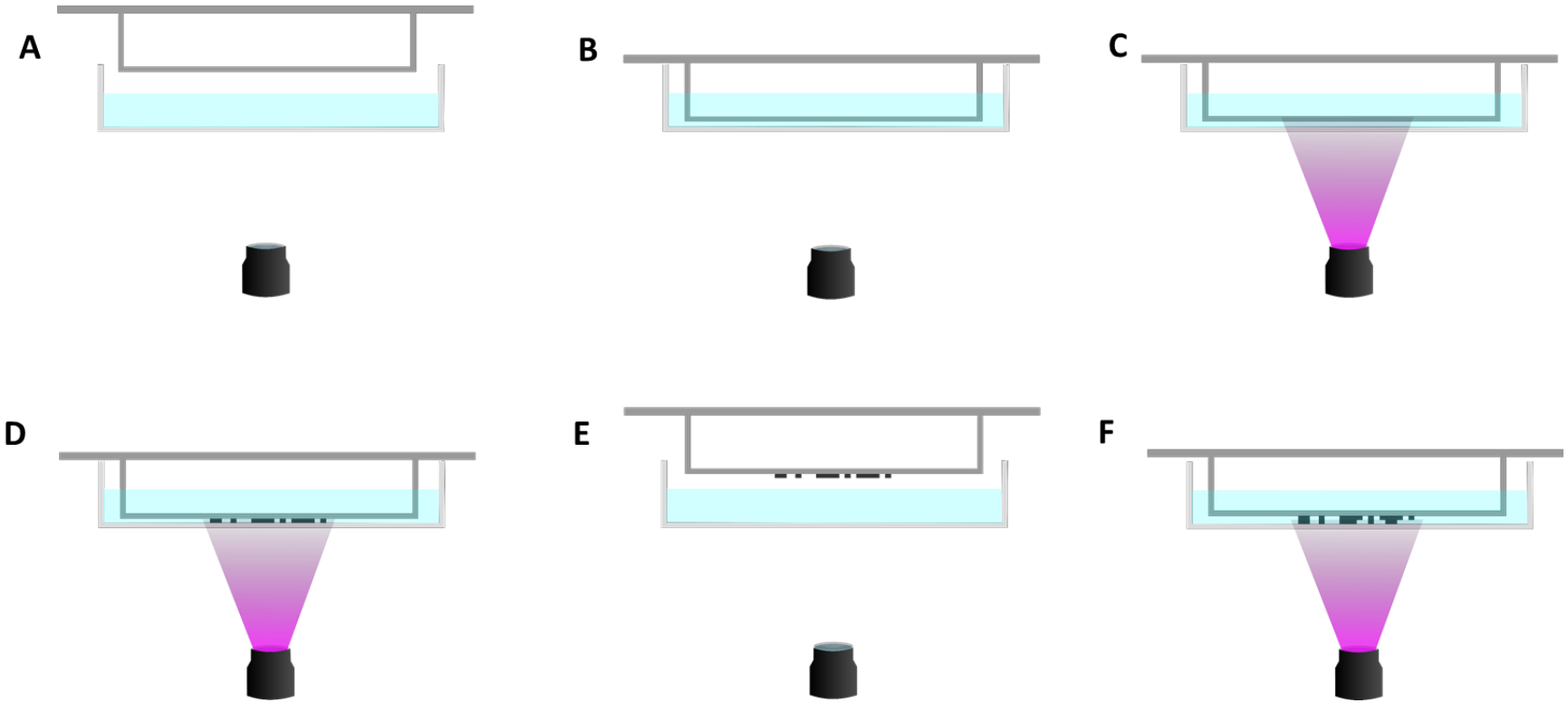

Figure 1.11 – Inverted DLP printing side-view. (A) When idle, the printer leaves the projector off, resin in the tank and build platform suspended out of the tank. (B) The build platform is lowered to the specified layer height above the lower surface of the resin tank. (C-D) A UV projector projects an entire layer at once through the resin tank floor window and cures resin to the tank and build platform. (E) The printed layer is peeled from the resin tank surface and the build platform raised out to enable flow of fresh resin into the void. (F) The build platform is lowered back into the tank but the specified layer height above the previous layer, the next layer is projected onto the first.

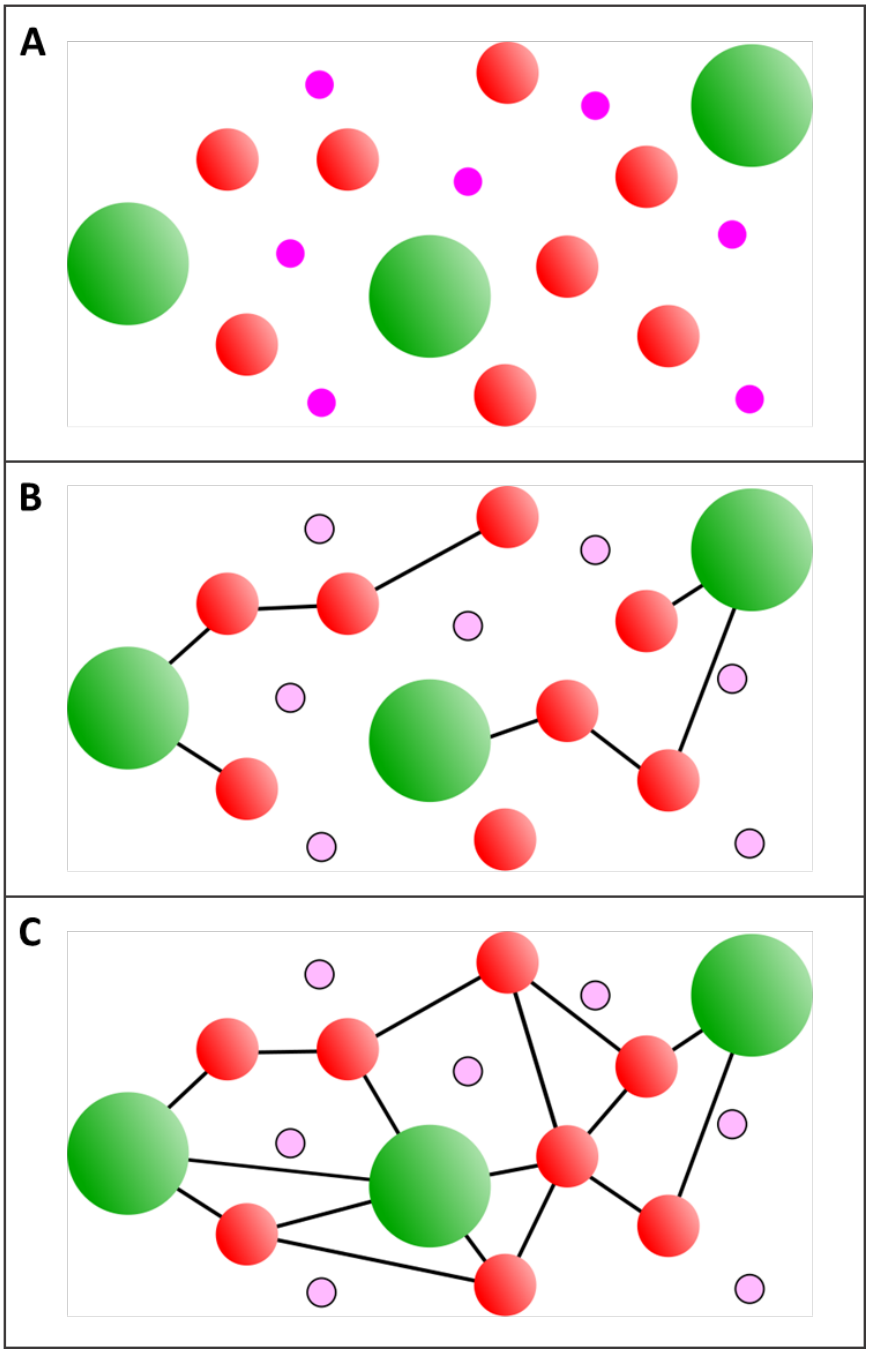

Figure 1.12 – Illustration of Photopolymerisaion. (A) Liquid resin consisting of Oligomers (green), Monomers (red) and Photoinitiators (pink). (B) Localised exposure to UV light triggers photoinitiators to release radicals which cause cross-linking of monomers and oligomers into polymers (C) Cross-linking produces a chain reaction, leading to chain-growth polymerisation of monomers and oligomers, resulting in a solidified polymer.

1.4.6: *Choice of 3D Printing Technology*

The main drawback of all resin-based printers is both the lack of material choice and the cost. Formlabs have their own proprietary range of resins, ranging from £144 per litre for their standard clear resin to £264 per litre for their Castable Wax resin. These resins offer a variety of properties comparable to engineering materials such as nylon (Durable Resin), ABS (Tough Resin) and Rubber (Flexible Resin). Formlabs have recently released their Elastic resin, which may lend itself to PDMS-like fluidic control devices. Budget third party resins equivalent to standard resins can be found for under £50 per KG (roughly equivalent to 1L), such as 'Funtodo Standard Blend' (www.funtodo.net) however, the range of material properties at this price point is extremely limited compared to FFF filaments.

Another advantage to certain FFF printers like the Ultimaker 3, is the ability to utilise two different materials in one print. Commonly this is used for multi-coloured prints however, perhaps the most important use for this system is the ability to print with water-soluble PVA support structures. On a printer like the Ultimaker 3, a print head contains two independently temperature-controlled nozzles, each with their own extruder and material input. Nozzles are located adjacent to one another on the same print head, so X/Y control is inter-linked. When changing material, the printer automatically moves by a calibrated offset value to position the second nozzle over a print before extruding material. The idle nozzle is kept hot but the extruder does not push material through until it is required again.

For low-cost and larger printed part, FFF is usually preferable. For high detail, resin-based printers are superior. Where plastic filament extrusion is always slightly ballooned to ensure proper layer adhesion, layers in DLP and SLA prints are not, they are far more vertical and layering lines for less prevalent. Resin printers produce solid parts which are impermeable to liquids, where FFF is usually permeable to air and liquid due to gaps forming between layers. Resin printers also produce more reliable tolerances because they are not subject to vibrations caused by moving print heads. DLP has no moving parts when a layer is being cured and SLA has only small mirrors which have no effect on print quality.

Between DLP and SLA is a more difficult choice. SLA offers near perfect curves, as the mirrors can move continuously, where DLP has pixels, so any shape is made up of square voxels. The counter argument to this, is that the laser on a Form 2 has a 140µm spot size compared to 50µm pixel size for the W2P SolFlex350, so absolute minimum feature size is theoretically smaller with DLP. DLP is faster, particularly with large prints as it projects an entire layer at once, rather than scanning the outline and infill with a laser spot. For the purposes of this research, the 50µm pixel size was preferred to the ability to produce better curves.

It should be mentioned that this is by no means an exhaustive list of 3D printing technologies, but a brief summary of the most common desktop 3D printers. Selective laser sintering (SLS) melts powders into solid shapes, inkjet technology similarly uses powder as a base material and selectively solidifies it in layers. Powder technologies have many advantages such as the ability to produce colour parts with inkjet printers like the HP Jet Fusion series (www.hp.com) and the ability to print without support. This research focuses on affordable desktop series 3D printers, most powder-based and other technologies are aimed at industrial settings and incur special expertise and higher costs.

1.4.7: *Design for 3D Printing*

As with any fabrication technique, there are design considerations for creating models to 3D print. Manufacturers usually provide a design guide for various details including minimum feature sizes and hole sizes, and the information here is based on design guides for all the manufacturers mentioned. Whether support material is necessary depends largely on the design of the model and whether it is optimised for 3D printing on a given machine. FFF printers generally advise support material on angles at 45° from the build platform or shallower, this is because the molten plastic extruded cannot hold its shape without sufficient support from the layer beneath. This either comes from the model, or support material. Resin printers can print more reliably at shallower angles than FFF printers, this is because they do not extrude molten plastic into space, but cure liquid resin into a solid, where it is surrounded by uncured resin. Instead of gravity, peel force is the limiting factor for a resin printer.

Peel force is the result of the mechanism by which a resin printer separates layers. For in inverted resin machine like a Form 2 or Solflex350, resin is cured at the bottom of the resin tank. While curing, the model is adhered both to the build plate, and the tank surface, which is usually made of PDMS. The peel force occurs when the model is ‘peeled’ off the tank surface and the model is moved away, adhering only to the build platform. The mechanism by which printers perform this varies from one manufacturer to another but it is critical to the reliability of a resin printer. Model design and orientation also has a significant effect on peel force, as the larger the area cured on a single layer, the more that layer adheres to the tank surface and the higher the peel forces.

The complex nature of model, printer and material interactions mean that the sum of design considerations cannot be adequately described in this work, and varies between model geometries. Those which apply to all parts and those relevant to laboratory applications and microfluidics will be discussed.

1.4.8: *Support Material Placement*

Support material is placed when a particular layer or set of layers on a print either begin as an island or a layer builds over an area that is not sufficiently supported by the previous layer on the model. Unsupported islands must have supports on any 3D printer using FFF or SLA/DLP, otherwise the first layer of this section of the part will print ‘in thin air’, unattached to the rest of the print and with no base to stick to. Parts of a model which require supports are generally known as bridges and overhangs. Bridging is where material is deposited between two previously printed walls in the sample plane as the layer deposition, with an unsupported section in between. Some level of bridging without support is possible with all 3D printing technologies, depending largely on the length which is unsupported and the layer height. Overhangs are cantilever structures in which the model is printed at an angle shallower than is self-supporting, relative to the build platform. Though commonly 45°, inverted resin-based printers are often capable of angles closer to 30° or lower, depending on part geometry. This is because they place an entire layer bonded with the resin vat before peeling and are not subject to gravitational forces deforming the layer as it is deposited. This means only the completed layer is subject to peel forces, which can

help provide structure for overhanging sections of a layer when compared with FFF extrusion.

Given the small scale of the printed features that would be required for microfluidics relative to the printer's capability and the potential fragility of the 3D templates, it is essential that models can be printed without support structure on the channels. Support would be impossible to adequately remove without breaking thin features, as the contact points would be as large as the diameter of the channels. Cutting supports off would be impossible to do by hand and would produce inconsistencies in the channel walls after casting. For this reason, it is important to test how small a diameter cylinder can be printed at 45 degrees from the build plate. This would enable building of channels at different angles, if cylinders can only be built at steeper angles or vertical, then it limits the differences between angles of different channels in a final device.

1.4.9: *3D Printing and Microfluidics*

The issues preventing widespread uptake of microfluidics in biological research are largely related to device production. Recent innovations in 3D printing technology provide a more accessible, more versatile alternative to typical construction methods. There are promising examples of 3D printing technology developed specifically for biological applications. Gong et al[68] from the laboratory of Professor Gregory Nordin, Brigham Young University, developed a DLP-SLA 3D printer capable of producing microfluidic channels as small as 18 μm × 20 μm. The ability to produce microfluidics on this scale would offer an alternative to traditional construction in all but the smallest microfluidic devices. As this is a custom printer, it demonstrates the potential for 3D printing as a fabrication method but does not currently offer non-specialised labs the ability to produce microfluidics. Research by the same group utilised an ultra-high resolution, commercially available DLP 3D printer (Asiga Pico Plus 27) and custom formulated resin to produce microfluidic channels[69]. This particular printer is intended for jewellery and has a 35 × 21.8 × 76 mm build area and pixel spacing of 27μm. When combined with their custom resin, the printer is capable of producing channels with a minimum of 60μm in height and 108μm diameter. Using this combination, the authors are able to fabricate functional 3D printed pneumatic valves, pumps and

mixers. Key findings from this work are that the minimum reliable channel size produced by this printer and resin combination is approximately four times the pixel size in the X/Y plane and that the resin absorption coefficient dictates the minimum void height. This issue is characteristic of DLP or SLA printing, a negative feature is likely to be less reliable than a positive feature due to light scattering (X/Y) and penetration of light further into resin than the specified layer height causing excess curing in the Z axis. This characteristic means that printing of positive features in a master mould or sacrificial template, followed by soft lithography, is likely to yield better resolutions than direct printing of devices with DLP or SLA printers.

Two photon polymerisation (2PP) is a microfabrication which uses photosensitive substrates to generate 2D or 3D structures at resolutions as small as 100nm[70]. The process uses similar substrates to the photosensitive resins in DLP and SLA but uses femtosecond laser pulses to produce high resolution structures in 3D space. In 2PP, polymerisation of the target substrate occurs when two photons are absorbed simultaneously, which can be carefully controlled by the laser pulses. This technique has been used to produce devices for cell growth, such as those fabricated by Otuka et al to monitor growth of *E.coli* in different microenvironments[71]. These devices demonstrate the potential of rapid, versatile microfluidic fabrication, producing two different devices with relative ease. Using 2PP, their first device contained column features of radius 15 μm and height 45 μm (with a height variation of 1-3μm), comparing favourably with current methods in the literature and out-performing the most precise commercial DLP and SLA printers by almost an order of magnitude in the X/Y plane. 2PP is a promising technology and there are now commercially available printers such as those made by Nanoscribe which employ this technology. Despite the potential of 2PP as a fabrication technique, it is likely to suffer from some of the same issues as current techniques when it comes to widespread uptake of microfluidics in biology. Accessibility for non-specialised research groups will be limited by the price and availability of the specialised technology. While current general-purpose 3D printers are not capable of the same detail as these specialised units, if they can produce microfluidic devices then they are likely to pave the way for wider adoption of the technology, as biological labs acquire them for other purposes. The research presented here evaluates one such general-purpose DLP 3D printer to see how precise it is at high resolution to evaluate the capability of currently available units.

FFF 3D printing of microfluidics is limited, largely due to the minimum achievable feature size with this technology relative to those based on photopolymerisation. Other drawbacks are that structures printed with FFF tend to be porous without post-processing and the surface finish tends to be inferior, due to the ballooning effect described previously. Advantages of FFF printing are that both machines and materials tend to be cheaper, there are more materials available, they are easy to customise, there is the potential for inserting components between print layers, and there is less post-processing of printed parts as there is no uncured resin to wash off. These advantages mean that FFF printers are the most common in laboratory groups currently, especially for general purpose use. FFF 3D printed microfluidics has been demonstrated[72], with the authors using 3D SIMO pen to extrude and ABS material to fabricate an acetone-soluble scaffold for soft lithography. Channels as small as 500μm were created with a single extrusion and either manually formed to a specific shape with a soldering set or 3D printed with a Craftbot 3D printer (200μm nozzle). The single pen extrusion had a consistent diameter from the nozzle, enabling modification post-extrusion, however, a typical layer-by-layer approach to 3D printing would not produce this dimension in 2D or 3D space. A more realistic target for FFF 3D printing using current devices is general labware and millifluidic devices with channels closer to 1mm in diameter, as shown in[73] where 0.8mm channels were achieved using an Ultimaker 2 3D printer. This research fabricated a droplet generator with pneumatic valves and integrated components which were inserted manually during printing for culture of *E.coli*. The devices in this publication were printed with PLA and vapour treated, a post-processing technique which smooths and seals FFF prints, making them airtight. FFF 3D printers can produce satisfactory results for creating custom reaction-ware in the lab, which is encouraging progress for changing the way research is conducted in biolabs. Despite these capabilities, their application in microfluidics remains limited and photopolymerisation-based 3D printing is the most likely technology to achieve resolutions necessary from commercially available, multi-purpose units.

In addition to these common technologies, research groups such as that of Professor Jennifer A Lewis at Harvard have developed 3D printing technologies specifically for micro and bioprinting. Using an organic ink as a sacrificial template, deposited via a syringe, they were able to produce channels between 10 and 300μm[74]. Using this technology, they were able to create square tower microfluidic mixers with smooth

channels as the channels themselves consisted of single layer extrusions stacked and connected by points of contact in the printed scaffold. The scaffold was than cast in resin before being melted out at 60°C to form microchannels. Using a similar syringe and ink-based technique, they were able to make single layer microfluidic devices with the same channel dimensions and rubber tubes inserted as attachment points. In addition to this work, several other novel 3D printing technologies were published by this group including a dual material PDMS extrusion nozzle[75] for direct printing of devices, and embedded 3D printing (e-3DP)[76]. E-3DP is a particularly interesting technique as it enables embedding of flexible, conductive materials to enhance the capability of 3D printed devices.

The outlook for 3D printed microfluidics is positive, with numerous research groups providing proof of concept using a variety of technologies. While it is clear from the review above that custom, specialist technology can rival or surpass current photolithography and soft lithography techniques in terms of versatility, the ability of off-the-shelf, general purpose 3D printers to produce microfluidic devices would accelerate the adoption of microfluidics as a research tool. Research presented in this work is intended to evaluate the capability of current, general purpose 3D printers to produce sub-200µm features using the W2P SolFlex350 as a model system. The relevance of this is based on the premise that 3D printers are likely to be purchased to produce general labware and research groups are more likely to use microfluidics if the 3D printers they use for general purpose are also capable of producing these devices.

1.4.9: *Factors Affecting the Resolution of DLP 3D Printing*

The spatial resolution of a DLP 3D printer is affected by the resin, the technological specifications and the maintenance of the printer. The X/Y resolution of a printer is principally controlled by the X/Y pixel size and spacing, however, the power of the light source, the depth of focus and the exposure time can also affect the resolution (*figure 1.13*). The exposure time is a parameter that can be controlled manually on open-source printers such as the W2P SolFlex 350 and requires optimisation for different resins. Over-exposure can result in light scattering, causing light to deviate from the intended location and trigger photopolymerisation outside the specified

voxel. This phenomenon can also occur as the light passes through the lower surface of the resin tank. It will be scattered by any optical abnormality including, dirt, damage or defects in the tank surface. In practice this typically means a loss of resolution and definition on fine features or debris from solidified resin floating in the tank. For this reason, it is paramount that the tank is clean and the resin is fresh, particularly if a part has failed. Under-exposure is likely to result in under-curing, leading to part delamination or poor build platform adhesion.

As previously discussed, the Z dimension is affected by the resin itself and the movement of the printer's Z axis. The depth of light penetration is affected by the opacity of the resin and exposure time. Over-exposure can lead to light bleeding, with light penetrating further into the resin than the specified layer height, causing inconsistency in layer height if there is a void in the previous layer. Opaque resins are less likely to suffer from light-bleeding, as the pigment can block excess light from passing too far into the resin tank.

Optimisation of water-soluble resin RORSD420 is part of the work presented in chapter 2. Parameters were altered based on these factors in an attempt to produce reliable results.

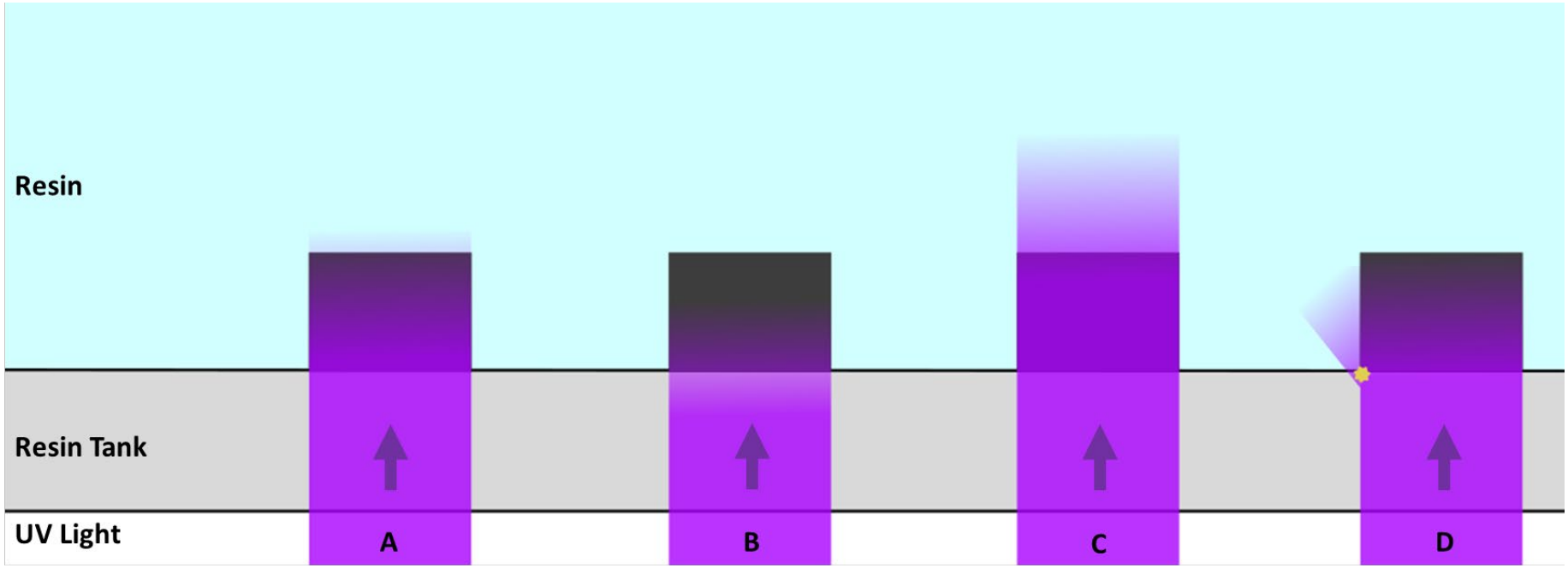

Figure 1.13 – Factors Affecting Voxel Formation in DLP Printing. (A) UV light penetrates to the specified voxel volume (grey box) and there is no light bleeding either in the X/Y or Z. (B) Under-exposure, light does not penetrate to the specified voxel depth, leading to under-curing. (C) Over-exposure with light penetrating deeper than the specified voxel height, leads to over curing and decreased resolution. (D) Light scattering due to contamination (can also happen as a result of over-exposure), leads curing outside the voxel area in the X/Y plane.

Chapter 2: 3D Printing Experiments

2.1: Abstract:

In this chapter, the capability of the W2P Solflex350 to produce 3D features in a water-soluble resin, and features of sub-100μm with manufacturer produced resin was tested. It was shown that the water-soluble resin did not produce reliable prints and could not therefore be used to produce microfluidic devices. Comparison of prints with sub-100μm features with their original 3D models revealed that additional considerations relating to part orientation need to be considered when printing at this small scale. The conclusions from this chapter are that the printer cannot reliably produce features in sub-100μm scale.

2.2: 3D Printing Experimental Aims:

2.2.1: *Outline*

The aim for this project was to evaluate the capabilities of the W2P SolFlex350, comparing them to current microfluidic devices similar to those mentioned earlier in this report. The eventual goal would be to fabricate a device with similar features those previously described, before designing an optimised system for 3D printing.

It is apparent from specifications that certain device features are not possible with an X/Y voxel size of 50μm^2, and a minimum Z layer height of 25μm. The channels with Z heights of 0.6μm in the chemostat by Groisman et al (*figure 1.3*) for example are an order of magnitude smaller than the minimum layer height provided by this printer, as is a channel width of 20μm. As these channels are core components of the function of this device, it is impossible to reproduce this device using only a current desktop 3D printer as a fabrication technique.

Given this fact, the focus of the research is on how well the system produces prints at the limits of its resolution, and how suitable this is for producing microfluidics. As previously stated, fabrication of fluidic channels has been successfully achieved using several different approaches illustrated in *Figure 1.8*. The first is direct printing of a fluidic device, where the channel walls and surrounding material is formed directly through 3D printing[64]. The second approach is 3D printing the channels themselves in a negative mould, or 'sacrificial template'[67]. Both methods have merit and limitations, which are affected by the capabilities of current desktop 3D printers. Disregarding anything but resin-based printers for this research due to the limitations previously discussed, there are several important factors to consider when choosing which approach to take.

2.2.2: *Sacrificial Template Fabrication*

A novel and enabling property of this type of design is that components can potentially be attached to the template, cast in the final device material and remain in place when the template is dissolved away. This could include light sources, heaters, pH sensors and more. Another advantage to this approach is that the material the final device is fabricated from is independent of the template material, provided the casting material is not soluble in the same solvent as the template. It means that the industry standard material PDMS, which is cheap and readily available, could be used in the same way it currently is and would not need to lend itself to 3D printing. This process is essentially the same as soft-lithography but with the advantage of complex, three-dimensional master moulds. With this in mind, a resin which is water soluble post-curing was sourced from Bucktown Polymers, called 'Rinse Out Resin SD420' (ROR SD420) (www.bucktownpolymers.com). This resin cures at wavelengths up to 420nm, meeting the specification for SLA printers and more importantly, the SolFlex350, which provides light at wavelength 385nm. Water solubility is ideal for this purpose, as the majority of cells grow in water-based culture medium. Any material which dissolves in water is unsuitable for long term culture of these cells, so it does not limit potential casting materials. It is also readily available in all biological laboratories and non-hazardous to the user or environment.

Microfluidic control using pneumatic and hydraulic pumps is cumbersome and specialist equipment. An important step to introducing microfluidic devices into biological laboratories would be to generate plug-and-play devices with a standard connection. While beyond the scope of this project, the ultimate aim for this research would be to develop micro-valves and standardised control plugs/software, which can be integrated into devices before casting. This would dramatically enhance the usability of microfluidics in a non-specialist setting.

The experimental aim of this part of the research was to evaluate the capability of the combination of Bucktown Polymers RORSD420 with the W2P SolFlex350 printer, in relation to the requirements for microfluidic fabrication.

2.2.3: *Negative Device Prints*

Truly 3D microfluidic device fabrication without the need for layer bonding would revolutionise device design and capability of microfluidics. While this is the eventual target for research into 3D printing and microfluidics, a positive first step would be to closely replicate the devices currently manufactured. 3D printing a single layer negative master mould such as that illustrated in *Figure 1.1* would provide rapid, in-house iteration of device, offering many advantages over the methods of generating photomasks described previously.

Alongside testing of soluble resin, this research utilises W2P NextDent Purple resin to establish the resolution and detail that could be created in a two-dimensional channel layout. Printing of a set of embossed channels with this resin with different sizes and properties provides essential information about the nature of channels which could feasibly be printed and later cast with PDMS.

2.2.4: *Positive Device Prints*

Positive prints mean that the device itself is 3D printed directly. There have been examples of this being successfully performed for simple geometries as previously mentioned. The primary advantage to this approach is that device manufacture would be possible in a single step, rather than the printing/casting/dissolving procedure required for a soluble sacrificial template, meaning fewer reagents and fewer possible errors in fabrication. A directly printed device would offer most of the potential benefits of sacrificial template casting, other than the ability to embed components easily within a device. Limitations of this method would be that small channels in a resin printer are prone to closing during printing.

As mentioned in chapter 1, the nature of resin that is cured by a light source, is that any contamination or degradation of the optical pathway of either the laser (SLA) or projector/LCD (DLP) will result in light scattering. This contamination can be dust, resin smears, finger grease or any other contaminant which interferes with light passage. This means that a feature is likely to be printed slightly larger than if the

pathway were clear. Over-curing can often result in light-bleeding around the focal area, leading to the effect of channels being inconsistent or closing up. This issue is present for sacrificial template fabrication, but positive features are less likely to suffer at high detail, as they will get larger rather than smaller like negative features.

As an example of the result of this phenomenon, the Formlabs design guide for a Form 2 suggests minimum positive embossed features of 0.1mm in each of x, y and z. The minimum engraved feature is four times this at 0.4mm. Similarly, the minimum 'wire' size (ie the minimum suggested channel size relevant to this research) is suggested at 0.3mm diameter up to 7mm tall. The minimum hole size is suggested at 0.5mm. (www.formlabs.com) The caveat to this is that small, thin channels such as the ones this research investigates are more likely to deform or break if printed as unsupported positive features, where a positive device print has significantly more structural integrity and is more likely to maintain its form throughout printing and post-processing.

A major limitation of a positive print is that the final device material must be modified to make it suitable for 3D printing. In this case, it must be a liquid photopolymer which is stable and biologically inert. It must print reliably at high resolution and generally it is preferred to be optically clear.

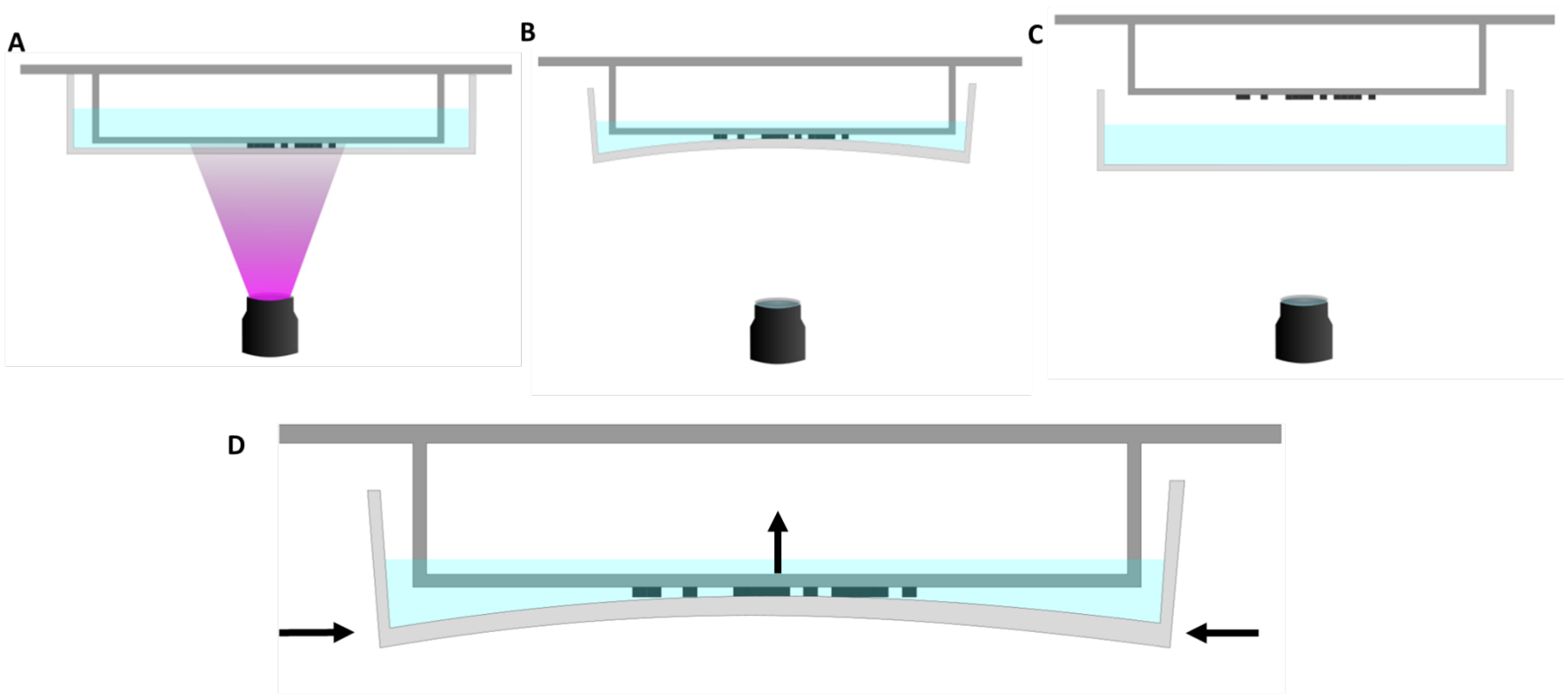

Figure 2.1 – Side view of W2P SolFlex350 peel process. (A) UV projector projects an entire layer at once through the resin tank floor and cures resin to the tank and build platform. (B) The printed layer is peeled from the resin tank surface. As the build platform raised out, the edges of the tank are pressed inward to push the tank floor up in a curve. (C) The build plate is raised out of the tank as it is released to restore the flat curing surface. (D) Close up of part B, showing the direction of forces. The parts at the edge are peeled off with the surface at an angle, while the parts in the centre remain touching the resin tank.

2.3: 3D Printing Experimental Procedures:

2.3.1: *3D Printing with the W2P SolFlex350*

The printer used for this research was a W2P SolFlex350 DLP resin printer from Austrian manufacturer Way2Production (www.way2production.at). Suitability for this research is provided by the fact that the print profiles are highly customisable for open source material. At 50µm X/Y pixel size and 25µm minimum layer height, it is representative of the capabilities of high-end desktop 3D printers. The printer uses UV LEDs to provide a light source at 385nm, with a projector system providing pixel control. The build platform is lowered from above and parts printed in inverted orientation from the lower surface of the resin tank (called the resin vat by W2P). The resin tanks are designed to flex as the build platform is raised after curing, reducing layer peel forces to retain part geometry (*Figure 2.1*). To aid in this process, the tanks are mechanically pushed inward towards the centre of the x axis as the platform is raised. This pushes the centre of the tank in the x axis to rise slowly in the Z axis with the build platform. As the edges of the tank in the x axis are fixed at the base of the Z axis, this means that the model is peeled from the edges inward as the build plate rises and the vat centre flexes upward in relation to the edges.

Material profiles enable close control of individual layer curing times, along with layer height and speed of peeling. Peel speed could more closely be modified by editing instructions in a .sfb file (SolFlexBuild) on a computer using Notepad. These instructions were modified to change the speed of peel and wait time between layers before lowering the print to start the next layer. Initially, all prints were performed on ‘Gentle’, which is the slowest peel. This was chosen due to the high detail of the prints and prioritisation of print success over print speed.

Post processing of printed parts included washing with Propan-2-ol (commonly known as Isopropyl alcohol – IPA) from Fisher Scientific (www.fishersci.co.uk) for 10 minutes to remove uncured resin and cleaned off with compressed air. If necessary, a second round of cleaning was performed in clean IPA. RORSD420 is susceptible to IPA and was instead washed with Petroleum Ether from the same manufacturer in the same manner. Post curing of parts was performed in a G171 Otoflash from NK Optik, providing ultraviolet light in pulses or flashes to post-cure parts.

2.3.2: *Preparing Models for Printing*

Models were created using AutoCAD from Autodesk Inc. Models were exported into .STL format and imported into NetFabb software, using the SolFlex350 profile as advised by the manufacturer W2P. Files were sliced into layer images and exported into a .zip file for transfer to printer.

2.3.3: *Evaluating 3D Channel Printing Capabilities*

Two test pieces were drawn in AutoCAD to evaluate the ability of the W2P SolFlex350 to print unsupported channel features. The first piece consisted of a rectangular base with 1mm depth. Cylinders were placed at 45 degrees to the build plate. Cylinders were 4mm in length and their diameter increased from 0.1mm to 1mm in 0.1mm increments (*Figure 2.2)*. This is to test the limits of channels printed in three-dimensional space, as opposed to channels printed in the X/Y plane only.

The second test model was a box shape with two cylinders spanning between opposing walls, with the cylinders at 90 degrees to one another (*Figure 2.6*). This was to test printing of three-dimensional channels in different orientations, along with testing the bridging ability of the channels between walls. The ability of the printer to print discreet, separate channels in close proximity to one another was also tested as the perpendicular channels crossed over one another in the centre of the box. The box was placed at different angles on the print bed to ascertain which orientation printed most reliably.

2.3.4: *Rinse Out Resin SD420 Optimisation*

With DLP printers, the power of the light source along with the time of exposure are fundamental to optimising layer curing. Over-curing could lead to light bleeding and reduced dimensional accuracy, under-curing leaves the resin too soft to retain its shape effectively during the peel process. This process must be optimised for every individual resin on an open source printer such as the W2P SolFlex350. To achieve this, test models above were printed using different layer exposure times until the results were acceptable. Resins from W2P were all used according to manufacturer specifications.

To characterise RORSD420, the aim was to reproduce or better the result of W2P Prototype Clear Resin. To do this, a material curing profile for this resin needed to be tested and optimised. The profile determines the set layer height (the steps in the Z-axis between each layer), along with curing times for each layer of the resin. As previously described, many printers perform compression of the first layer (and in the case of a Form 2, for another 5mm) to help with adhesion of the print to the build surface. The SolFlex350 instead over-cures the first layers, ensuring the resin is properly cured and attached to the build plate. This first layer and subsequent layers are individually controlled in the material profile and are specific to the material and layer height.

A generic calibration procedure was attempted with ROR SD420. This procedure involves curing of 11 disc shapes, each cured with for a different length of time. In place of a resin tank and build platform, 16ml of resin was poured into a 60mm diameter petri dish and curing takes place directly on the petri surface. The thickness in the Z axis of each disc was compared with that of manufacturer resin (W2P Prototype Clear), presented in the table below. For the resin to be successful in general printing, layer exposures should be approximately 1.1-1.5x the depth of the designated layer height to ensure proper adhesion to the previous layer when printing. This could potentially cause issues with printing of small voids, as the curing would penetrate into the void on the previous layer, however, it is a good starting point for general printing.

	W2P Prototype Clear (100 µm)	
Layer	Exposure time [ms]	Polymerisation Thickness [µm]
1	25000	800
2	15000	683
3	10000	588
4	5000	425
5	3000	305
6	1700	172

Difficulties were encountered with the standard calibration test, so a test piece with rods at 45° from the build platform was printed, with settings adjusted according to the outcome until an acceptable print quality was achieved.

2.3.5: *Solubility Experiments*

Printed test pieces were placed in distilled water to determine the nature of solubility. Experiments were run at room temperature and 60°C to assess the optimal dissolving process for the resin.

2.3.6: *Resin Vat Modifications*

Following advice from the manufacturer, a 0.1mm thick film of fluorinated ethylene propylene (FEP) was cut to size and placed in the base of the vat at the curing surface. This was sealed at the edges using Polycraft Mould Making Silicone (www.mbfg.com) to prevent resin from permeating between the vat and FEP film (FEP 100 from www.fepshop.com). No adhesion was necessary in the optically important areas of the vat, as the film was applied to a layer of IPA and pressed firmly to the surface before allowing the IPA to evaporate.

2.3.7: Resin Dye

RORSD420 is shipped with a small volume of resin dye. 100µl of this dye was added to 100ml of resin to produce a 0.1% solution.

2.3.8: *Optical Examination of Printed Parts*

3D Printed parts were observed using a 10x magnification optical microscope. Photographs were taken using a Xiaomi Mi 5S mobile phone camera.

2.4: 3D Printing Results:

2.4.1: *Initial Evaluation of the W2P SolFlex350.*

A test part was drawn up to represent certain basic requirements for 3D fluidic channel printing. It consisted of ten cylindrical extrusions, at 45 degrees from the build platform, anchored to a rectangular base. Cylinders were chosen to represent the ideal shape of channels to prevent corners where biofilms can form, flow can be disrupted, and material may not be easily dissolved. The ideal fabrication technique would be able to produce cylindrical channels at any angle from the build platform however due to the layering effect of 3D printing, shallow angles do not print reliably, and surface quality is degraded at these angles due to 'stepping' appearance from Z-layer height. Support material is not an option if channels are to be fabricated using a sacrificial template, as they would be larger than the print they are supporting and impossible to remove without causing failures of the sacrificial template. 45 degrees was chosen as a reasonable angle at which channels should be printable on this printer, while enabling some complexity in design geometry. 90 degree cylinders would be most likely to form correctly, however, shallower angles would be required to create any kind of branches from a vertical channel. 45 degrees was chosen, as it would enable printing of channel networks in 3D space. Printing of vertical channels has already been shown in the literature referred to in chapter 1 and can be achieved by printing a channel in the X/Y plane and manually placing at 90 degrees after printing, before casting.

W2P Prototype Clear resin was used as a comparison for RORSD420. The test piece was printed at a layer height of 25μm as this is the smallest layer height available with the printer, and the closest to what will be required for fabricating microfluidic channels. Three identical models were printed in the same print. Of the cylinder shapes attempted, 0.7mm and 0.8mm diameters printed successfully on all three models based on optical observation and comparison of print with intended model. Below 0.6mm diameter failed to complete on any of the sample parts (*Figure 2.2)*. The implication of this result is that true three-dimensional microfluidics at the scales

currently desired is not feasible on this printer, as this resin has been optimised by the manufacturer, for this printer.

Automated fluidic control of cell culture would be hugely advantageous, even if the capability of traditional microfluidics cannot be replicated exactly. Culture volumes in 0.6-0.8mm channels may provide benefits over traditional culture methods, while providing a gateway to future microfluidic design. For example, a 0.8mm diameter cylindrical channel measuring 100mm in length would provide ample length for complex geometry. This shape would have a volume of approximately $50mm^3$ – or 0.05ml. This volume compares favourably to a 1.5ml or even a 0.5ml microcentrifuge tube, meeting the target of reducing waste while providing a platform for automation and customisation of experiments.

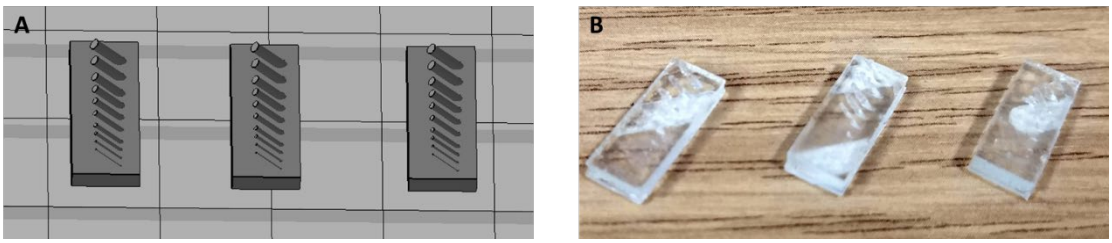

Figure 2.2 – Printing with W2P Prototype Clear (A) Three identical CAD models prepared to print using NetFabb software. Cylinders of 4mm length and sizes increasing from 0.1mm to 1mm diameter in 0.1mm increments (bottom to top) were placed at 45° from the build plate. (B) Actual prints using W2P Prototype Clear resin at 25µm layer height with 'Gentle' profile.

2.4.2: *Characterising RORSD420*

The idea of the generic calibration is to determine optimal curing time for a given layer height, by curing different discs for different lengths of time directly to the curing surface, in this case a petri dish, and measuring the height of each disc. The ideal curing time would result in around 1.5x the thickness of the intended layer. As shown in *Figure 1*.13, longer curing times result in thicker layers. The results of the test were inconclusive with RORSD420. All of the discs were sticky and could not be removed to measure their depth. The over-adherence of this resin to the build platform was a common observation throughout testing, meaning removal of parts intact was difficult.

Failure of the planned calibration meant that optimisation of the resin curing times had to be based on the characteristics of printed test pieces. Initial layers were cured for 15000ms to ensure adhesion. The layer curing times were tapered down to an eventual time of 1500ms for the rest of the print, individual layer curing times are shown in *Figure 2.3*. 50µm layer height was chosen for initial tests because it was presumed to be more reliable than 25µm. Optimisation of the resin profile for both 50µm and 25µm was the eventual goal. The model in *Figure 2.3* is the same as that in *Figure 2.2*, rotated at 90° around the Z axis and printed only once.

Initial prints shown in *Figure 2.3* were unsuccessful, with several layers adhered to the build platform, and the rest of the model adhered to the vat surface. This means that delamination occurred during printing, suggesting several things. Firstly, the initial layers were adhered to the build platform, so the problem did not occur due to initial layer cure times being too short. Second, it suggested that the resin, when cured at 1500ms for 50µm layer height, did not have the structural integrity to retain its shape during the peel process, delaminating and adhering to the vat surface instead.

Final layer cure times (ie the exposure time for every layer after initial over-curing section) were increased to 1750ms without improvement and it was observed that initial layers were solid and difficult to remove from the build platform. Initial curing times were reduced to ascertain whether over-curing initial layers was negatively affecting adhesion of layers later in the print. Reduction to 10000ms instead of 15000ms for initial layers resulted in more of the part detaching from the build platform, this was consistent for several prints, leading to the conclusion that initial layer curing required more than 10000ms for 50µm layer height to ensure proper adhesion to the build platform. Since reduction of initial curing time appeared to exacerbate the detachment problem, it was reasonable to assume the opposite change may help. Increasing initial cure times to 25000ms did not appear to solve the issue so a different modification to the process was necessary.

Given that the original test with W2P Prototype Clear was successful, the orientation and models were replicated for the next stage of this optimisation process. The addition of two further models offered more information about the nature of any print failures, with the added advantage of testing printing in different areas of the peel action. This peel action was assumed to be consistent before beginning experimentation, however, as shown in *Figure 2.4*, the location of the printed model

with respect to the peel action (in the x axis) had a large role to play in the outcome of the print. In this test, the two off-centre models printed successfully, while the piece in the centre showed similar characteristics to earlier test (where model was printed only in the centre). The peel process on this printer is symmetrical along the x axis, as described in the experimental procedures section (illustrated in *Figure 2.1*) of this report.

For the remainder of the process, models were placed off-centre in the x-axis, this led to dramatically improved performance and enabled further optimisation. The final layer cure time was adjusted several times, making it shorter and longer over the course of numerous prints. A final layer cure time of 3000ms, used in *Figure 2.4* appeared to consistently produce results comparable to expectations of the resin printing appropriately, provided this was coupled with off-centre location of the model on the build platform.

The remaining issue which had not been a priority until this point, was the inability to remove parts from the build platform without damaging or destroying them. Such was the adherence of initial layers to the build platform, levering or chiselling at parts always resulted in cracking and snapping the bulk of the part, leaving a solid remains on the build platform. The inability to remove intact parts from the platform meant that they could not be washed and post-cured, as the printer's build platform would not fit in the post-curing machine.

On the basis that the base of the part was not strong enough to withstand levering, thickening this from 2mm to 4mm was the first modification to address the issue of removal. The result was unchanged, with the part sticking so strongly to the build platform that it was destroyed during removal. Instead of further file modification, another setting in the printer was altered. The distance between the build platform and the resin vat surface can be modified for the first layer. With the initial layer curing time set to 15000ms, the offset was increased by +0.2mm. The offset value is in addition to the predetermined layer height, which was 50µm. This was ineffective, with removal of parts still difficult, so the value was increased in 0.1mm increments, with results gradually improving until an offset of +0.7mm was settled on as an acceptable value. If the offset were too large, the part would not adhere to the platform, leaving debris in the resin vat instead as was seen in earlier tests. Fine tuning of the initial layer curing time down to 12500ms at +0.7mm offset still resulted in strong adhesion

to build platform, though it was possible to remove most of the test piece intact for washing and post-curing (*Figure 2.5*). This offset would mean that the initial layers were not exactly true to the model, which is not unusual but should be considered when designing sensitive geometries for printing.

Several methods were attempted to alter the nature of contact with the build platform and make removal easier. These included placing the part on a hatching and a series of cylinders. The aim of this development was to create a standard platform on which to place parts with easy removal and reliable platform adhesion. Of the patterns tested, none produced the desired outcome. As lack of bed adhesion no longer seemed an issue with all the developments previously outlined, reducing the contact with the build platform considerably relative to the overall size of the model seemed a logical change of approach.

The test piece was altered to reduce platform adhesion and to test an additional, crucial capability required for complex microfluidics – the ability to produce multiple channels at different angles, in close proximity to one another. This test piece was also designed to act as a container for PDMS during moulding. *Figure 2.6* shows the cube piece with the two 500µm diameter, perpendicular rods, overlapping in the centre 0.3mm apart and attached to the box walls at either end. As the rods printed in this test piece were unsupported and perpendicular to one-another, the theoretical optimal angle would place them both at 45° from the build platform. This would mean neither rod would print at a shallower, unsupported angle relative the build platform and therefore minimising and equalising the peel force across both rods. To verify this theory and optimise orientation for this part, initial prints were performed at this angle, followed by additional prints with the cube test piece at different angles on the build platform (*Figure 2.7).*

The results in *Figures 2.6 and 2.7* show that despite optimising print profiles for printing the first test file, results do not translate to other geometries. Rods and walls consistently deformed during printing. Rather than the expected orientation of 45° for both rods in both the x and y planes (*Figure 2.6*) being the most successful, the results in *Figure 2.7* show that orientating so that one rod is parallel to the build platform and one is at 45° in the y plane but not the x plane produced results closest to the prepared model (*Figure 2.7 D*). The fact that the other rod printed successfully at 45° in one plane agrees with expectations. The results are unexpected mostly because printing

horizontal to the build platform should exert significant peel forces on this rod, resulting in more deformation than the rods printed at 45° in both x and y planes, which did not seem to be the case.

A likely explanation for this result is that, rather than an unsupported overhang, the rod printed as a bridge between the two walls of the cube. Bridging exerts different forces on a given layer than unsupported overhang, as it is fixed at both ends and so is less likely to fail. It is likely that if the rod were angled slightly, so that the first layers of the rod were not connected at both ends, that this print would have produced the worst results in relation to the prepared model, rather than the best. Bridging alone does not explain the result, as in prints C, D and E, both rods were bridges, where only one of the two was bridging in F. It is possible that a combination of bridging and self-supporting rod fabrication is more successful than an excess of either. Regardless, complex devices would require a variety of angles to be printable, this test emphasises the importance of orientation on any given model but does not provide a universally applicable guide to what orientation is most successful.

Even in the orientation producing the best results of those tested, this level of inconsistency would not be acceptable in a microfluidic device requiring precise geometries and location of channels to control flow. The difference between the model and printed part is not repeatable, with the models identically prepared but producing poor, non-identical results. The implication of this finding is that initial optimisation was successful only for the one test part and that further optimisation would be needed if RORSD420 were to provide a viable method of microfluidic fabrication. Results to this point did not show much potential for this resin to print these kinds of geometries reliably.

Assuming that the printer and resin are capable of printing parts like this, two possible causes presented. Firstly, that the resin was not curing optimally on each layer and therefore failing to maintain its structure during the peel process. Second was that resin curing produces heat and this resin in particular seemed to produce a great deal of heat during post-curing. It is possible that this increase in temperature was causing expansion of the semi-cured resin and the elongation of the rods was forcing them to warp, as they were fixed at either end.

To address the first issue, additional cure times were trialled, starting from 3000ms and increasing to 3250ms, up to 3500ms and 3750ms. All models were orientated in

the position which produced the best results previously, with four identical models in each print. Results in *Figure 2.8* tended towards increased deformation of the internal rods as layer cure duration was increased. This result implied that not only did increasing cure times not produce better results but was detrimental to the quality of the printing of this particular model. A normal symptom of over-curing would be loss of resolution due to light bleeding. This was not the result presented here, as the definition of the part appeared unchanged through additional curing time. This therefore pointed toward the other hypothesised cause of model deformation during printing – increased temperature. As layer curing was producing heat, and increased layer duration was increasing both curing and deformation, it was logical that this temperature may be the cause.

To address the temperature concern, a new test model was created. The current test model has features enclosed in a small space, surrounded closely by walls. As this is a DLP printer, all of this would be curing simultaneously, creating localised temperature increases. A similar model was designed but with longer rods and wider aperture, so curing and temperature changes were not clustered in a small space and negatively affecting overall print quality. *Figure 2.9* shows that deformation is not improved with a less dense part, rods were observed to be disconnected in the centre and the parts are severely warped at the edges. Given the warping at the edges is was possible that the rods were damaged because their anchor point was unstable, *Figure 2.10* shows a part with thicker walls to negate the deformation of the anchor points. This print resulted in catastrophic damage to the resin vat. Though there was no partially cured resin on the vat surface, meaning the parts had not delaminated during the peel action, the resin vat itself was severely damaged and it was fortunate that it remained sealed, preventing uncured resin from spilling onto the window.

At this point, the printer manufacturer (W2P) was contacted for advice before performing any further testing. Bucktown Polymers were also contacted but were not able to offer advice on curing times with specific machines. It was noted that RORSD420 is far less viscous than the majority of resins provided by the manufacturer. Less viscous resins, according to W2P support, bond more strongly to the resin vat during peeling, as they can be stickier in their printed form. This was consistent with observations of prints with RORSD420. To overcome this issue, W2P were in the process of developing a new vat type for their range of printers. In testing, they were using a film of 0.1mm thick FEP film covering the surface of their vat to

reduce adhesion. Further prints used a replicated version of this vat system, as it served both to reduce peel force and form an additional protective layer over the resin vat. *Figure 2.11* shows the modified vat. The results were not noticeably improved with this setup, longer curing times up to 4000ms per layer were attempted (*Figure 2.11* C) but this also did not provide acceptable performance for the specified goal of printing microfluidic channels.

To address the concern of heat build-up, W2P provided a printer peel profile with additional wait time in between layers. The additional wait time would enable the part to cool before curing the next layer, with the goal of preventing this heat from causing distortions in the part. This did not seem to improve results during testing, and it was deemed unlikely to lead to positive results with this resin.

The final modification to the system in order to yield acceptable results was to add resin dye to the resin. The resin dye was provided with the RORSD420, with its purpose to reduce light bleeding and increase absorption of light. The goal is to produce increased reliability of parts and reduce unwanted curing. If resin was cross-linking outside the designated light applied by the printer, it could lead to partially cured (and therefore highly sticky) resin extending from the boundaries of the model, causing increased adhesion with the resin vat and resulting in the symptoms previously shown. *Figure 2.12* shows the result of the first print with added dye. At 3500ms final cure time, no resin was adhered to the build platform, instead all curing occurred on the FEP vat surface. At 4500ms cure time, the parts were present, but the internal rods show no sign of improvement over previous tests.

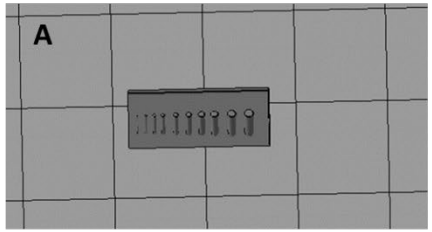

B Layer	Cure time (ms)
1	15000
2	15000
3	15000
4	10000
5	7500
6	5000
7	3000
8+	1500

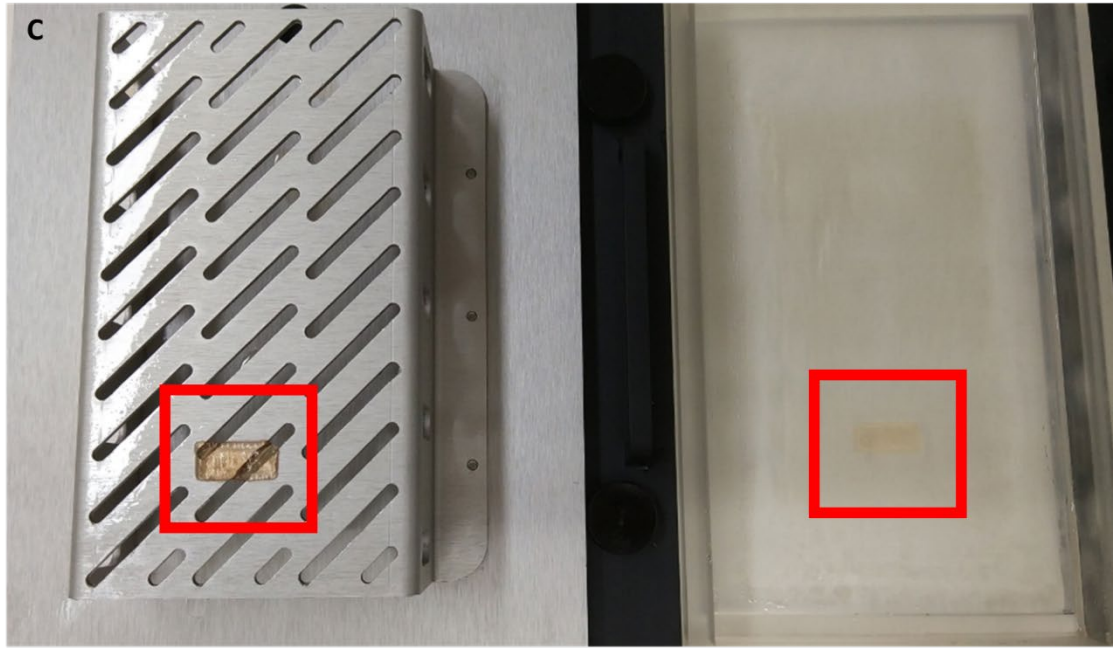

Figure 2.3 – Initial Printing with Rinse Out Resin (A) Initial Printing with CAD model prepared to print using NetFabb software. Cylinders of 4mm length and sizes increasing from 0.1mm to 1mm diameter in 0.1mm increments (left to right) placed at 45° from the build plate. (B) Layer cure times in ms. (C) Result of print, showing some of model cured on build platform (left) and some in resin vat (right)

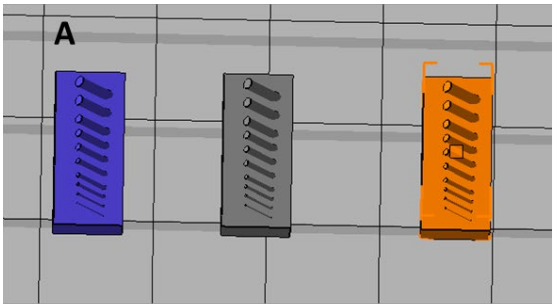

B Layer	Cure time (ms)
1	25000
2	15000
3	10000
4	5000
5+	3000

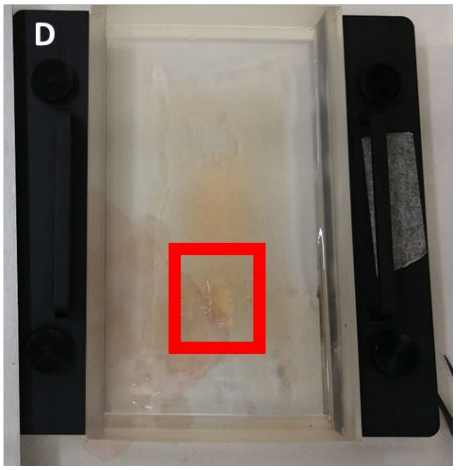

Figure 2.4 – Optimising Rinse Out Resin (A) CAD model prepared to print using NetFabb software. Cylinders of 4mm length and sizes increasing from 0.1mm to 1mm diameter in 0.1mm increments (bottom to top) placed at 45° from the build plate. (B) Layer cure times in ms. (C, D) Result of print, showing two models cured on build plate (left) and centrally located model in resin vat (right) (E) Parts were adhered so strongly to platform that they could not be removed for washing without severe damage.

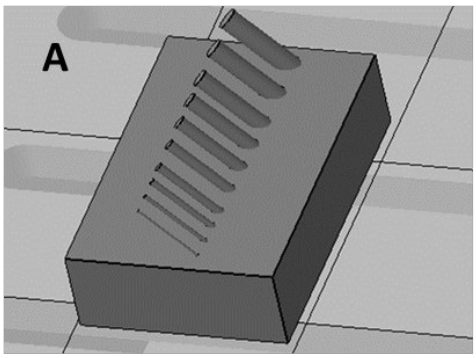

B Layer	Cure time (ms)
1	12500
2	12500
3	10000
4	5000
5+	3000

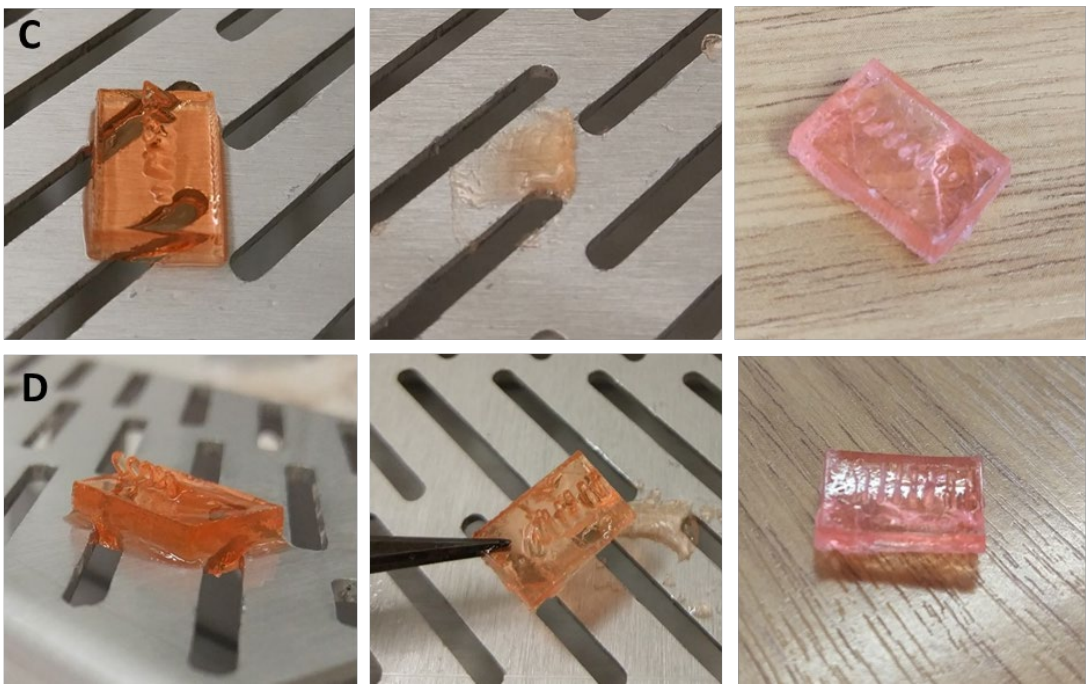

Figure 2.5 – Optimising Model for Rinse Out Resin (A) Revised CAD model, prepared to print using NetFabb software. Cylinders of 4mm length and sizes increasing from 0.1mm to 1mm diameter in 0.1mm increments (bottom to top) placed at 45° from the build plate, 4mm thick base. (B) Layer cure times in ms. (C) Printed model on build platform before removal (left) Chunks of model remaining on build platform post removal (centre) Damaged part, post removal, washing and post-curing (right). (D) Second model before and after removal from build platform

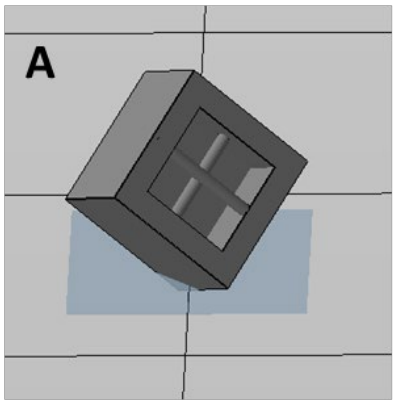

B Layer	Cure time (ms)
1	12500
2	12500
3	10000
4	5000
5+	3000

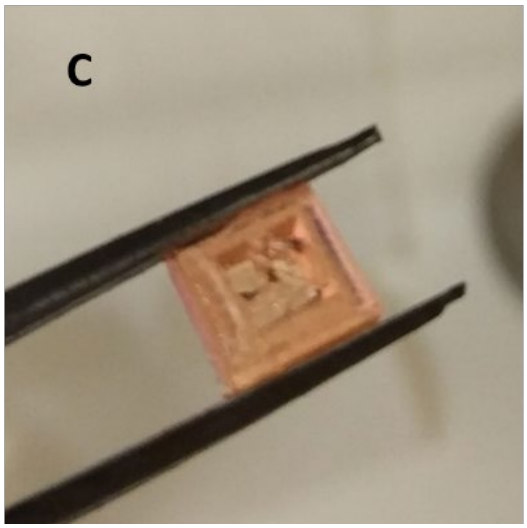

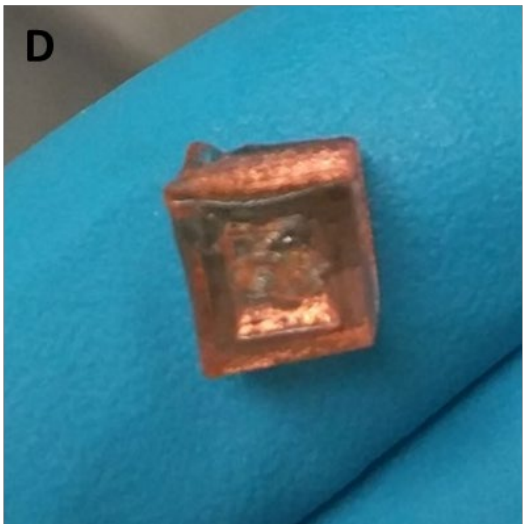

Figure 2.6 – Initial Cube Model Prints (A) Revised Cube CAD model, prepared to print using NetFabb software. Two perpendicular rods of 4mm length, 50mμm diameter, spanning the walls of a hollow 6mmx6mmx4mm cuboid. Rods pass over one another in the centre of 4mmx4mmx4mm void, 0.3mm apart in the Z axis. (B) Layer cure times in ms. (C, D) Printed model in two separate print attempts. Faces are not straight and rods have not printed correctly.

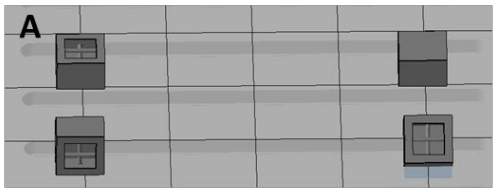

B Layer	Cure time (ms)
1	12500
2	12500
3	10000
4	5000
5+	3000

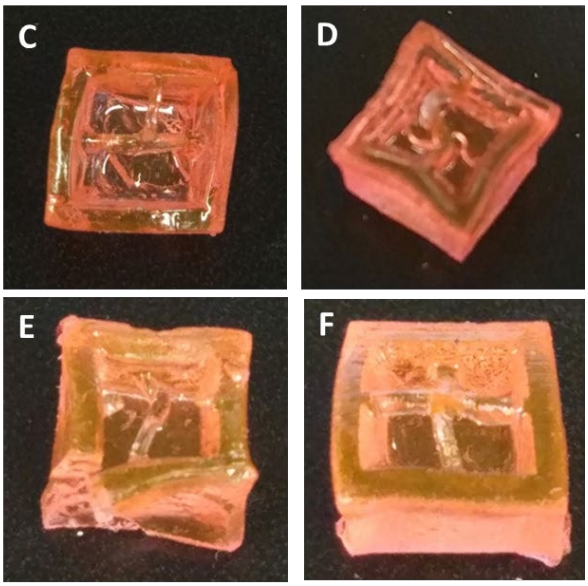

Figure 2.7 – Optimising Cube Orientation (A) Revised Cube CAD model, prepared to print using NetFabb software. Two perpendicular rods of 4mm length, 50mμm diameter, spanning the walls of a hollow 6mmx6mmx4mm cuboid. Rods pass over one another in the centre of 4mmx4mmx4mm void, 0.3mm apart in the Z axis. Four identical models were printed in different orientations on the build platform (B) Layer cure times in ms. (C, D, E, F) Printed models corresponding to their positions in part A. Print F appears to produce results closest to the model.

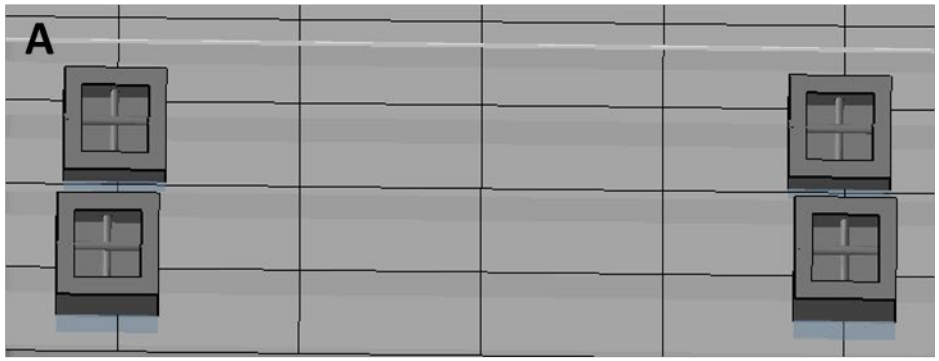

B Layer	Cure time (ms)
1	12500
2	12500
3	10000
4	5000
5+	Variable*

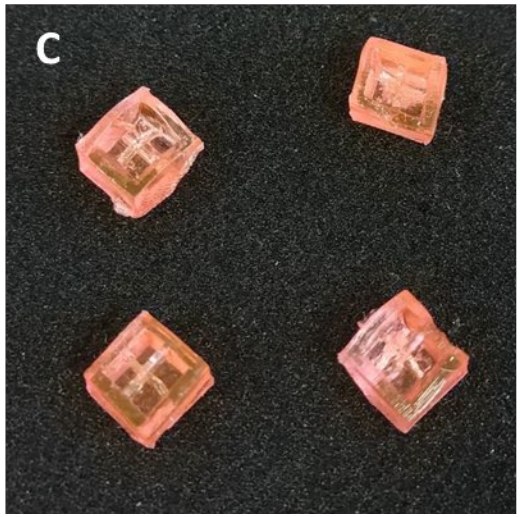

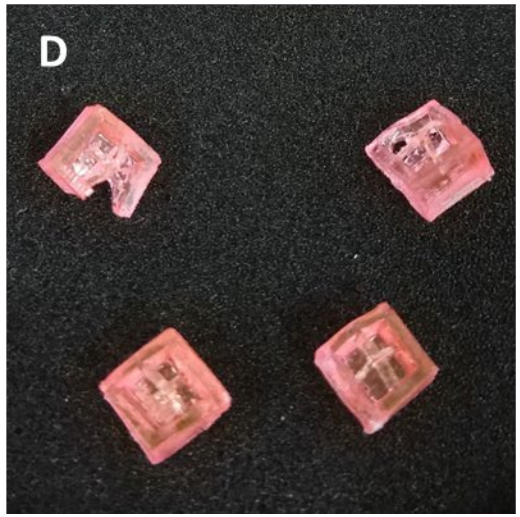

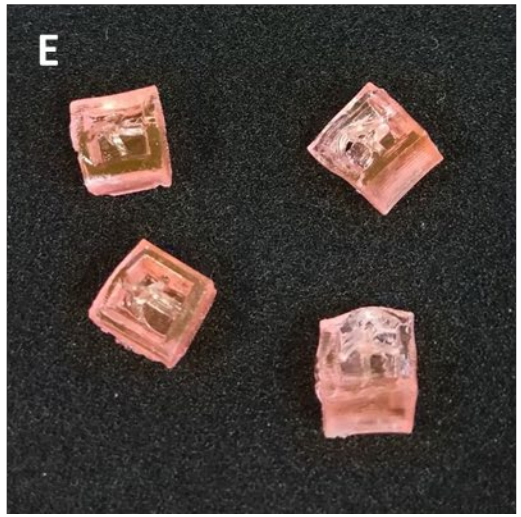

Figure 2.8 – Optimising Layer Cure Times (A) Revised Cube CAD model, prepared to print using NetFabb software. Two perpendicular rods of 4mm length, 50mμm diameter, spanning the walls of a hollow 6mmx6mmx4mm cuboid. Rods pass over one another in the centre of 4mmx4mmx4mm void, 0.3mm apart in the Z axis. Four identical models were positioned on the build platform (B) Layer cure times in ms. (C) Models printed with a final layer curing time of 3250ms after removal and post-curing. (D) Models printed with a final layer curing time of 3500ms after removal and post-curing. (E) Models printed with a final layer curing time of 3750ms after removal and post-curing.

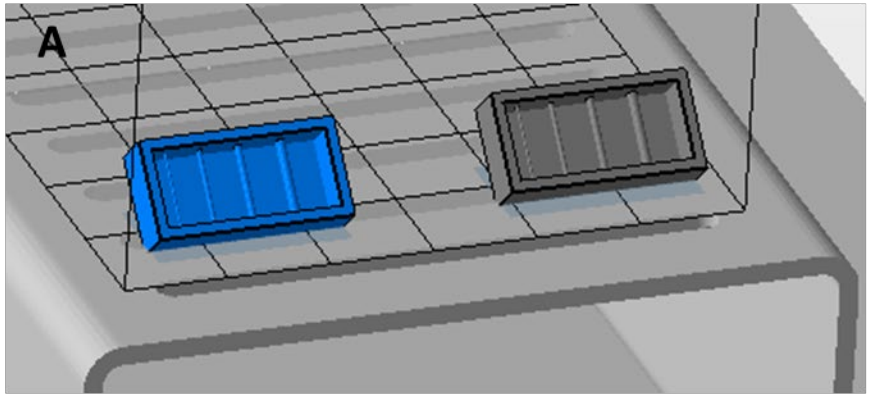

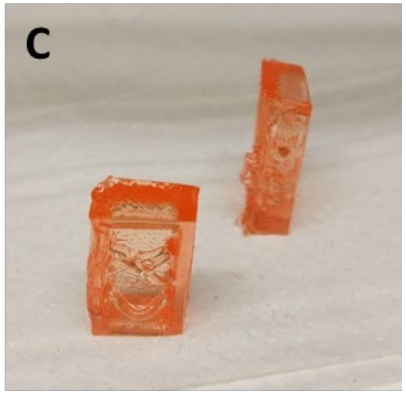

B Layer	Cure time (ms)
1	12500
2	12500
3	10000
4	5000
5+	3750

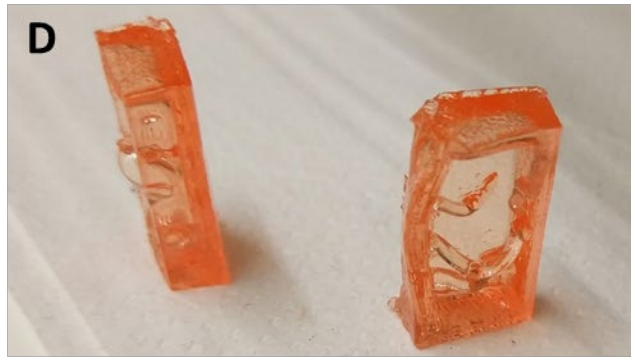

Figure 2.9 – Reduced Density Model (A) Model orientated at 45° from the build platform in the y axis. Model contains four rods of 250μm, 500μm, 750μm and 1mm diameter (left-right). Two identical models were positioned on the build platform (B) Layer cure times in ms. (C, D) Printed models, post removal and washing showing failure of rods and deformation of edges.

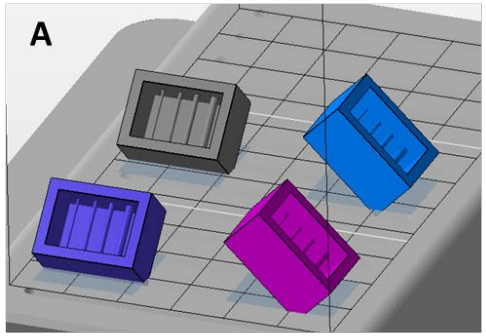

B Layer	Cure time (ms)
1	12500
2	12500
3	10000
4	5000
5+	3750

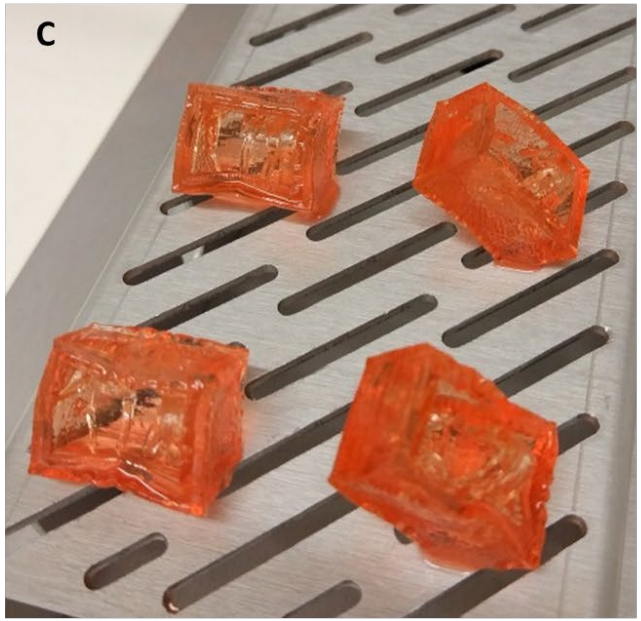

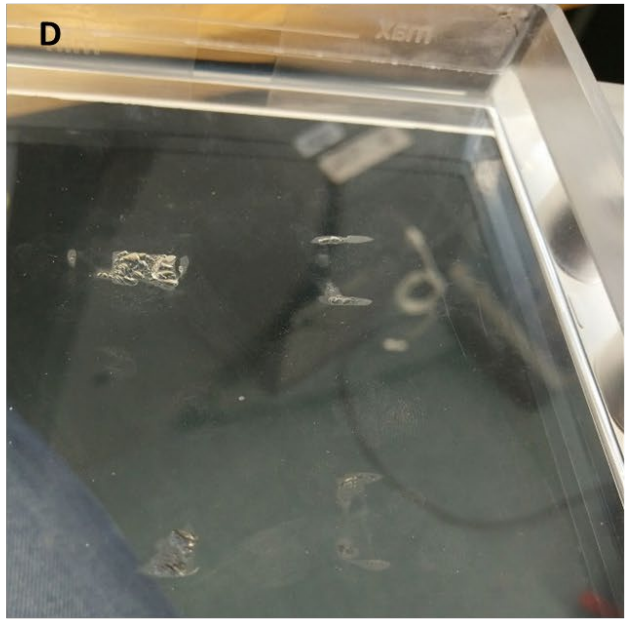

Figure 2.10 – Resin Vat Damage (A) Model orientated at 45° from the build platform in the y axis. Model contains four rods of 250µm, 500µm, 750µm and 1mm diameter (left-right). Two identical models were positioned on the build platform (B) Layer cure times in ms. (C) Printed models, showing failure of rods and deformation of edges. (D) Resin vat after removal of resin and cleaning with IPA showing severe scarring caused during printing.

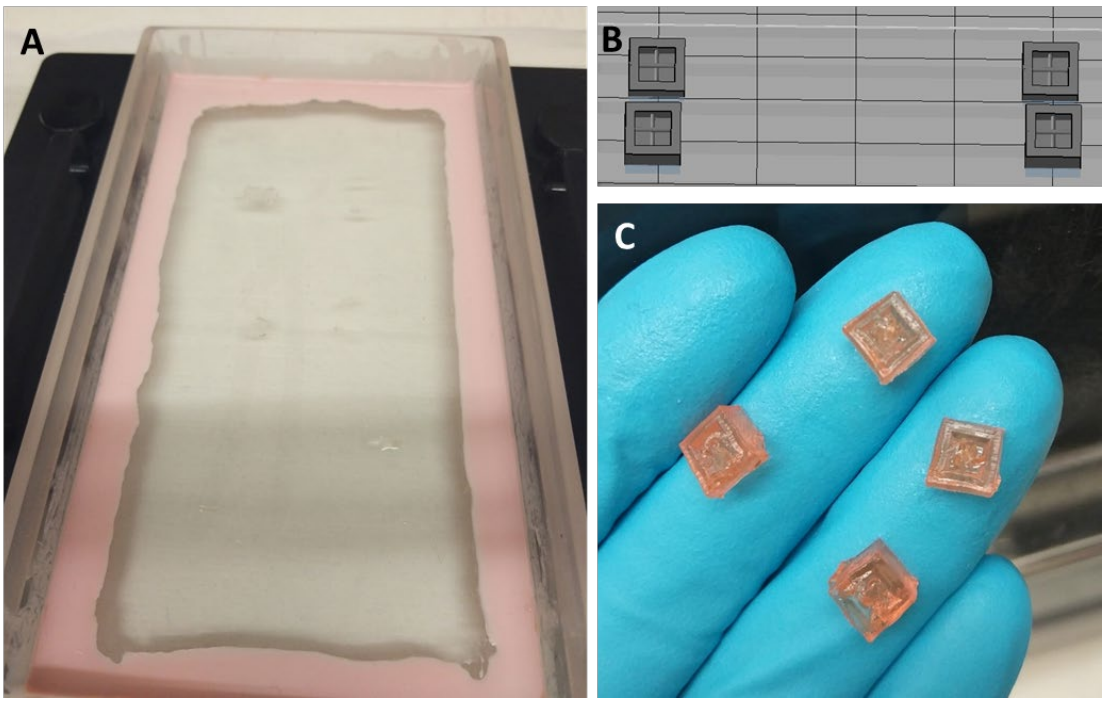

Figure 2.11 – Resin Vat Modification (A) Resin vat modification – a 0.1mm thick FEP film applied to the entire resin vat lower surface, sealed with soft dental silicone to enable movement during peel action. (B) Test file from previous figures, sliced in NetFabb software. (C) Prints with final layer cure time of 4000ms, showing consistent deformation of internal details.

A Layer	Cure time (ms)
1	12500
2	12500
3	10000
4	5000
5+	4500

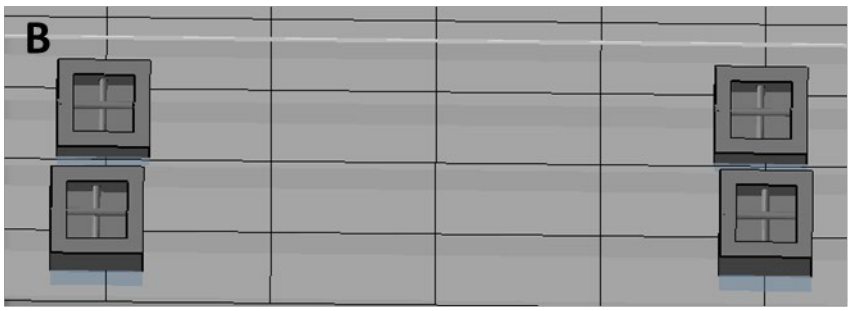

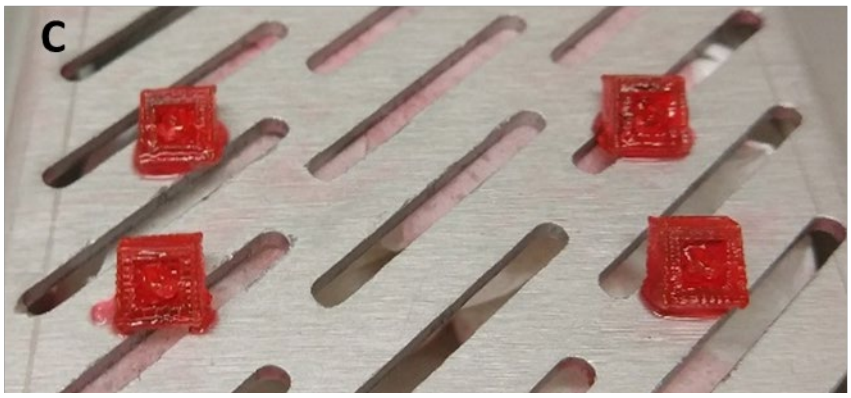

Figure 2.12 – Resin Dye Test (A) Layer cure times in ms. (B) Test file from previous figures, sliced in NetFabb software. (C) Prints with 0.1%v/v resin dye added to RORSD420. As with previous attempts, showing consistent deformation of internal details.

2.4.3: *Solubility of RORSD420*

This resin was purchased because of the advertised property of water solubility. The manufacturer claims that this resin ‘dissolves rapidly in hot water’, providing a set of photographs suggesting 1 hour in 60°C water is enough to dissolve printed parts, though there is no specification for size or geometric effect on this. The purpose of this resin, according to the manufacturer, is to ‘replace the burn out cycle’ in investment casting by simply dissolving out with water instead. This fits with this application of casting PDMS around a soluble sacrificial template.

Using printed parts from previous tests, the solubility of printed parts in water was tested in both room temperature (RT) water and 60°C water. Results in *Figure 2.13* show that box prints from previous figures were not dissolved after one hour, even after over seven days at this temperature the parts were not dissolved. Water did influence the properties of the prints, with those submerged in water swelling, losing their colour pigment and becoming soft and spongy. This change would not be sufficient to dissolve scaffold from a complex network of channels after casting and performs poorly compared with the stated properties of the resin.

Figure 2.13 – Solubility Tests (A) RORSD420 prints submerged at room temperature for 0 hours, 1 hour, 24 hours and 1 week in 25ml measuring flasks. Water was replenished with fresh once every 24 hours. Parts show swelling an loss of colour pigment but remained structurally intact after a week of submersion. (B) RORSD420 prints submerged at 60°C for 0 hours, 1 hour, 24 hours and 1 week in sample jars. Water was replaced every 24 hours and samples stored in incubator for heating. Parts show swelling an loss of colour pigment but remained structurally intact after a week of submersion, similar to those in cold water.

2.4.4: *Concluding Testing with RORSD420*

The unfortunate conclusion from the results in *Figures 2.2 - 2.12* is that RORSD420 does not produce results adequate for printing details and geometries which would be required for 3D printed microfluidic sacrificial templates. The results are unreliable in both similarity to the CAD model and to other prints of identical setup. Progression onto evaluating the dimensions and surface finish of these models would not have provided useful information given the poor printing results and so was not performed in this research.

Results in *Figure 2.13* demonstrate that even if printing was of an acceptable quality, solubility will not be adequate to remove the template from the PDMS device after casting. The combination of these results leads to the conclusion that RORSD420 does not have the properties to fulfil the target of 3D printed microfluidic sacrificial scaffold printing. It does not print adequately, and it does not dissolve in water when it is printed. Unfortunately, at this point it was deemed unproductive to continue research into the combination of RORSD420 and the SolFlex350 DLP printer.

2.4.5: *Printing Templates for 2D Channel Layouts*

The potential for complex, 3D layout of microfluidics in space facilitated by soluble scaffold material has been demonstrated as unachievable with the materials and equipment tested. While this would enable advances in the capability and design of microfluidic devices, the ability to replicate current device layouts with low-cost, user-friendly desktop 3D printers would still be a step towards mass adoption of automated microfluidics in biological laboratories. For this reason, examination of the capability of the printer to produce a mould to cast a two-dimensional network of channels was performed using W2P NextDent Purple. This resin was chosen as it is a manufacturer optimised resin, which the manufacturer suggests using for the finest detailed prints.

To test the limits of resolution on the printer, a test model was generated with a cuboidal base and embossed lines of varying width and height from this base. The lines represent the required geometry for printing basic fluidic channels. *Figure 2.14* shows a diagram of this model, which tests several aspects of the printer. The first

aspect tested is the minimum line width that the printer will print. This is tested through the inclusion of clusters of lines of increasing width, from 50µm (cluster 1), which is the minimum theoretical width of exposure due to the 50µm pixel size, up to 100µm (cluster 2), 150µm (cluster 3) and 200µm (cluster 4) (*Figure 2.14 B*). The sets of lines that came out in the print can demonstrate how small in the X/Y plane positive features can be printed on the printer. The second aspect of this test piece was a set of staircase-like increases in Z height, starting with 25µm – the smallest layer height the printer is capable of – and stepping up to 50µm, 100µm and 200µm in groups of four (*Figure 2.14 C*). These steps demonstrate any difference between stated layer height and the minimum printable feature height. The final aspect of this test piece was to repeat these staircases three times for each line width, increasing the gaps between the lines in each set, to see how close together positive features can be printed before they merge into one. The gaps for the first staircase were 50µm, then 100µm and finally 150µm. The first cluster of 50µm width also contained an additional staircase with 200µm gap. The result of a completely successful print therefore would have a cluster of 16 lines of 50µm width and three clusters of 12 lines, corresponding to 100µm, 150µm and 200µm clusters.

As can be seen in *Figure 2.15*, lines of 50µm and 100µm in the CAD model did not come out in the printed parts. This was a surprising result, given that the pixels of 50µm should be perfectly capable of producing features of 100µm in width, even if they cannot actually produce the stated 50µm. Clusters with widths of 150µm and 200µm printed staircases as expected. *Figure 2.15 B* shows a print at 50µm layer height, each staircase consists of 3/4 steps, with the first 25µm step not present. This is expected, as a print with layer height 50µm cannot print a feature that is small than 50µm. This is verified by the print in *Figure 2.15 C*, which was printed at 25µm layer height and includes all steps for clusters 3 and 4, including the 25µm steps that were not present in the previous print.

These results show that the printer is not capable of printing positive features equivalent to pixel sizes in the X/Y plane. Features in the Z plane behaved as expected, with steps only present if they were equal to or larger than the specified layer height. Prints were placed under a 10x optical microscope and lit from beneath to try to ascertain what was causing the lack of detail in the X/Y plane. The image in *Figure 2.15 D* shows a grid pattern at 45° to the direction of the printed lines. This means that it is at 45° to the edges of the build platform and resin vat. The result is

that lines printed parallel to the edges of the vat cannot be printed as smooth, straight lines. Lines of only a single pixel width are printed resembling a chain of beads, where the beads correspond to pixels. Wider lines which require illumination of more than one pixel are smooth and solid in the centre and resemble saw-teeth on the outer edges. Given the fact that a line of 50µm width would be exactly one pixel wide, the 45° angle of the pixel grid to the part will likely affect the number of pixels actually illuminated, which could potentially have led to the absence of small features.

Figure 2.15 (E-G) shows the same part orientated at 45° from the edge of the resin vat and build platform, in an attempt to align the pixel grid of the printer with the features of the model. At first glance, it appears that the results are worse in this orientation, with the only complete cluster being cluster 4, at 200µm width. Under closer inspection with a 10x optical microscope, (*Figure 2.16 F-G*) the results are mixed. Some lines are indeed perfectly formed, with no sawtooth edges as seen in the previous orientation, other lines show intermittent illumination of the adjacent pixels which result in wavy edges and staircase 2 in cluster 3 did not form at all. What was consistent between the two alignments was the absence of clusters 1 or 2.

To investigate this, the print file was examined. When slicing parts for the printer, NetFabb software uses a profile specifically for the W2P SolFlex350, though NetFabb is a highly versatile software used for slicing or examining models for printing with any printer for which a profile can be made. The profile contains the dimensions of the build area, enabling the placement of models within the area and slicing them into individual layer images for the printer to convert into illuminated pixels. The actual file transferred to the SolFlex350 is simply a .zip folder containing .png image files. Because DLP printers project an entire layer at once, there is no complex pathing as there would be for SLA or FFF printers, instead there is simply an image for each layer consisting of a white footprint of the layer of a model, for illumination, surrounded by black, for no illumination. The key layer to generating the line features on this model in a 25µm layer height print is layer 200. This layer is the first layer after the base is completed and should illuminate lines of widths corresponding to clusters 1-4. The image file for layer 200 of prints from both 90° and 45° orientated models are shown in *Figure 2.16 B and H* respectively, this angle assumes the x axis as 0°.

The printer translates the images and layer height specification into pixels which need to be illuminated on each layer and the layer height in the z-axis between each layer.

As previously discussed, when attempting to optimise RORSD420 resin, the individual layer cure times are set in a resin profile, which is stored on the printer itself and selected when setting a print up on the printer interface. The final layer curing time for this resin was calculated based on the manufacturer specification at 980ms for 25μm layer height. This means that while NetFabb is responsible for instructing the image to be illuminated, the printer firmware is responsible for converting the images into actual pixel illumination.

Results in *Figures 2.15 and 2.16* show disparity between the expected printer output given the specifications and the models sliced for printing. Correct printing of this file would illuminate a single line of pixels for cluster 1, two lines of pixels for cluster 2, three lines of pixels for cluster 3 and four lines of pixels for cluster 4. Assuming the specified 50μm pixel size is accurate, this would result in 50μm wide lines, 100μm wide lines, 150μm wide lines and 200μm wide lines, matching exactly the number of pixel columns illuminated. This is not the case in the results presented here, which imply that it is not possible to reliably print lines of 200μm or below in any orientation by simply importing and slicing a given model in NetFabb with the correct printer profile. Lines of 100μm or smaller do not form at all. The results show several stages at which errors are introduced to prevent correct model formation in the final part.

The flow of data starting with the model and ending up as an actual print was traced back to ascertain the causes of inaccuracies in the final printed part. A summary of the pathway would be: Model generation in AutoCAD > Model export to .STL file > Model import into NetFabb > Print file generation with NetFabb > Print file translation by printer > Illumination of pixels and curing of resin. Issues somewhere in this process were responsible for the differences between the intended and actual prints. The most obvious issue with the printed parts is the complete absence of clusters 1 or 2 in either print orientation, this can be seen by eye in *Figures 2.15 and 2.16* Images of layer 200 on each print show that this issue was not down to the printer, but due to a failure of NetFabb to incorporate the finer features of the model into the sliced layer. The images in the print file include only clusters 3 and 4. Another difference between the model and print file can be seen in cluster 4, (*Figure 2.16 B*) where the lines have pointed or rounded tips. This is not consistent with the model, which can be seen in *Figure 2.14 B* to not have rounded tips. Interestingly, this top did not appear in all of the printed features (*Figure 2.16 D*), which is a sign that there is some level of mis-matching between the sliced file and the array of pixels actually illuminated by the

printer based on this file. A similar discrepancy in the shape of the lines is present in the layer 200 image for the part printed at 45° to the x axis of the printer build area. *Figure 2.16 H* shows an image which should match that of the other print, with solid lines for each cluster. Instead, the lines are inconsistent, wavy and poorly defined. This waviness resembles that of lines formed by square pixels which are arranged at 45 ° to the line direction. This pattern of line construction clearly indicates a grid of virtual pixels used by the NetFabb software, which is aligned to the x and y axes of the build area.

Figures 2.15 and 2.16 show the actual alignment of pixels in the printer to be at 45° to the x and y axes of the build area – i.e. at 45° to the virtual array generated by the NetFabb software as described above. This is demonstrated when printed lines are orientated parallel to the x and y axes of the build area in NetFabb. The pixel grid can be clearly seen at 45° to the printed lines in *Figure 2.16 C and D*. This is again demonstrated when these models are rotated so that the printed lines are at 45° to the x axis of the build area. In this case, the printer pixels are aligned in the x and y with the printed lines on the model (*Figure 2.16 E and F*), though the shape and width of the lines is inconsistent. The misalignment of these two grids means that NetFabb is incapable of aligning features directly with pixels on the printer, explaining some of the inconsistencies in the printed parts. It also explains why the models orientated at 45° from the virtual grid in NetFabb (*Figure 2.16 H*) are not smooth solid lines and show inconsistent widths as the software tries to align its virtual array with features in the model orientated at 45° to this grid.

After accounting for the discrepancy between the model and print file, there are still issues with the part in relation to the layer images it is processing. Cluster 4 in the 90° print (*Figure 2.16 D*) seems to print fairly consistently. All the lines have sawtooth edges but they are consistent in width of approximately 3 diagonal pixels. Cluster 3 appears less consistent, varying from 1-2 diagonal line of pixels, with the first line barely forming. The diagonal nature of the lines in relation to the pixels is evident on all printed lines for this part. In contrast, the part printed in line with the pixel grid (*Figure 16 E-G*) showed a high degree of variability between lines which on the model were the same width. The 200µm wide lines in cluster 4 should theoretically all be exactly 4 pixels wide. As can be seen in staircase 3 of this cluster, lines vary from a consistent 2 or 3 pixels wide, to lines which have one smooth edge and one edge with intermittent pixel activation along the length. Staircase 1 in this cluster is the closest

to a correct print, with smooth edges on all lines, though the lines are only 2 pixels in width, rather than the predicted 4. Cluster 3 in part *Figure 16 E* shows a high degree of variability, with the first two steps of staircase 1 printing identical positive features to the equivalent in cluster 4, even though they should have been 50µm/1 pixel column smaller. Staircase 2 in this cluster was not present, despite it being so in the print file. Staircase 3 appeared to miss steps 1 and 3 from the print, with steps 2 and 4 bot showing severe waviness and inconsistent pixel activation on one edge. Looking at the image in the print file itself, stairs 1 and 3 of staircase 3 in this cluster are clearly thinner. This would explain why the printer processed steps 1 and 3 differently to steps 2 and 4.

In general, pixels are not translating from the model to the printed part – 150µm features are printing 1-2 pixels wide. This should be 50µm pixels and 3 pixels wide. 200µm features are printing 2-3 pixels wide where they should consistently be 4. The results and analysis above outline two key areas where this mis-translation is occurring, firstly small features are not being processed into the print images by NetFabb. Features that are translated are based on a virtual array of pixels parallel to the x and y axes of the build area, where the software appears to interpret the actual model features and illuminate the nearest approximate combination of pixels. This interpretation means that features placed at different angles cannot be exactly assigned pixels in this array, which can be seen when the lines in this part are angled at 45° from the arrangement of the virtual array. Instead, the software exports the nearest combination of pixels to the actual model, and, depending on the exact location of the features on the model in relation to the individual pixels in the virtual array, they are translated differently – resulting in the errors seen in *Figure 2.16*.

Due to the fact that NetFabb appears to translate and approximate features into a virtual array at 45° to the actual pixel grid on the printer, errors in translation are doubled, meaning the final print is twice removed from the original model. The model in *Figure 2.15 E*, orientated at 45° to the x and y axes of the build area is an example of this twofold error. The virtual array NetFabb translates these lines into is at 45° to the line features in the model. As demonstrated by the image of the layer given to the printer in *Figure 2.16 H*, these lines have been approximated from straight and consistent in the model, to inconsistent widths and wavy edges. This is the result of the difference in angle between the columns of virtual pixels and the direction of the actual model line features, coupled with the locations of these features in relation to

the pixels. The actual printed file shown in *Figure 2.16 E-G* shows the result of the printer interpreting the array from NetFabb and re-approximating a shape representative of the image it is provided back into the original direction of the 45° features. Some of these have straight edges such as staircase 1 in cluster 3, but others appear to be lost completely or significantly deformed in the final printed part.

This means that even if a part is designed with features which exactly correspond to pixels on the printer's projector, they will never be 100% correct in the final part due to the conflicting array orientations. At this point, it is evident that the printer's software is a major limitation in producing features close to the limit of the printer's capability. Without a more reliable method of printing small details it is not possible to tell whether the size of the pixels is 50µm as specified or larger, as it would appear to be from these results. The interaction of NetFabb and the printer's interpretation of the sliced file is distorting the image before it is printed. The conclusion is that the W2P SolFlex350 cannot provide a reliable fabrication technique for microfluidic moulds with features smaller than 200µm in its current format. This does not mean that 3D printers are not capable of achieving this, but it would be desirable for a printer and software to be developed in unison with the sole objective of achieving the necessary resolution for this application.

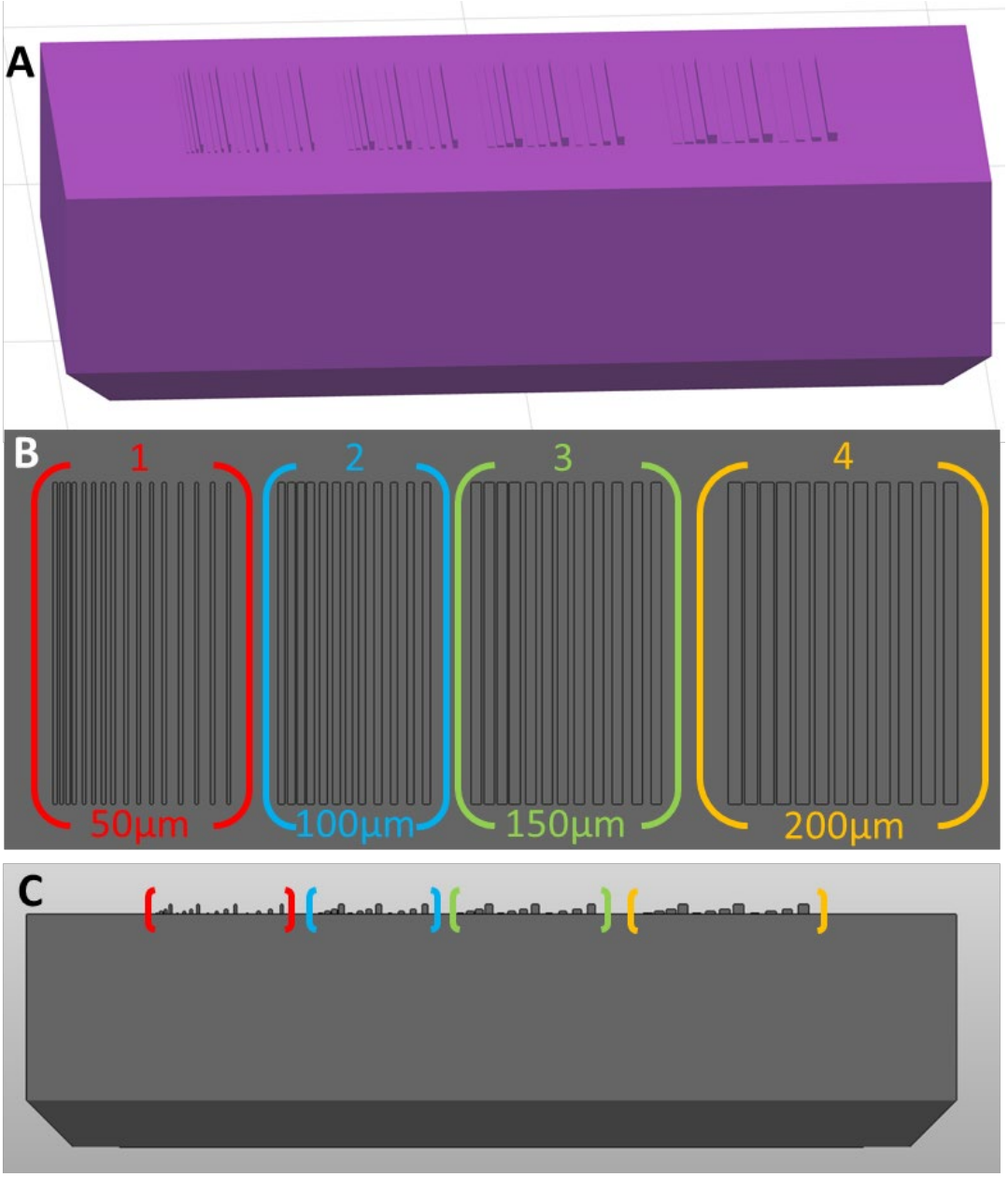

Figure 2.14 – Model to test resolution of channels in x/y and z. Four clusters were drawn with different line widths. Cluster one (left) contained lines of 50µm width, as this is the listed pixel size of the printer. Cluster two was 100µm, cluster three was 150µm and cluster four 200µm. Each group contains staircases of four lines of 25µm, 50µm, 100µm and 200µm in Z height to test the resolution of the printer in the Z axis. Staircases were repeated four times for the first group and three times for all other groups. Repeats were the same line dimensions however the spacing between the lines increased from 50µm spacing in staircase 1 of 4, to 100µm (staircase 2), 150µm (staircase 3) and one additional 200µm staircase in cluster 1. This was to test whether lines in close proximity merged into one another or remained separate. (A) Rendered image of part. (B) Top-down view of lines. (C) Side-view of part showing staircase.

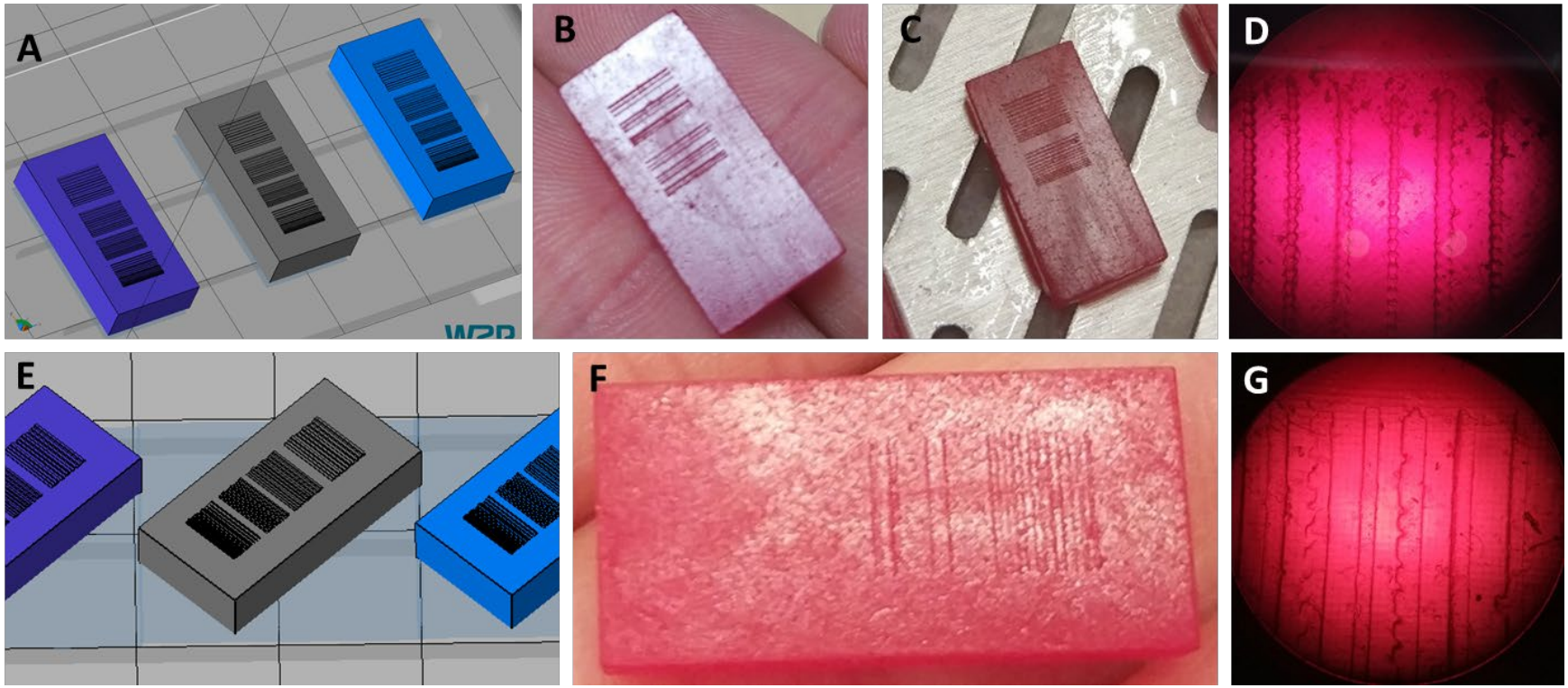

Figure 2.15 – Staircase Resolution Prints (A) Models prepared in NetFabb software. Orientated at 90° from platform edge. Grid lines correspond to x and y axes on build platform. (B) Print at 50µm layer height, showing features in 150µm and 200µm clusters, missing the 25µm step in each staircase. (C) The same print at 25µm layer height, showing features in 150µm and 200µm clusters (3&4) with all stairs present, including 25µm first step in each staircase. (D) Features third staircase (ascending) from cluster 3 (150µm width) in print C, viewed using a 10x optical microscope showing pixel grid. (E) Re-orientated models from print C to print at 45° from the platform edge. (F) Printed part at 45° orientation, staircases in cluster 4 were the only complete set. (G) 10x magnification image of final staircase in cluster 4 (right hand lines in F).

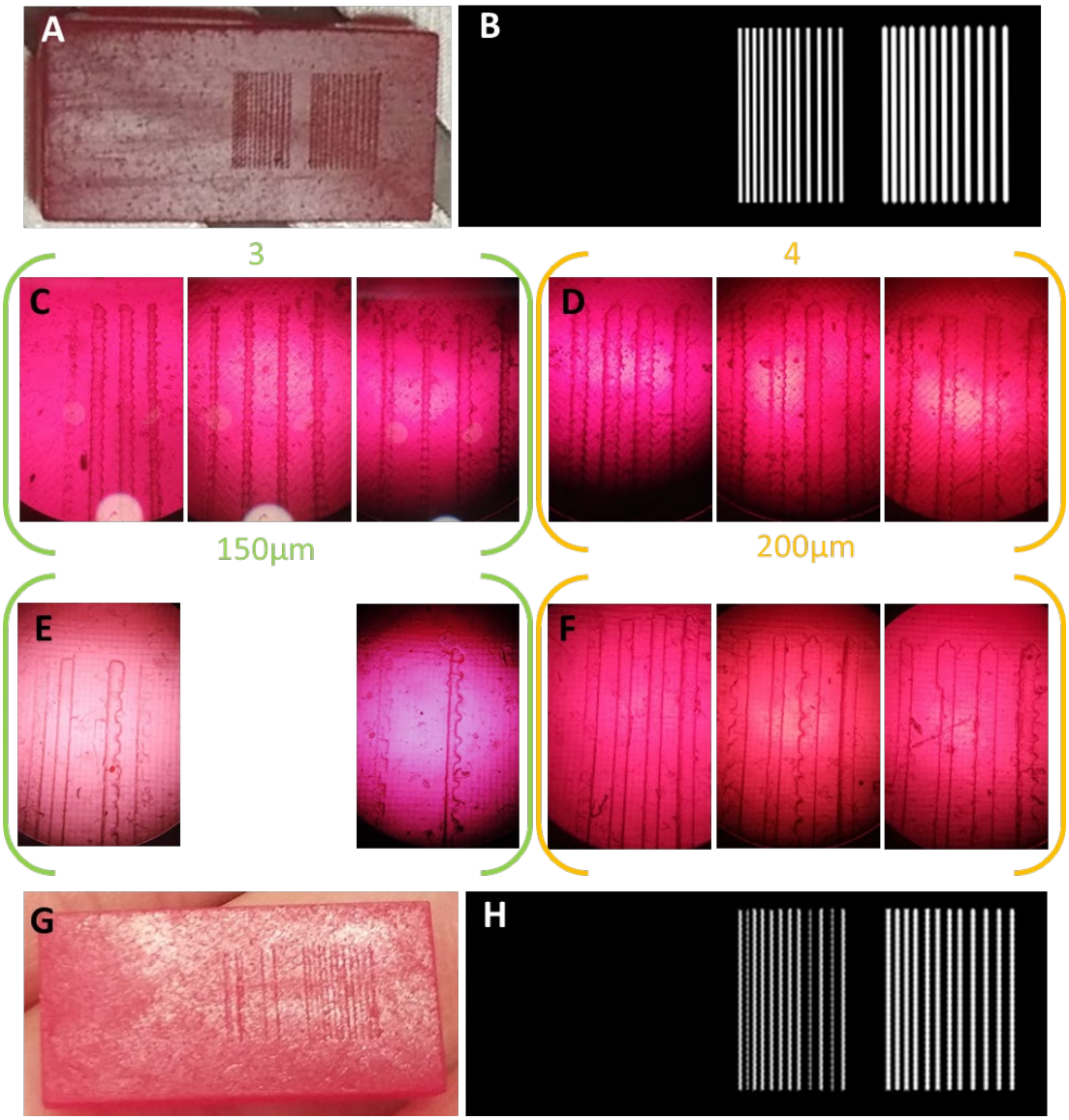

Figure 2.16 – Staircase Resolution Prints Under 10X Optical Microscope (A) Printed part from figure R14 C, orientated at 90° from platform edge. Layer image lacks clusters 1 and 2 but contains 3 and 4 (B) Image of layer 200 (the first layer of lines) from the print file sent to the printer for print job in A. (C) Cluster 3 (150µm model line width), showing sawtooth pattern and inconsistent print width of printed lines on part A. (D) Cluster 4 (200µm model line width), showing sawtooth pattern and inconsistent print width of printed lines on part A (E) Cluster 3 (150µm model line width), showing the two sets of positive staircases (spacing 50µm/staircase 1 and 150µm/staircase 3) on printed part G. Lines are either straight or show inconsistent edges. (F) Cluster 4 (200µm model line width) displaying some straight lines and some with wavy edges. (G) Printed part from figure R14 F, orientated at 45° from the platform edge, lines parallel to pixel grid. (H) Image of layer 200 (the first layer of lines) from the print file sent to the printer for print job in G, rotated to match layout.

Chapter 3: Streptomyces and Raman Spectroscopy

3.1: Abstract

Research in this chapter aimed to test the ability to detect C-F bonds with in aqueous solution Raman spectroscopy at different concentrations, in order to evaluate this as a potential target and detection method in a directed evolution device. It was shown that C-F bonds have a strong signal in dilutions down to 2mM using the setup described. Concentrations lower than this require signal post-processing to improve signal to noise ratio. *Streptomyces* species MA37 and cattleya were characterised for their suitability as targets in a directed evolution device and unsuccessful attempts were made to produce a knockout of the fluorinase enzyme in MA37. It was shown that these bacteria do not lend themselves to growth in a free-flowing reactor design.

3.2: Experimental Aims

3.2.1: *Streptomyces MA37*

In conjunction with the evaluation of 3D printed microfluidics to create a microchemostat fabrication platform, a candidate was chosen as a potential application for the technology. The ability to incorporate components into a device before PDMS casting would enable the incorporation of an optical window. The target is to use this window to take Raman spectra of single cells within the population in the device, on the assumption that a 3D printed device were able to produce a small enough reaction volume to make selection based on these spectra effective in influencing the evolution of the culture as a whole. Sorting cells based on their spectral properties is not a new idea in itself, nor is applying Raman spectroscopy to microfluidics. The novel development in this research is the partnership of 3D printed device fabrication to enable creation of a microchemostat, with the ability to monitor cells *in vivo* and either discard or retain them in the general population based on their Raman spectrum. This would create the potential to create a selection pressure based not on antibiotic resistance or cellular modification, but by any property which could

be observed and characterised by Raman spectroscopy and without the need for cellular engineering. This would be a powerful directed evolution device.

As mentioned previously, discovery and optimisation of novel, pharmaceutically, pesticidally or herbicidally active compounds is a perpetual challenge for industry. High throughput screening of small molecules followed by lead compound optimisation is now a fundamental paradigm for drug discovery, and it is the process of optimisation to which this project contributes. A directed evolution device would be a fitting partner to this paradigm, enabling rapid and controlled analysis and development of lead compounds and synthetic biology.

The fluorinase enzymes discovered in Streptomyces *cattleya* and then a further three bacteria performs a potentially high value and industrially relevant process incorporating fluoride ions, meaning it would be a good target application for this technology. There are two primary issues with the wild-type enzyme which prohibit industrial use. The enzymes currently described in the literature act exclusively on S-Adenosylmethionine (SAM) as a substrate and are substrate dependent, limiting their application. They are extremely inefficient compared with industrial enzymes such as penicillin G acylase (PGA) (K_{cat}/K_M of 0.05mM^{-1} S^{-1} for MA37 fluorinase vs 16.1mM^{-1} S^{-1} for wild type *Alcaligenes faecalis* PGA)[77]. The fact that even this PGA enzyme has been modified to improve efficiency 800-fold to suit pharmaceutical production is an indication as to how far from industrial application wild-type fluorinases are. A combination of Raman-based microfluidic selection and genetic engineering approaches could modify the enzyme to act on other substrates and increase its efficiency to meet the requirements of industrial fluorination.

3.2.2: *Streptomyces MA37 Characterisation*

If Streptomyces cattleya and the more recently discovered Streptomyces MA37, which has a more efficient enzyme[43] are to be candidates for this device, their growth pattern and characteristics must be suitable for continuous liquid culture. By growing the bacteria using general laboratory culture methods, this research aims to evaluate the suitability of the bacteria themselves for growth in a microfluidic chemostat similar to those previously described. Streptomyces are of general interest as an effective chassis for producing an array of secondary metabolites for use in the pharmaceutical

industry[78], making their manipulation and maintenance important for synthetic biology. Given that MA37 has a more efficient enzyme, it was chosen as the primary avenue of research over S.*cattleya.*

3.2.3: *Deletion of FlA1 Fluorinase Gene in Streptomyces MA37*

Further to assessing the growth patterns of these bacteria in a laboratory, it would be beneficial to produce a fluorination negative strain of Streptomyces MA37, which could be used as a direct negative comparison in Raman testing. Using the system described in[79], the aim was to make a Streptomyces MA37 with a deletion of the FlA fluorinase gene as a negative control for testing with the functional enzyme. This would be particularly useful for comparison with Raman spectroscopy.

3.2.4: *Raman Spectroscopy*

Another key element making the fluorinase suitable for this type of device is that the C-F (Carbon-Fluorine) bond also produces a strong Raman peak. Research by Menaa et al.[80] viewed several organofluorines with a patented fluorocarbon targeted Raman spectroscopy, Carbon-Fluorine Spectroscopy (CFS) or Fluoro-Raman Spectroscopy (FRS), which uses a 510.6nm wavelength pulsed laser. These compounds included 3-fluoroaniline (3-FA), fluoxetine hydrochloride, perfluorodecalin, 5-fluorouracil (5-FU) and 3-fluorophenylalanine. The measurements published indicate that characteristic Raman peaks associated with carbon-fluorine bonds shift within the region of 500-800cm^{-1} depending on the context of the bond. With this setup, 3-fluoroaniline produces a C-F peak at 752cm^{-1}, fluoxetine hydrochloride at 782cm^{-1}, perfluorodecalin at 692cm^{-1}, 5-fluorouracil (5-FU) at 770cm^{-1} and 3-fluorophenylalanine at 758cm^{-1}. A target of this research is to evaluate the possibility of being able to detect the fluorinated compounds in Streptomyces species, at the concentration they current appear in cells using Raman spectroscopy. 5-FU and its unfluorinated counterpart Uracil are readily available organic fluorine compounds. They offer a suitable chemical for testing of C-F bond detection in this

setting due to the direct comparison between identical molecules with and without a C-F bond present.

3.3: Streptomyces Experimental Procedures:

3.3.1: *Culture of Streptomyces*

Streptomyces was cultured in replicated Difco ISP1 (International Streptomyces Project) or ISP2 media formulations. Culture protocols follow those first described in[81].

3.3.2: *Culture of E.coli*

E.*coli* were cultured in LB media at 37°C. Culture on solid media used LB media plus 5% agar. Standard procedures for handling E.*coli* were followed.

3.3.3: *DNA Extraction from Streptomyces*

Extraction of DNA from Streptomyces species used the following modified TRIzol protocol from Invitrogen (www.thermofisher.com). ~50mg cells were suspended in DNA extraction buffer (50mM Tris-HCl, 20mM EDTA, pH8) and vortexed for 20 seconds. The mixture was centrifuged at 16000g for 4 minutes (Room temperature), supernatant discarded, and cells resuspended in 1ml ice cold acetone. This mixture was centrifuged at 16000g for 4 minutes (Room temperature), before discarding acetone supernatant and allowing residual acetone evaporation at 42°C. Cells were resuspended in 500µl DNA extraction buffer with 1mg/ml lyzosyme and incubated at 37°C for 1-2 hours. 75µl SDS (10%) and 125µl 5M NaCl were added to reaction and mixed by inversion before incubating at -70°C for 3 minutes (dry ice or ethanol bath). Reaction was transferred to 65°C for 3 minutes (water bath or heat block). This freeze/thaw step was repeated a further three times before incubation on ice for 10 minutes. Cells were centrifuged at 16000g for 5 minutes, before transferring the supernatant to a new tube. An equal volume of TRIzol was added to the reaction and incubated at 15-30°C (RT) for 5 minutes. 200µl of chloroform was added for every 1ml TRIzol and vortexed for 15 seconds before 15 minute incubation at room temperature. Mixture was centrifuged at 16000g (4°C) for 15 minutes and upper

aqueous phase containing RNA fraction discarded. 300µl ethanol per 1ml TRIzol was added to remaining phases and vortexed, before incubation for 2-3 minutes at room temperature. The mixture was centrifuged at 16000g for 5 minutes at room temperature and protein supernatant discarded. The pellet was twice washed with 0.1M Sodium Citrate, equal volume to TRIzol before incubation at room temperature for 10-20 minutes with periodic mixing. The pellet was centrifuged at 16000g for 5 minutes at room temperature and supernatant discarded. 75% ethanol was used to wash the pellet for 10 minutes before supernatant discarded and remaining solvent left to evaporate at room temperature. Final resuspension of DNA was in ddH_2O and storage at -20°C or -80°C for long term storage.

3.3.4*: Antibiotic Selection of Bacterial Cells*

Antibiotics were added from stock solutions to working concentrations: Ampicillin 50ng/µl, Chloramphenicol 34ng/µl, Kanamycin 25ng/µl, Gentamycin 20ng/µl.

3.3.5: *Engineering of Streptomyces*

PCR primers were designed to generate DNA insert containing homologous sequences to DNA flanking the FlA1 gene, without the gene present. The insert contained EcoRI restriction enzyme sequences at either end for cloning into plasmid vector. Plasmid pSEVA612S (Gentamycin resistant) was used as a donor plasmid, with pSEVA628S the ISce-I expression plasmid. Donor strains of E.*coli* for final conjugation/electroporation plasmids would be ET12567(pUZ8002), as this methylation deficient strain is generally used for Streptomyces transformation to prevent the degradation of methylated target DNA in the target strain[82].

Key Primer sequences listed 5’ – 3’

P1 – GAATTCCCATCCCGTCCCCGAAGAAC

P2 – TCAGCGCGCTTCCACGCGGCGAACTCCTTCTGCCTGTG

P3 – CACAGGCAGAAGGAGTTCGCCGCGTGGAAGCGCGCTGA

P4 – GAATTCGGTCGATGTCCACGGACATGTT

3.2.6: *Polymerase Chain Reaction (PCR)*

All standard PCR reactions were performed in 50µl reaction tubes using Bioline MyTaq DNA polymerase according to manufacturer instructions (www.bioline.com). PCR amplification of cloning regions was performed using Promega Pfu (www.promega.com) or NEB Phusion (www.neb.com) enzymes according to manufacturer specifications.

3.3.7: *Raman Spectroscopy*

Raman microscopy was performed using a Renishaw inVia Raman microspectrometer with a 785nm diode laser of 40mW power at the sample (Toptica, Germany. A 100x/0.9 NA objective (11566202, Leica Microsystems, Germany) objective lenses was used with grating of 1200gr/mm. Simple background subtraction was performed by repeating conditions of sample with a negative comparison and subtracting one spectrum from the other. Further background correction was performed using 'moving window' automated baseline correction as described by Schulze *et al*[83]. Spectra were taken through CaFl cover slides.

3.4: **Streptomyces and Raman Results**

3.4.1: *Culture of Streptomyces*

Typical model organisms in the laboratory such as E.*coli* are fast growing and easy to culture, with results achievable in a matter of hours. The rate of growth, coupled with their versatility in homogeneous liquid and solid cultures of LB media or LB agar mean that E.*coli* are near ubiquitous in bacterial laboratories and extremely well characterised. Streptomyces *Cattleya* and MA37 have not been characterised with respect to genetic engineering, meaning this was the first step required before further techniques could be employed.

Homogeneous culture of E.*coli* is a large factor in their success as a laboratory tool, it means cultures can be mixed with reagents, bacterial cells can interact with one another and division of cultures into aliquots or sub-culture can be easily achieved. It

also means that individual bacteria can be separated in smears on plates to form homogeneous colonies on a solid medium such as LB agar, which is a standard precursor to any experiment, as it means starting with a monoclonal culture. Figure 3.1 shows growth of both S.*cattleya* and S.MA37 in culture dishes with ISP2 media and 5% agar after 48 hours at 30°C. There is no antibiotic in these cultures, so the growth was not inhibited in any way. After 2 days, the cultures appear similar to what would be expected for E.*coli* after 5-10 hours. After this point however it becomes clear that Streptomyces do not continue in colonies for the entirety of their life cycle, instead they behave like a fungus, growing mycelium and sporulating after 7-14 days. S.*cattleya* produces purple spores as can be seen in *Figure 3.1 D*, where MA37 produces pale yellow spores.

The behaviour of these cells in a petri dish is close enough in the early stages to E.*coli* that the same methods can be used. Plates are generally used for antibiotic selection or isolation of monoclonal colonies, both of which can be done with the observed characteristics. Most processing of cells occurs in liquid culture, optical density is often used to determine the saturation of a culture for example. More importantly, addition of reagents such as plasmids, buffers or lysing agents is usually performed in homogeneous liquid cultures. Results in *Figure 3.2* show that Streptomyces MA37 does not exhibit desirable characteristics when grown in ISP2 media in a rotary shaker, instead bacteria grow in tightly bound clumps. Disrupting the bacterial clumps in liquid culture would be paramount if they were to be grown in a microfluidic device, as they would quickly block small channels. Disrupting the adhesion of these clumps with addition of detergents to disrupt cell membranes was attempted with Tween20 and Triton (*Figure 3.2D and E* respectively.) with little success. Mechanical separation of these clumps using a P1000 pipette or increasing the RPM of the rotary shaker during growth were also ineffective.

This characteristic poses a problem for microfluidics and indeed general laboratory manipulation. It seems likely that to develop the FIA1 fluorinase enzyme, it would have to be transferred to a more suitable host organism. E.*coli* does not contain the downstream genes for processing of fluorinated metabolites, but it is possible that introducing the FIA1 gene into this species would prove fruitful. Figure S3 demonstrates that the addition of potassium fluoride (KFl) to E.*coli* media, which would provide a source of fluoride ions in aqueous solution, does not negatively affect

their growth. This is promising, as it means that fluoride ions are not toxic and could potentially be processed by these cells.

The issue with the clumping for general laboratory manipulation could arise if cells in the centre of clumps are not exposed to plasmids or DNA which are introduced to transform. Subsequent antibiotic selection may also be less effective against the cells in the centre of clumps. These characteristics aren't necessarily prohibitive to genetic engineering of the species, indeed Streptomyces are a widely utilised production chassis for antibiotics[84]. Given that antibiotic production and therefore resistance is a common trait among Streptomyces species, it was necessary to test the effectiveness of antibiotics again S.MA37 before resistance markers could be chosen. Results in *Figure 3.4* show resistance to Ampicillin and Chloramphenicol, but susceptibility to Kanamycin and Gentamycin at the concentrations listed, meaning they can be used as selection markers.

3.4.2: *Streptomyces MA37 FlA1 Gene Deletion*

To remove the FlA1 gene from the genome of MA37, two homologous regions flanking the gene itself needed to be cloned into suicidal donor plasmid pSEVA212S. Coupled with plasmid pSEVA228S expressed in an E.*coli* host, this enables I-SceI mediated deletion of the gene, without leaving scarring. Clean deletion of the entire coding region of the gene was important to ensure no remnant of the enzyme could perform any fluorine incorporation after modification. It should be noted that this technique was developed for *Pseudomonas putida*, a gram-negative bacterium. Streptomyces are gram-positive, meaning they have a different membrane structure than gram-negative bacteria. Conjugation from E.*coli* strain ET12567 using plasmids with RP4 (also known as RK2) origin of replication has been demonstrated previously[82], so it was hoped that this method could be applied successfully.

To amplify regions of DNA flanking the gene, the first step was to extract and verify DNA from S.MA37. The protocol used is described in the experimental procedures section of this chapter. As the full genome sequence for MA37 is unavailable, verification was performed on the known section of DNA – the FlA1 gene. Primers 1 and 4, when used together, should amplify a region containing both homology arms along with the FlA1 gene itself, totalling a region of ~2.1kb. For cloning it is best

practice to use a polymerase enzyme with proof reading capability. These enzymes tend to be slower and more susceptible to contaminants such as salts but ensure that the DNA sequence is correct. Several attempts were made to amplify the DNA with proof reading enzymes Pfu and Phusion but none were successful. This could have been due to residual contamination from the DNA extraction, so MyTaq was used with these primers to amplify the fragment for cloning (*Figure 3.6 B*). Sequencing of the final insert would verify whether the enzyme had produced any errors in amplification.

Using this DNA as a template, homology regions HR1 and HR2 (upstream and downstream respectively) could be generated. HR1 uses primers 1 and 2, HR2 uses primers 3 and 4. Primers 2 and 3 have additional sequences which are complementary to one another, this enables both fragments individually to be turned into one long fragment using overlap extension with primers 1 and 4, as the fragments will be complementary to one another at the 3` (HR1) and 5` (HR2) ends. Primers 1 and 4 incorporate EcoRI restriction enzyme sites, enabling digestion and cloning into a donor plasmid (pSEVA612S). pSEVA612S is a non-replicating plasmid[85], so it can only convey its antibiotic resistance (Gentamycin) to the target strain upon integration into the genome. Integration into the genome occurs at homology sites, with the aim to replace the FlA1 gene region with homology arms, which bookend two ISce-I restriction sites and the antibiotic cassette from the plasmid. ISce-I is an enzyme which has no recognition sites in wild-type bacterial species, meaning that its activity can only occur at the newly introduced target regions. It is transiently introduced by the second plasmid pSEVA628S. Double stranded DNA breaks mediated by ISce-I are repaired by the host cell DNA repair machinery. Failure to repair dsDNA breaks is terminal for the bacterium, so only those who have successfully repaired their chromosomes will survive. Gene transfer mechanism is illustrated in *Figure 3.5*.

An illustration of the insert generation can be seen in *Figure 3.6 A*, along with gel electrophoresis of fragments for extraction in *Figure 3.6 B*. PCR with primers 1 and 4 was successful when amplifying the entire sequence and amplification of each fragment individually appears correct in gels for HR1 and HR2. The final gel of the overlap extension PCR shows significant non-specific amplification of DNA, and extraction of the band corresponding to the expected amplicon did not provide enough DNA for sequencing or further analysis. Several attempts were made to repeat the reaction, with higher annealing temperatures to reduce off target binding and indeed repeating the entire amplification method but a functional, verified insert was never

produced to put into the target plasmid. This could be due to a number of reasons, amplification with MyTaq may have induced errors into the sequence which resulted in incorrect template DNA.

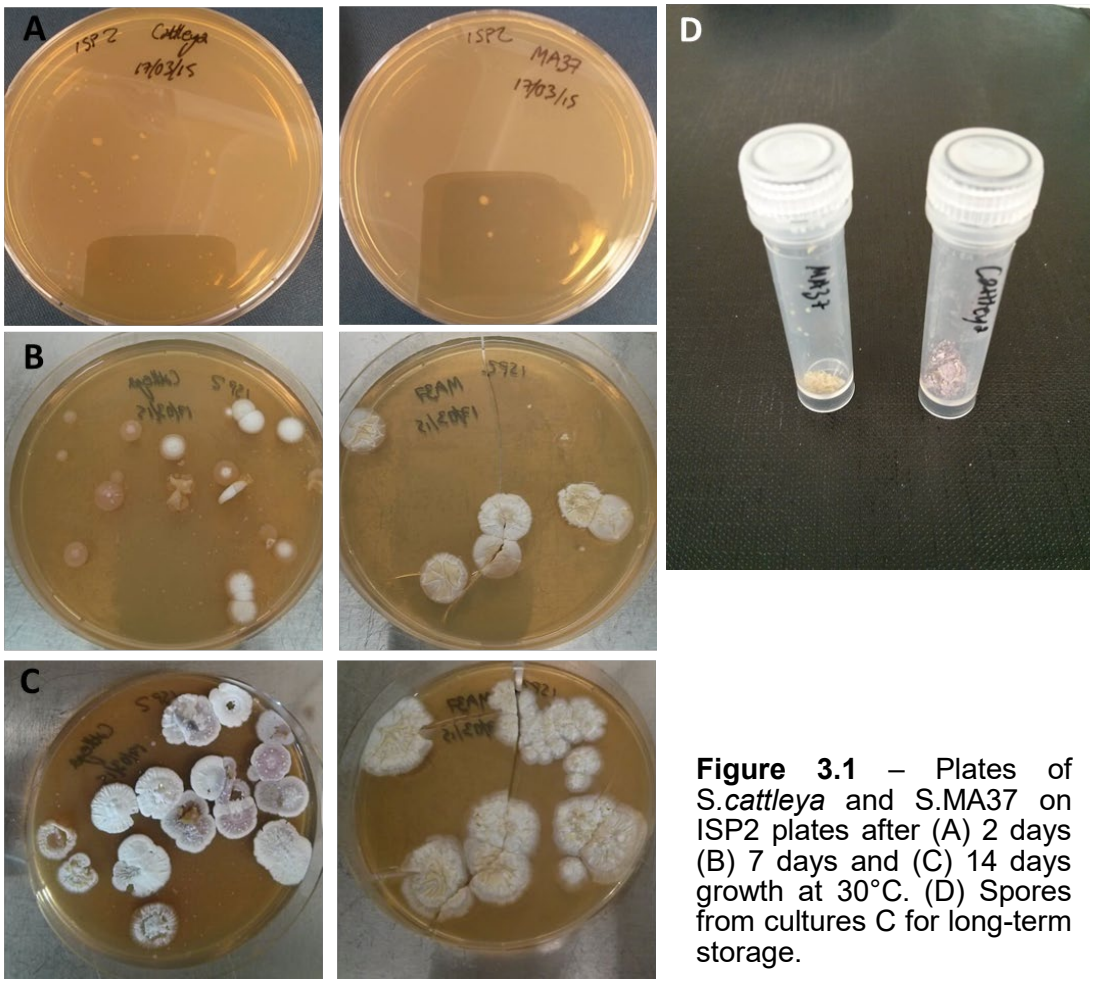

Figure 3.1 – Plates of S.*cattleya* and S.MA37 on ISP2 plates after (A) 2 days (B) 7 days and (C) 14 days growth at 30°C. (D) Spores from cultures C for long-term storage.

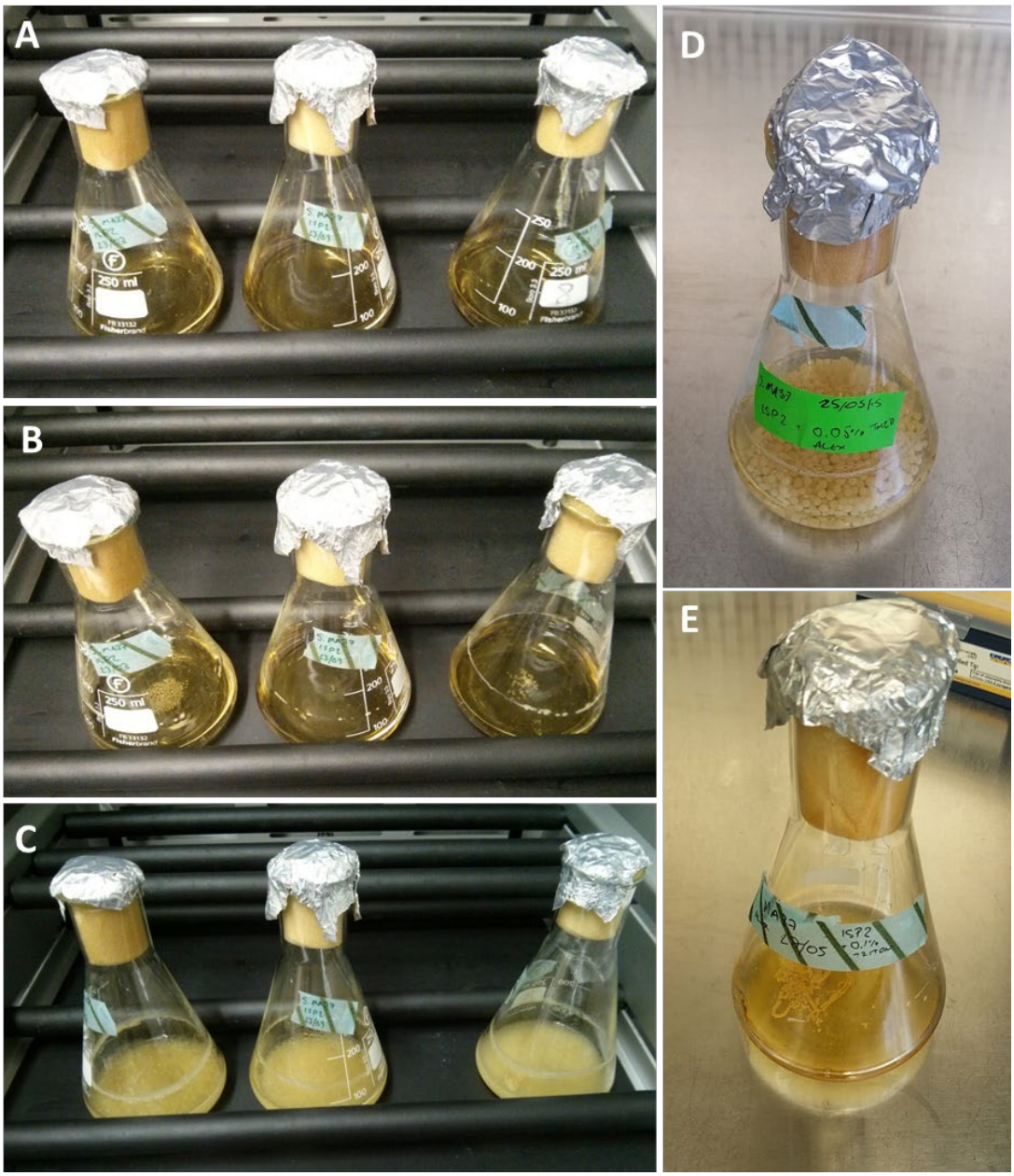

Figure 3.2 – Liquid Culture of S.MA37 in ISP2, grown in a rotary shaker at 90RPM, 30°C after (A) 1 day. (B) 2 days (C) 7 days. (D) Culture after 7 days of growth in ISP2 plus 0.05% volume Tween20. (E) Culture after 5 days of growth in ISP2 plus 0.1% Triton.

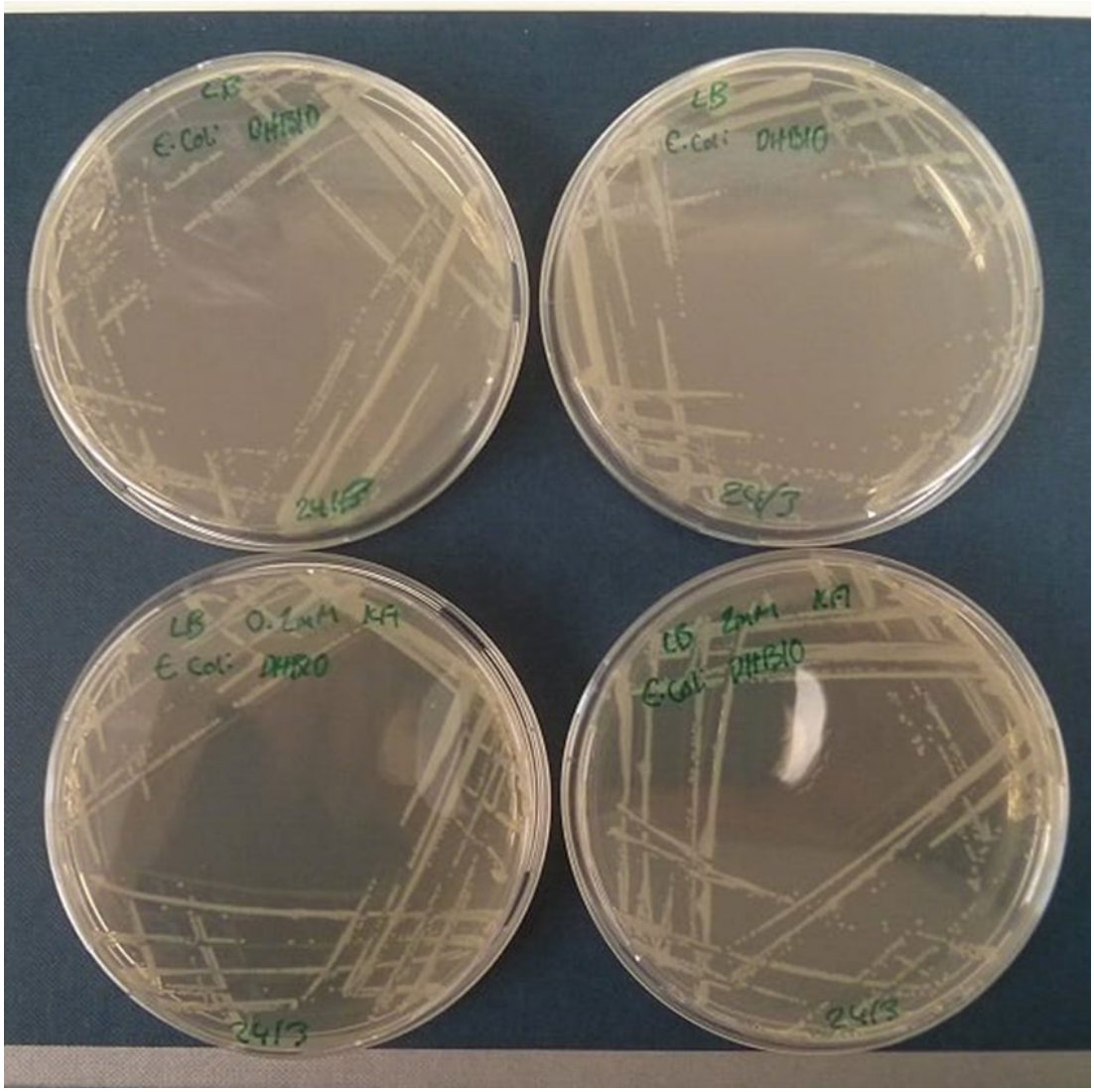

Figure 3.3 – Culture of E.*coli* DHB10 with added Potassium Fluoride (KFI). Cultures were incubated at 37°C for 16 hours. Top row shows control plates without KFI. Lower left plate contains 0.2mM KFI and lower right contains 2mM KFI.

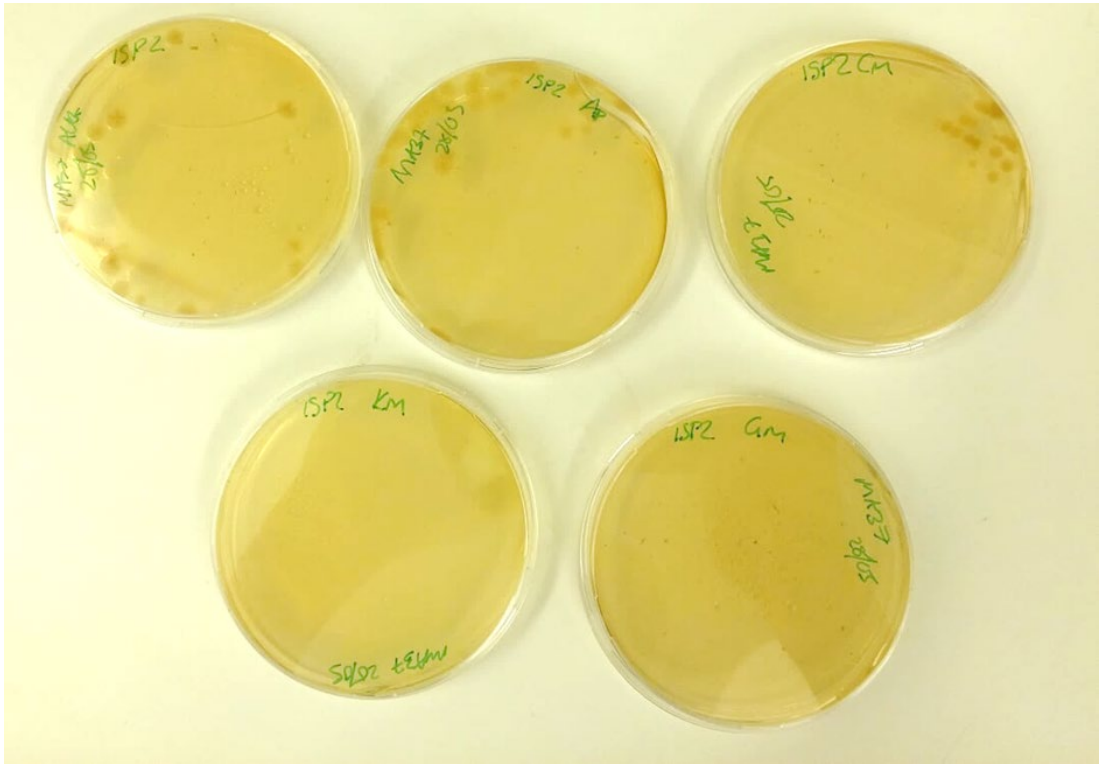

Figure 3.4 – Culture of Streptomyces MA37 on ISP2 media plus antibiotic after day incubation at 30°C. Row 1: no antibiotic selection (left), Ampicillin 50ng/µl (centre), Chloramphenicol 34ng/µl (right). Row 2: Kanamycin 25ng/µl (left), Gentamycin 20ng/µl (right).

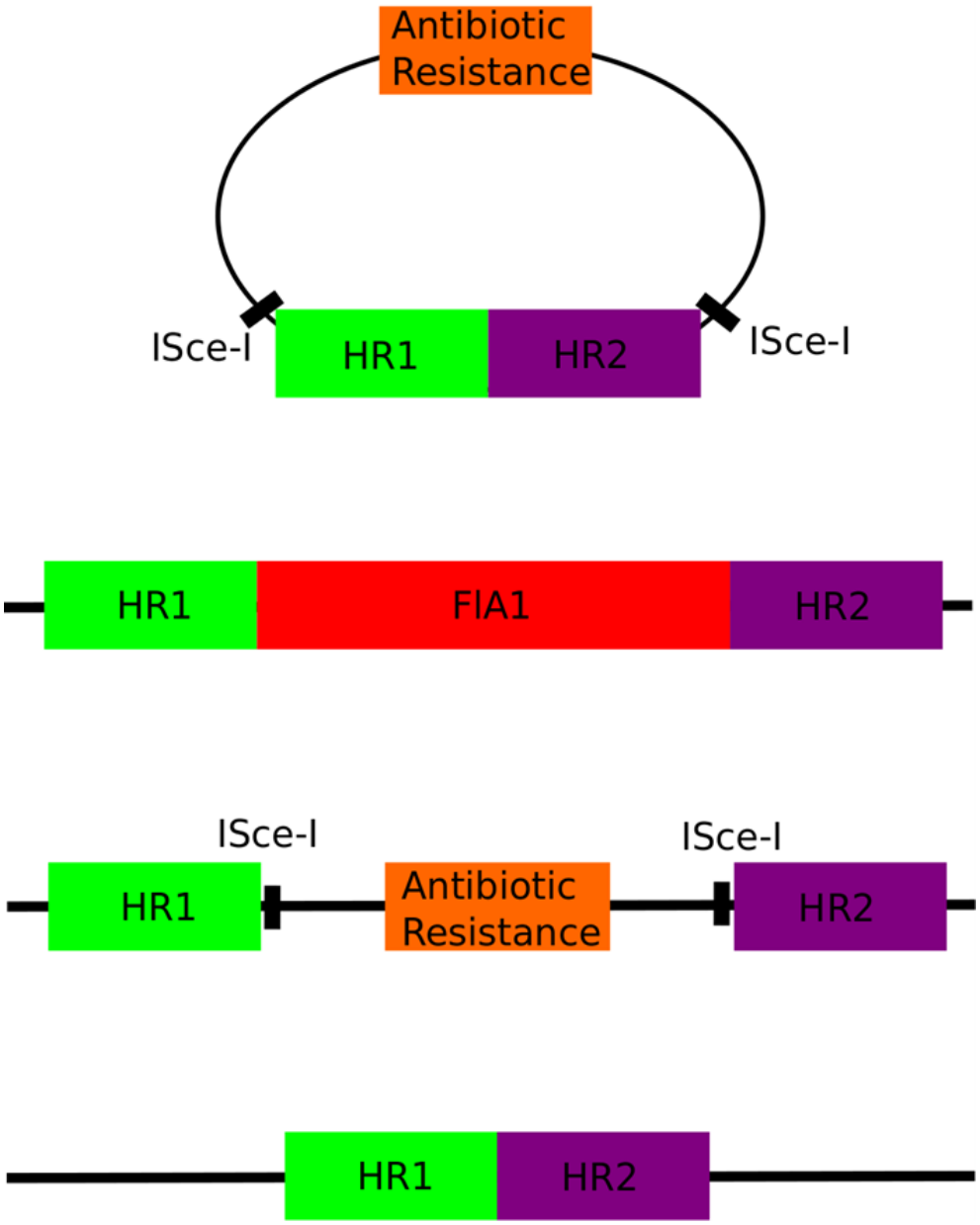

Figure 3.5 – Illustration of pSEVA suicidal vector mediated gene deletion. pSEVA612S non-replicating plasmid containing ISce-I sites, antibiotic resistance (Gentamycin) and two homology regions for DNA flanking target FIA1 gene. Plasmid integrates by swapping FIA1 gene with antibiotic resistance and ISce-I sites. Transient expression of ISce-I enzyme by second plasmid excises intervening section and host DNA repair mechanisms repair region, leaving clean deletion of FIA1 gene.

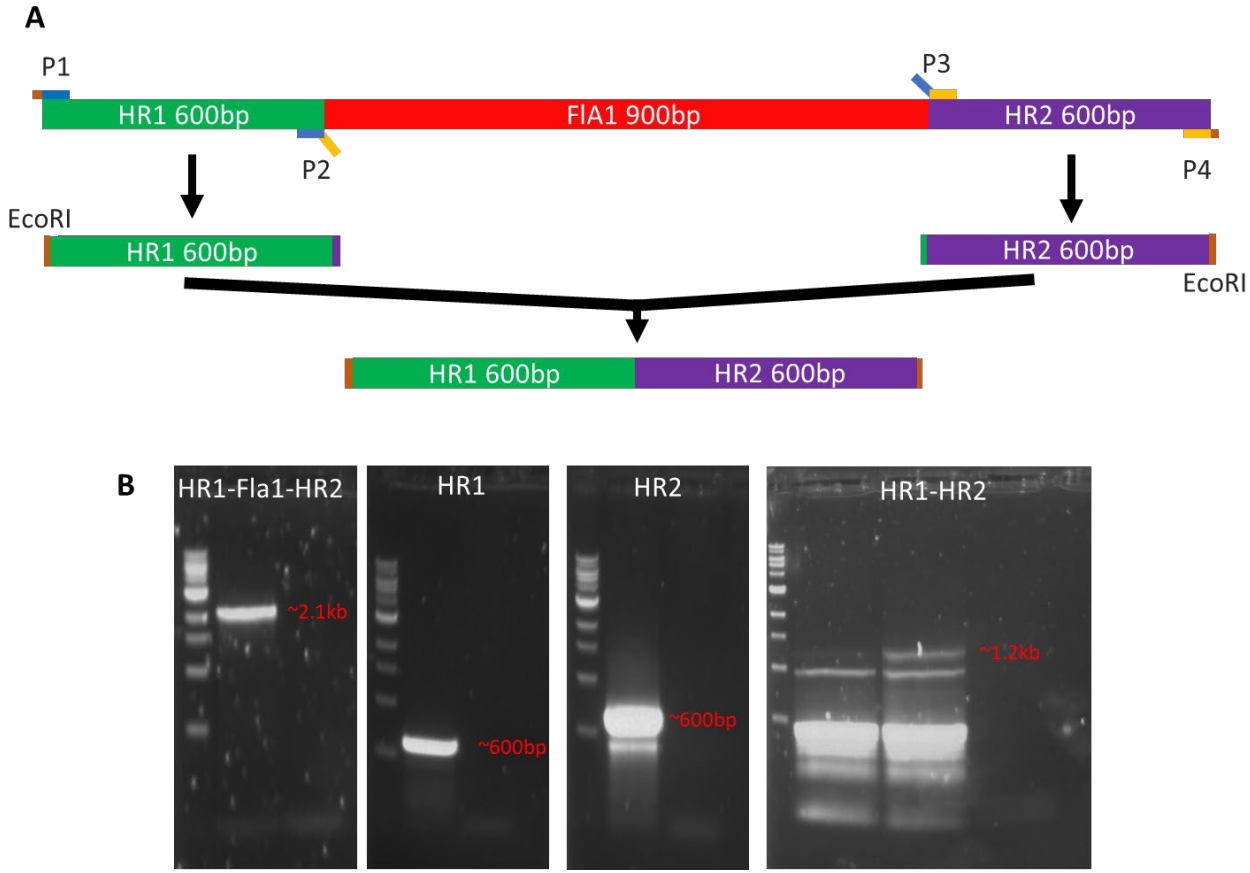

Figure 3.6 – Cloning of FlA1 Homology Regions for Insert. (A) Genomic region containing FlA1 gene and target flanking regions. Primers 1-2 amplify upsteam homology region (HR1) and 3-4 amplify downstream homology region (HR2). Fragments are amplified separately, then put into the same PCR reaction with primers 1 and 4 to amplify whole insert via overlap extension. (B) Gel electrophoresis of each fragment, showing amplicons to be extracted. NEB 1kb+ DNA ladder was run in lane 1 on all gels, along with a negative control PCR in the right-hand lanes.

3.4.3: *Organofluorine Raman Spectroscopy*

Preliminary data for Raman spectra was acquired using crystalline and aqueous solution of 5-FU, along with the un-fluorinated Uracil molecule. The aim for this was to characterise the effect of adding a carbon-fluorine bond to a molecule's Raman fingerprint. Many enzyme products are transient in nature, this is true for the fluorinated product of the FlA1 enzyme in Streptomyces, 5-FDA, which is rapidly processed into other compounds[86]. For this reason, it may not always be possible to acquire the spectrum of a particular fluorinated compound prior to screening. Results in *Figure 3.7* show the different spectra for Uracil and 5-FU. It is apparent that the addition of a C-F in the place of a C-H can significantly alter the Raman fingerprint of a given molecule. The peaks of these two compounds show little overlap, indicating the influence a C-F bond in place of a C-H has on the entire molecule's Raman scattering properties. The strongest signal in the 5-FU spectrum was at 769cm^{-1}, almost identical to the 770cm^{-1} signal designated as the C-F bond by Menaa et al[80]. this peak is not present in uracil. This shows that the C-F bond signal is consistent between Raman acquisition setups.

In order to detect these compounds *in vivo* it is essential to be able to identify compounds in aqueous solution. To test the capability of this kind of Raman setup to identify 5-FU in low concentrations, spectra were acquired for serial dilutions of 15.2mm, 7.6mm, 3.8mm and 1.9mm, and a sample of water alone was subtracted from the results. The spectra displayed in *Figure 3.8* show that minimal post-processing is required to see the C-F peak down to 3.8mM concentration in aqueous solution. O'Hagan grew Streptomyces in 2mM fluoride solution[43], and at 1.9mM the signal becomes difficult to see against background. Post-processing of Raman spectra to remove background information can be a powerful tool, *Figure 3.9* shows processing of the 1.9mM signal using 'moving window' automated baseline correction as described by Schulze et al.[83]. On first look, a far clearer spectrum can be obtained for 1.9mM 5-FU, however, the peak for the C-F bond at 758cm^{-1} is not shown as clearly as those around it, even though it should be present. This is a good indication of the limitations of any model-free baseline subtraction method, emphasising the importance of knowing the molecule's fingerprint in advance, if possible.

While clear spectra were acquired in this research, it should be noted that the acquisition time of 300s, using a 100x optical lens, would be far too long for practical use on live cells in a microfluidic device. Using a laser of shorter wavelength such as 532nm would enable faster acquisition of Raman signal, at the expense of increased background signal. Future work should investigate the prospect of detection with shorter acquisition times using a shorter wavelength laser and automated baseline correction.

Acquisition of spectra from individual cells suspended in culture solution was attempted, but this was not possible as the heat of the laser spot creates currents in the culture that move cells away from the focal point during the detection period. This phenomenon means that a 3D printed chamber with cells in suspension would not enable single-cell detection with Raman spectroscopy. For practical uses, it would be necessary to temporarily trap cells in the Raman focal point, as performed in[87], or acquire a signal from a larger area, averaging the signal from all the cells present in the area.

Another drawback is that in a complex solution containing the sum of metabolites present in a bacterial species, the Raman shifts from an individual molecule, at low concentration, would be far more difficult to isolate from the background spectrum. It would be highly desirable to increase the specificity of the Raman detection methods. This is possible using more advanced methods of Raman spectroscopy, and is covered in the discussion section of this thesis.

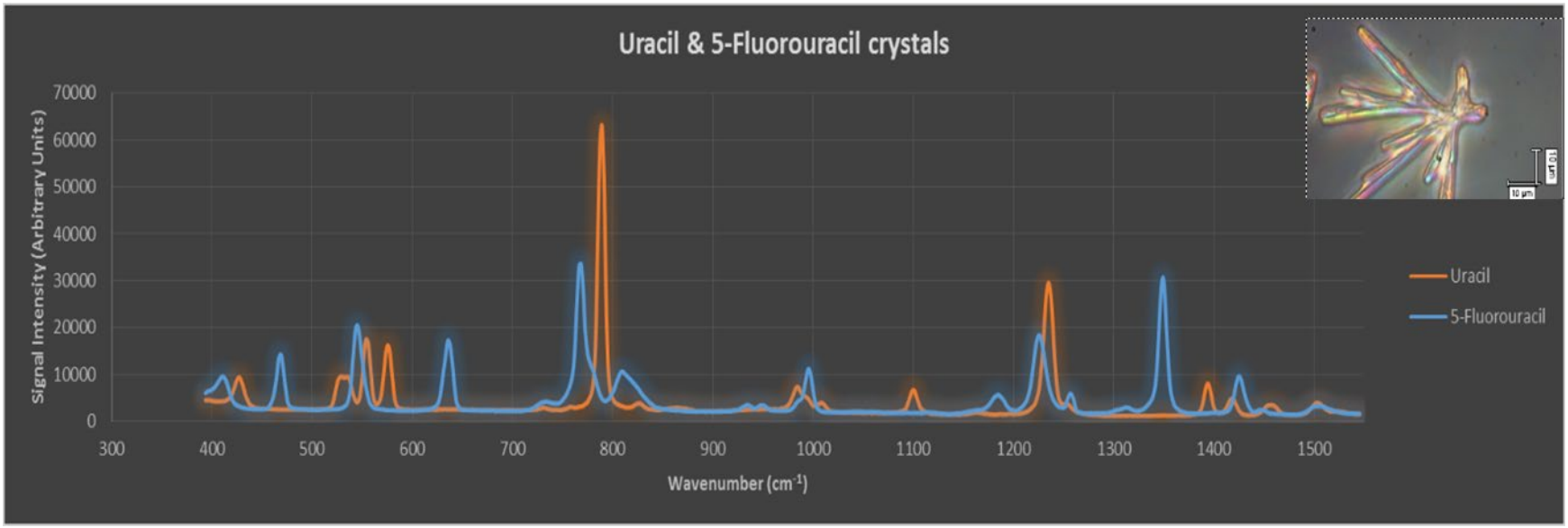

Figure 3.7 – Raman spectra of crystals of 5-FU (pictured) and its non-fluorinated counterpart uracil. The strongest signal in the 5-FU spectrum is at 769cm^{-1}, correlating with the expected peak of the C-F bond.

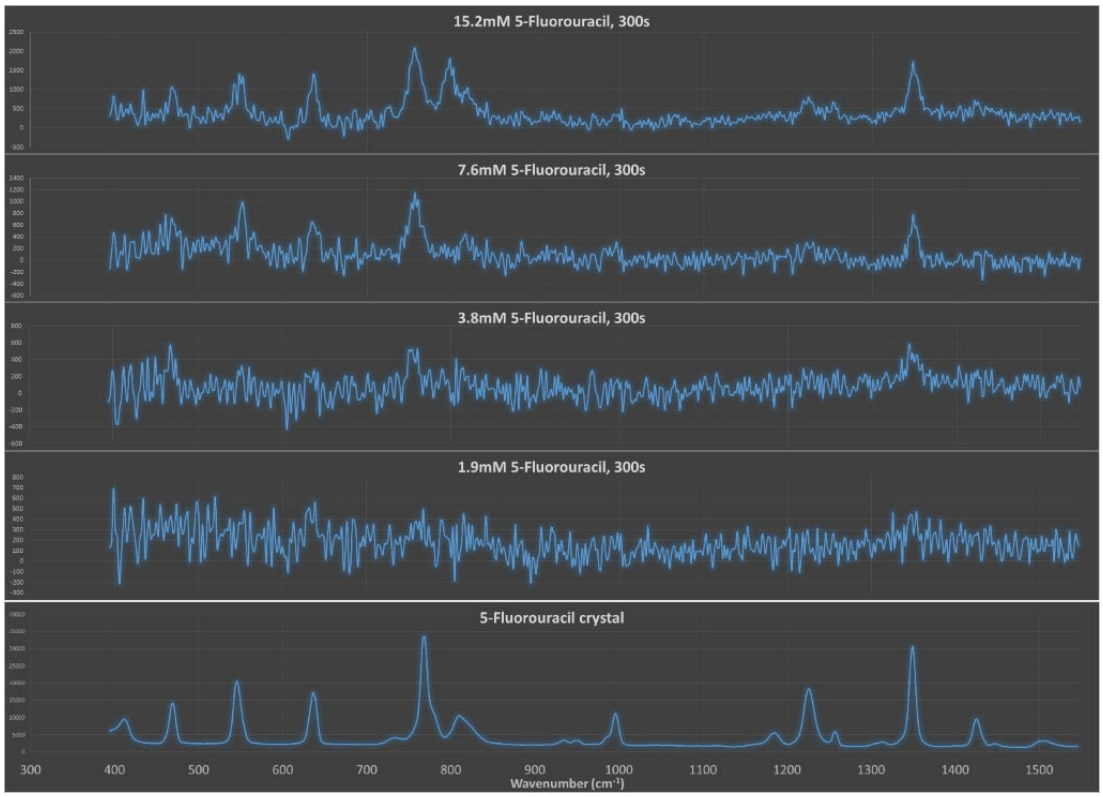

Figure 3.8 – Serial dilution of 5-FU in water with rudimentary background subtraction. 300s exposure, grating 1200gr/mm, 100x optical zoom. Two peaks of 5-FU can be seen by eye, without processing, in concentrations as low as 3.8mM. These peaks are located at ~758cm-1 in solution, corresponding to the C-F peak at 769cm-1 in the crystal and ~1348cm-1, which is not shifted from the corresponding crystalline peak.

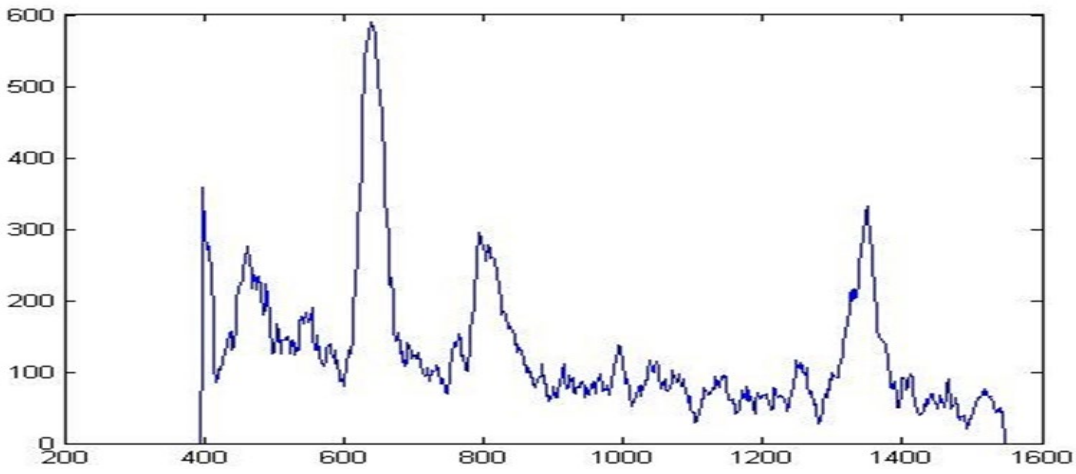

Figure 3.9 - 1.9mM 5-FU spectrum after analysis with moving window baseline correction, described by Schulze et al.

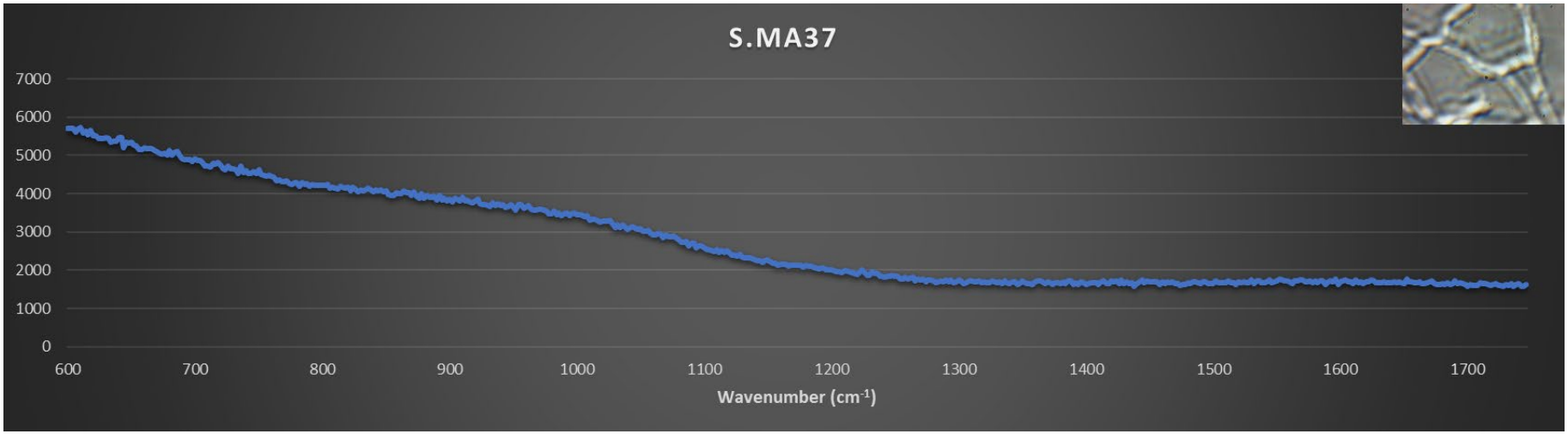

Figure 3.10 - Raman Spectrum of S.MA37. A Raman spectrum of filamentous S.MA37 dried from liquid culture containing 2mM potassium fluoride to provide source of inorganic fluorine for incorporation by FIA enzyme. Spectrum acquired using 50 second acquisition time. No clear peaks are visible in the raw spectrum.

3.5: Summary

In summary of the work presented here, 3D printing of features at the extreme of resolution with the W2P SolFlex350 does not produce reliable results for features smaller than 200µm. Features smaller than 100µm in the CAD model often do not form at all, despite their presence in the image provided to the printer by the NetFabb slicing software. Discrepancies between the CAD model and the sliced layer images, along with misalignment of the pixel grids of the exported layer images and the pixels on the printer limit the reliability of producing features at this scale. Information from previous publications presented in chapter 1 suggests that the minimum reliable features are approximately 4* the pixel size, meaning that 200µm features should be formed reliably here. This was shown not to be the case, meaning that any microfluidic device produced with this printer will require scales larger than 200µm.

Optimisation of RORSD420 on this printer was not achieved over the course of this work. This could be due to faulty resin, or failure to test the correct parameters. Even if printing were successful, dissolving of RORSD420 with water as described by the manufacturer was shown to be ineffective, meaning it would not be suitable for production of a sacrificial template for microfluidics.

Growth of Streptomyces in different conditions suggests that it would be unsuitable for a suspended culture microfluidic device due to the aggregation of cells into clumps. It is likely that expression of the FIA gene in another organism such as *E.coli* would make it more suitable for this type of device.

Raman spectroscopy of organofluorine compounds showed a strong signal for the C-F bond using this setup. Though it may be possible to distinguish fluorinated from non-fluorinated organic compounds such as those produced by Streptomyces species presented here, the 300s exposure time with this Raman setup would be prohibitive for selection in any kind of directed evolution device, whether using single-cell analysis or cell aggregate analysis. The spectrum acquired for S.MA37 using a 50s acquisition time shows no clear peaks, meaning further development of the Raman setup and protocol is required to produce improved signal and exposure times.

Chapter 4: Discussion and Conclusions

4.1: *3D Printed Microfluidics*

The data presented in this research strongly indicates that the best desktop 3D printers on the market are not capable of producing microfluidics at sub-200μm scale. While this is disappointing, it is not surprising as 3D printers such as the W2P SolFlex350 are designed to be versatile, catering for a wide range of parts which rarely require features as small as those attempted here. This research focused solely on the capability of the printer to produce microfluidics at the limit of the resolution, as a directed evolution device would function more effectively the smaller the overall reaction volume. Due to the nature of a directed evolution device requiring a sorting mechanism which could influence the culture as a whole, it is unlikely that this resolution would produce devices with culture volumes small enough for this effect to occur.

For general biological research it may not be necessary to achieve such scales in all cases. While the results in chapter 2 show that features of 200μm and below are unreliable, features above 300μm are likely to print more successfully and would produce useful channels for many experiments. Replacing general cell culture such as growth in volumes in the millilitre or litre scale with micro or millifluidic devices would still be a positive step in updating laboratory techniques. Future research should focus on producing complex micro and millifluidic devices reliably with a general-purpose 3D printer such as the W2P SolFlex350. This should focus on producing pumps and valves which require minimal input from the user to make the technology accessible to non-specialised researchers.

As mentioned in chapter 1, sacrificial, soluble scaffolds such as those attempted here have been successfully printed with FFF printers using PVA at larger scales. Many devices of larger scale have been successfully generated using both negative[88] and positive[65] device prints, which in themselves offer significant improvement in efficiency of biological research. The research referenced on positive device prints found results similar to those presented here, producing minimum channel dimensions in the region

of 250μm in both X/Y and Z planes. Highlighted in that paper is the problem of over-curing making features larger and therefore enclosed channels smaller, which is why the Z dimension of the channels is 250μm, despite a Z-layer height of 50μm. The authors found this problem to primarily be due to the resin itself, stating that the minimum Z-height of a printed channel is ~3.5–5.5h_a where h_a is the inverse of the resin absorption coefficient. For this reason, negative moulds can offer advantages when it comes to producing reliably open channels.

The problems with printing of RORSD420 could have been the result of a number of factors. The resin used here was from a single batch and could simply have been faulty or out-of-date, meaning the photoinitiators were not producing radicals and cross-linking as they were intended. This would explain the poor results produced with all the different settings used here. Acquiring new resin from the manufacturer could yield improved results. If further batches of RORSD420 repeat the results shown here, an alternative resin with similar soluble properties should be developed. Resin development is a huge factor in the development of resin-based printing and the development of a purpose-made microfluidic scaffold resin which can be used on open-source printers would be an important step for uptake of the technology. Resin which can be used on a variety of popular desktop printers but has the properties required to produce 3D structures as fine resolutions would provide would help reduce entry barriers that a purpose build 3D printer may not.

The benefits of single layer 3D printed moulds over laser etched or photolithographic master moulds is demonstrated in[89], using multiple depths in the same mould for PDMS casting. FFF based printing of materials such as ABS, which is soluble in acetone, have been shown to enable complex three dimensional channels using a special 500μm nozzle and manual modification post-printing[72]. This allows for the integration of components prior to casting in the same way as was targeted in this project with Rinse Out Resin, enabling fabrication of extremely capable devices, albeit orders of magnitude larger than some of the features required for some chemostat designs.

The general trend in the literature, along with results in this research suggest that to achieve the resolution required for a true microfluidic platform, a 3D printer and software to process the models for printing would have to be developed specifically for the task. Microfluidics require higher resolution but a smaller build volume than

desktop printers such as the Formlabs Form 2 or the W2P SolFlex350 investigated here. There are printers with details in mind and indeed some marketed specifically for microfluidics, such as the Fluidic Factory 3D Printer – claiming to be the world's first commercial 3D fluidic device printer (www.dolomite-microfluidics.com). Despite this, there is currently no industry standard system for designing, fabricating and operating microfluidics devices and until there is, uptake of the technology where it is sorely needed in biological research will not be widespread.

New additions to 3D printing technologies are being added regularly, Formlabs Elastic Resin was released in February 2019 and offers PDMS-like qualities for a positive device print. This resin and indeed formation of new resins with desirable properties should be a target of further investigation. Many simple devices may not require the scale to handle cells on an individual level. Devices that are already within the capabilities of 3D printers can offer many of the advantages of the microfluidics described here, automation and miniaturisation most importantly.

Future research on this topic should focus on methods of fabricating reliable devices at the scales required to recreate those described in the literature here. The next, and possibly most important step would be plug-and-play type device operation. It is almost certainly the future of biological research to incorporate microfluidics into everyday experimental design and the advancement of fabrication technology is one of the primary enabling factors in this. This research however also demonstrates, that even with appropriate printing capabilities, the software can play a vital role in the success or failure of a platform.

4.2: *Microfluidics and Cell Culture*

It is well documented in the literature that Streptomyces species grow in a manner consistent with that seen here, so the results were not unexpected. While Streptomyces species are extremely useful due to their antibiotic production capability, they would not lend themselves to the kind of suspended culture device described here. Their tendency to produce filamentous hyphae and join together in clumps when suspended would lead to device blockages. Given that the cells do not grow separately to one another, the interactions between cells that this kind of device enables, and the advantages that brings for directed evolution would not be

possible. That is not to say that 3D printed microfluidics cannot offer a platform for growth of Streptomyces, static culture in simple devices such as the one described in[90] demonstrate the ability of different device designs to cater for different organisms.

The focus of this research evaluating whether microfluidics for directed evolution could be feasibly fabricated using 3D printing. If instead, microfluidics was employed as a method of antibiotic production, with many devices in parallel enabling higher yields of product, there is every possibility that a device could be designed and optimised using 3D printing. If single cell isolation and cellular mobility is not desired, culture of cells in devices of various sizes and formats could produce results. For example, seeding a microfluidic device with immobilised cells and passing growth media and reactants over the cell before removal of the culture media. This offers the ability to culture cells in an automated fashion, in parallel, and to isolate the chemical excretions of the cell in the depleted media. This offers the advantage of tight control over exactly what conditions individual cells in the bioreactor, along with the ability to remove and replace dysfunctional cells. Devices could act as cells in a battery.

This also expands the laboratory capabilities of an individual researcher, automating the culture of cells in devices specifically designed for a given experiment and cell line. This would reduce the complexity involved when culturing different cell types with different protocols. Incorporation of monitoring devices such as pH[91, 92] and temperature sensors[93] would give additional functionality into cell culture equipment itself, enabling tighter control of culture conditions and additional information to assess unexpected results. Crucially, a fully sealed experiment from start to completion would all but eradicate contamination from human error, which can be a major source of waste and frustration.

The breadth of device design and formats for specific research and cells would be impossible to describe here. The platform of 3D printed microfluidics with accompanying user-friendly design and operation would be an enabling technology for high throughput, high quality research that is currently not viable for individuals in a laboratory. The ideal platform would offer standardised components for general device design, e.g. pumps, heaters, sensors and a fabrication method to incorporate them all into a device, in whatever the desired format. Coupled with bespoke culture

chambers, this would offer a radical alternative to the labour intensive, wasteful practices that are ubiquitous in current research.

4.3: *Raman Spectroscopy, Microfluidics and Directed Evolution*

A directed evolution device to actively guide natural or stimulated evolution towards a target trait would be a revolution in approach to synthetic biology. Though some may not consider it to be truly synthetic biology, when coupled with lead compound identification for new drug discovery or optimising synthetic pathways it could be a capable partner to facilitate these approaches. Raman spectroscopy offers an ideal detection method for live cell analysis as it is non-invasive.

The results presented here would suggest that this system alone would not be capable of detection of individual cells at high speed. 300s acquisitions was used to characterise 5-FU in this research, where the samples were in pure water at higher concentrations than would likely be found *in vivo.* Surface Enhanced Raman Spectroscopy (SERS) increases Raman signal in a localised area, this means that acquisition times can be shorter for a given signal. An example of this is that 3s acquisition enabled characterisation of several cell types in a SERS-microfluidic cell analysis device using the same Renishaw InVia system used here, but with a longer wavelength 832nm laser to reduce background signal[59]. This system uses a 20μm x 2μm array of gold nanodimers to provide the surface enhancement of Raman signals. Using enhanced Raman would likely be fundamental to achieve speed and detail in a directed evolution device.

The fabrication of these nanodimers is not currently possible using 3D printing, due to their small size of 100nm and use of gold metal. This leads to the conclusion that multiple fabrication techniques may be required for specific purposes such as this. 3D printing lends itself to incorporating prefabricated components, as has already been referenced here with sacrificial template moulding. Some FFF 3D printers, such as the Markforged Mark Two (www.markforged.com) offer the ability to pause a print after a certain layer and resuming on command. This offers the capability of designing a void in a model, pausing the print after this void has printed, and then inserting a component before resuming printing and encapsulating it. While there is no system available which offers this at the scale required for incorporating

components like this array, it demonstrates the potential for incorporating external components within a printed part, be it through sacrificial template casting or direct printing.

For this type of device to function, the rate of Raman based cell sorting would need to be greater than or equal to the rate of cell division. E.*coli* for example double every 20 minutes under optimal 37°C, oxygen rich LB media conditions in the exponential phase of growth. Acquisition of 3s samples would enable analysis of only 400 cells in a 20-minute period, excluding time required to manoeuvre cells into place and resetting of the system. Growth conditions can be manipulated to slow growth through nutrient depletion[94], which may be necessary despite the potential to affect cell behaviour. As a point of reference, a common optical density at 600nm for stopping an E.*coli* culture for use would be OD_{600} 0.4. This is during the exponential phase of growth, and contains approximately $3.2x10^8$ E.*coli* cells per millilitre. A total cell population would have to be around 1nl for 3s acquisition to be fast enough to process all the cells before the population doubles (320 cells at OD_{600} 0.4). It should be stated that the overall volume of the culture chamber in Jason Kelly's chemostat was just 16nl. A combination of faster Raman spectroscopy techniques, using a different Raman setup, and detailed microfluidics would likely provide the necessary parameters.

Coherent Anti-Stokes Raman Spectroscopy (CARS)[95] and Stimulated Raman Spectroscopy (SRS)[96] are orders of magnitude more sensitive than Raman spectroscopy alone. Both CARS and SRS use multiple laser sources at different wavelengths to increase Raman photon emission compared with spontaneous Raman spectroscopy. This increase in probability is facilitated by the second laser wavelength matching the Stokes scattering wavenumber of the target bond, which serves to stimulate the vibrational transition with orders of magnitude higher probability than spontaneous Raman scattering. These techniques are powerful because they can stimulate targeted excitation of bonds which produce Raman photons, meaning a specific bond can be chosen to amplify[97] – the C-F bond would be a suitable target. SRS is generally considered to be preferable for low concentrations of target, as both Raman and CARS are susceptible to strong background signals, as seen in this research for spontaneous Raman spectroscopy. It has been demonstrated that to even further enhance the sensitivity of Raman based spectroscopy, CARS and SRS can be combined with SERS[98]. Application of

these technologies to a directed evolution device would be beneficial, if not essential, for proper function of the device.

4.4: *Concluding Remarks*

Results presented here suggest that the W2P SolFlex350 3D printer is unable to produce features smaller than 200µm. The reasons for this appear largely down to the software and firmware on the printer, rather than a fundamental problem with the technology itself. Close interaction with the manufacturer may provide a solution through software updates for this particular printer. The production of larger channels however could be extremely useful in encouraging the uptake of devices with larger volumes to replace resource intensive practices such as general culture and cell transformation. Future research should focus on integrating components such as valves and mixers with larger channels using this printer.

Raman spectroscopy as a non-invasive method of cell sorting is an established technique and there is evidence from the work here that the C-F bond could be used as a target. The setup used for this research is capable of acquiring signal with low background noise, however, the acquisition time of 300s used here is too long to be useful in cell sorting. Using a different laser wavelength such as 532nm, or more advanced methods such as SRS may produce more suitable results for cell-sorting.

The concept of a directed evolution device, capable of sorting individual cells was not realised in this research. The results shown here demonstrate that the 3D printer and Raman setup were not optimal for producing such a device. Realisation of a device like this may be possible using a specialist fabrication technique such as 2PP.

The widespread adoption of microfluidics through in-house production with desktop 3D printers is likely to occur in the coming years. Affordable, general-purpose printers such as the one used here and units like those from Formlabs are already capable of producing custom labware and the continuous improvement of both machines and resins will eventually displace photolithography and specialist equipment for the vast majority of microfluidic fabrication. Increase in knowledge and advancements in the technology mean that devices can already be produced

with specialist equipment and it is only a matter of time before general purpose 3D printers are capable of producing similar results.

The work presented here provides a useful insight into the function of desktop 3D printers at the limit of their resolutions and an oversight of the technology in the literature which can produce microfluidics. Future work should focus on integration of this technology into biological laboratories to improve the quality and output of research on biological materials.

References

1. Basketter, D. A., English, J. S. C., Wakelin, S. H. & White, I. R. Enzymes, detergents and skin: facts and fantasies. *Br. J. Dermatol.* **158**, 1177–81 (2008).
2. Mullis, K. B. & Faloona, F. A. [21] Specific synthesis of DNA in vitro via a polymerase-catalyzed chain reaction. *Methods Enzymol.* **155**, 335–350 (1987).
3. Sanger, F., Nicklen, S. & Coulson, A. R. DNA sequencing with chain-terminating inhibitors. *Proc. Natl. Acad. Sci. U. S. A.* **74**, 5463–7 (1977).
4. Wetterstrand KA. DNA Sequencing Costs: Data - National Human Genome Research Institute (NHGRI). Available at: https://www.genome.gov/sequencingcostsdata/. (Accessed: 11th December 2017)
5. Cong, L. *et al.* Multiplex Genome Engineering Using CRISPR/Cas Systems. *Science (80-.).* **339**, 819–823 (2013).
6. Movasaghi, Z., Rehman, S. & Rehman, I. U. Raman Spectroscopy of Biological Tissues. *Appl. Spectrosc. Rev.* **42**, 493–541 (2007).
7. Lee, J. W., Goulet, M.-A. & Kjeang, E. Microfluidic redox battery. *Lab Chip* **13**, 2504 (2013).
8. Licklider, L., Wang, X.-Q., Desai, A., Yu-Chong Tai, A. & Terry D. Lee*. A Micromachined Chip-Based Electrospray Source for Mass Spectrometry. (1999). doi:10.1021/AC990967P
9. Xia, Y. & Whitesides, G. M. SOFT LITHOGRAPHY. *Annu. Rev. Mater. Sci.* **28**, 153–184 (1998).
10. Whitesides, G. M. & Stroock, A. D. Flexible Methods for Microfluidics. *Phys. Today* **54**, 42–48 (2001).
11. Ng, J. M. K., Gitlin, I., Stroock, A. D. & Whitesides, G. M. Components for integrated poly(dimethylsiloxane) microfluidic systems. *Electrophoresis* **23**, 3461–3473 (2002).
12. Stone, H. A., Stroock, A. D. & Ajdari, A. ENGINEERING FLOWS IN SMALL DEVICES. *Annu. Rev. Fluid Mech.* **36**, 381–411 (2004).
13. Hong, J. W. & Quake, S. R. Integrated nanoliter systems. *Nat. Biotechnol.* **21**, 1179–1183 (2003).
14. Friend, J. & Yeo, L. Fabrication of microfluidic devices using polydimethylsiloxane. *Biomicrofluidics* **4**, (2010).
15. Lei, K. F. Chapter 1. Materials and Fabrication Techniques for Nano- and Microfluidic Devices. in 1–28 (Royal Society of Chemistry, 2015). doi:10.1039/9781849737609-00001
16. Unger, M. A., Chou, H.-P., Thorsen, T., Scherer, A. & Quake, S. R. Monolithic Microfabricated Valves and Pumps by Multilayer Soft Lithography. *Science (80-.).* **288**, (2000).
17. Lu, J.-C., Liao, W.-H. & Tung, Y.-C. Magnet-assisted device-level alignment for the fabrication of membrane-sandwiched polydimethylsiloxane microfluidic devices. *J. Micromechanics Microengineering* **22**, 075006 (2012).
18. Glick, C. C. *et al.* Rapid assembly of multilayer microfluidic structures via 3D-printed transfer molding and bonding. *Microsystems Nanoeng.* **2**, 16063 (2016).
19. Kim, J. Y., Baek, J. Y., Lee, K. A. & Lee, S. H. Automatic aligning and bonding system of PDMS layer for the fabrication of 3D microfluidic channels. *Sensors Actuators A* **119**, 593–598 (2005).
20. Levin, P. A. & Angert, E. R. Small but Mighty: Cell Size and Bacteria. *Cold Spring Harb. Perspect. Biol.* **7**, a019216 (2015).
21. Altschuler, S. J. & Wu, L. F. Cellular heterogeneity: do differences make a difference? *Cell* **141**, 559–63 (2010).
22. Balaban, N. Q., Merrin, J., Chait, R., Kowalik, L. & Leibler, S. Bacterial persistence as a phenotypic switch. *Science* **305**, 1622–5 (2004).
23. Bigger, J. TREATMENT OF STAPHYLOCOCCAL INFECTIONS WITH PENICILLIN BY INTERMITTENT STERILISATION. *Lancet* **244**, 497–500 (1944).
24. Urbina, M. A., Watts, A. J. R. & Reardon, E. E. Environment: Labs should cut plastic

waste too. *Nat. 2015 5287583* (2015).
25. Bistulfi, G. Sustainability: Reduce, reuse and recycle lab waste. *Nat. 2013 5027470* (2013).
26. Sezonov, G., Joseleau-Petit, D. & D'Ari, R. Escherichia coli physiology in Luria-Bertani broth. *J. Bacteriol.* **189**, 8746–9 (2007).
27. Wilm, M. S. & Mann, M. Electrospray and Taylor-Cone theory, Dole's beam of macromolecules at last? *Int. J. Mass Spectrom. Ion Process.* **136**, 167–180 (1994).
28. El-Faramawy, A., Siu, K. W. M. & Thomson, B. A. Efficiency of Nano-Electrospray Ionization. *J. Am. Soc. Mass Spectrom.* **16**, 1702–1707 (2005).
29. Mahmood, T. & Yang, P.-C. Western blot: technique, theory, and trouble shooting. *N. Am. J. Med. Sci.* **4**, 429–34 (2012).
30. Mccarthy, K. D. & De Vellis, J. *PREPARATION OF SEPARATE ASTROGLIAL AND OLIGODENDROGLIAL CELL CULTURES FROM RAT CEREBRAL TISSUE*. **85**, (1980).
31. Wu, D., Qin, J. & Lin, B. Electrophoretic separations on microfluidic chips. *J. Chromatogr. A* **1184**, 542–559 (2008).
32. AlJanahi, A. A., Danielsen, M. & Dunbar, C. E. An Introduction to the Analysis of Single-Cell RNA-Sequencing Data. *Mol. Ther. Methods Clin. Dev.* **10**, 189–196 (2018).
33. Delincé, M. J. *et al.* A microfluidic cell-trapping device for single-cell tracking of host–microbe interactions. *Lab Chip* **16**, 3276–3285 (2016).
34. Yang, J., Hurth, C., Nordquist, A., Smith, S. & Zenhausern, F. Integrated Microfluidic System for Rapid DNA Fingerprint Analysis: A Miniaturized Integrated DNA Analysis System (MiDAS)—Swab Sample-In to DNA Profile-Out. in 207–224 (Humana Press, New York, NY, 2019). doi:10.1007/978-1-4939-8964-5_14
35. Ylitervo, P., Franzén, C. J. & Taherzadeh, M. J. Continuous ethanol production with a membrane bioreactor at high acetic Acid concentrations. *Membranes (Basel).* **4**, 372–87 (2014).
36. NOVICK, A. & SZILARD, L. Description of the chemostat. *Science* **112**, 715–6 (1950).
37. Plouchart, D., Milferstedt, K., Guizard, G., Latrille, E. & Hamelin, J. Multiplexed chemostat system for quantification of biodiversity and ecosystem functioning in anaerobic digestion. *PLoS One* **13**, e0193748 (2018).
38. Ziv, N., Brandt, N. J. & Gresham, D. The use of chemostats in microbial systems biology. *J. Vis. Exp.* (2013). doi:10.3791/50168
39. O'Hagan, D. Understanding organofluorine chemistry. An introduction to the C–F bond. *Chem. Soc. Rev.* **37**, 308–319 (2008).
40. Hyohdoh, I. *et al.* Fluorine Scanning by Nonselective Fluorination: Enhancing Raf/MEK Inhibition while Keeping Physicochemical Properties. *ACS Med. Chem. Lett.* **4**, 1059–63 (2013).
41. Theodoridis, G. *Fluorine and the Environment - Agrochemicals, Archaeology, Green Chemistry & Water*. *Advances in Fluorine Science* **2**, (Elsevier, 2006).
42. Schaffrath, C., Deng, H. & O'Hagan, D. Isolation and characterisation of 5′-fluorodeoxyadenosine synthase, a fluorination enzyme from Streptomyces cattleya. *FEBS Lett.* **547**, 111–114 (2003).
43. Deng, H. *et al.* Identification of fluorinases from Streptomyces sp MA37, Norcardia brasiliensis, and Actinoplanes sp N902-109 by genome mining. *Chembiochem* **15**, 364–8 (2014).
44. French, C. E. *et al.* SYNTHETIC BIOLOGY AND THE ART OF BIOSENSOR DESIGN. (2011).
45. Pedley, A. M., Karras, G. I., Zhang, X., Lindquist, S. L. & Benkovic, S. J. The Role of HSP90 in the Regulation of de novo Purine Biosynthesis. *Biochemistry* acs.biochem.8b00140 (2018). doi:10.1021/acs.biochem.8b00140
46. Chiba, S. *et al.* An iterative compound screening contest method for identifying target protein inhibitors using the tyrosine-protein kinase Yes. *Sci. Rep.* **7**, 12038 (2017).
47. Hope, E. A. *et al.* Experimental Evolution Reveals Favored Adaptive Routes to Cell Aggregation in Yeast. *Genetics* **206**, 1153–1167 (2017).

48. Guccione, E. J. *et al.* Transcriptome and proteome dynamics in chemostat culture reveal how *Campylobacter jejuni* modulates metabolism, stress responses and virulence factors upon changes in oxygen availability. *Environ. Microbiol.* **19**, 4326–4348 (2017).
49. Groisman, A. *et al.* A microfluidic chemostat for experiments with bacterial and yeast cells. *Nat. Methods* **2**, 685–689 (2005).
50. Long, Z. *et al.* Microfluidic chemostat for measuring single cell dynamics in bacteria. *Lab Chip* **13**, 947 (2013).
51. Kelly, J. R. Tools and reference standards supporting the engineering and evolution of synthetic biological systems By. (2008).
52. Balagaddé, F. K., You, L., Hansen, C. L., Arnold, F. H. & Quake, S. R. Long-term monitoring of bacteria undergoing programmed population control in a microchemostat. *Science* **309**, 137–40 (2005).
53. Park, J., Wu, J., Polymenis, M. & Han, A. Microchemostat array with small-volume fraction replenishment for steady-state microbial culture. *Lab Chip* **13**, 4217–24 (2013).
54. Ochman, H., Lawrence, J. G. & Groisman, E. A. Lateral gene transfer and the nature of bacterial innovation. *Nature* **405**, 299–304 (2000).
55. Temiz, Y., Lovchik, R. D., Kaigala, G. V. & Delamarche, E. Lab-on-a-chip devices: How to close and plug the lab? *Microelectron. Eng.* **132**, 156–175 (2015).
56. Aaron R. Wheeler, †, Hyejin Moon, ‡, Chang-Jin “CJ” Kim, ‡, Joseph A. Loo, †,§ and & Robin L. Garrell*, †. Electrowetting-Based Microfluidics for Analysis of Peptides and Proteins by Matrix-Assisted Laser Desorption/Ionization Mass Spectrometry. (2004). doi:10.1021/AC0498112
57. Korczyk, P. M. *et al.* Scaling up the Throughput of Synthesis and Extraction in Droplet Microfluidic Reactors. (2015). doi:10.1556/JFC-D-14-00038
58. Mark, D., Haeberle, S., Roth, G., von Stetten, F. & Zengerle, R. Microfluidic lab-on-a-chip platforms: requirements, characteristics and applications. *Chem. Soc. Rev.* **39**, 1153 (2010).
59. Perozziello, G. *et al.* Microfluidic device for continuous single cells analysis via Raman spectroscopy enhanced by integrated plasmonic nanodimers. *Opt. Express* **24**, A180 (2016).
60. Matthews, T. E. *et al.* Glucose monitoring and adaptive feeding of mammalian cell culture in the presence of strong autofluorescence by near infrared Raman spectroscopy. *Biotechnol. Prog.* **34**, 1574–1580 (2018).
61. RAMAN, C. V. & KRISHNAN, K. S. A New Type of Secondary Radiation. *Nature* **121**, 501–502 (1928).
62. Kerr, L. T., Byrne, H. J. & Hennelly, B. M. Optimal choice of sample substrate and laser wavelength for Raman spectroscopic analysis of biological specimen. *Anal. Methods* **7**, 5041–5052 (2015).
63. Kong, X. *et al.* Comparative analysis of different laser systems to study cellular responses to DNA damage in mammalian cells. *Nucleic Acids Res.* **37**, e68 (2009).
64. Macdonald, N. P. *et al.* Comparing Microfluidic Performance of Three-Dimensional (3D) Printing Platforms. *Anal. Chem.* **89**, 3858–3866 (2017).
65. Shallan, A. I., Smejkal, P., Corban, M., Guijt, R. M. & Breadmore, M. C. Cost-effective three-dimensional printing of visibly transparent microchips within minutes. *Anal. Chem.* **86**, 3124–30 (2014).
66. Chan, H. N. *et al.* Direct, one-step molding of 3D-printed structures for convenient fabrication of truly 3D PDMS microfluidic chips. *Microfluid. Nanofluidics* **19**, 9–18 (2015).
67. Buchoux, A. *et al.* Manufacturing of microcirculation phantoms using rapid prototyping technologies. (2015).
68. Gong, H., Bickham, B. P., Woolley, A. T. & Nordin, G. P. Custom 3D printer and resin for 18 μm × 20 μm microfluidic flow channels. *Lab Chip* **17**, 2899–2909 (2017).
69. Gong, H., Woolley, A. T. & Nordin, G. P. High density 3D printed microfluidic valves, pumps, and multiplexers. *Lab Chip* **16**, 2450–2458 (2016).
70. Ostendorf, A. & Chichkov, B. N. Two-photon polymerization: A new approach to

micromachining. *Photonics Spectra* **40**, 72–80 (2006).
71. Otuka, A. J. G., Corrêa, D. S., Fontana, C. R. & Mendonça, C. R. Direct laser writing by two-photon polymerization as a tool for developing microenvironments for evaluation of bacterial growth. *Mater. Sci. Eng. C* **35**, 185–189 (2014).
72. Saggiomo, V. & Velders, A. H. Simple 3D Printed Scaffold-Removal Method for the Fabrication of Intricate Microfluidic Devices. *Adv. Sci.* **2**, 1500125 (2015).
73. Tsuda, S. *et al.* Customizable 3D Printed 'Plug and Play' Millifluidic Devices for Programmable Fluidics. *PLoS One* **10**, e0141640 (2015).
74. Therriault, D., White, S. R. & Lewis, J. A. Chaotic mixing in three-dimensional microvascular networks fabricated by direct-write assembly. *Nat. Mater.* **2**, 265–271 (2003).
75. Hardin, J. O., Ober, T. J., Valentine, A. D. & Lewis, J. A. Microfluidic Printheads for Multimaterial 3D Printing of Viscoelastic Inks. *Adv. Mater.* **27**, 3279–3284 (2015).
76. Muth, J. T. *et al.* Embedded 3D Printing of Strain Sensors within Highly Stretchable Elastomers. *Adv. Mater.* **26**, 6307–6312 (2014).
77. Deng, S., Su, E., Ma, X., Yang, S. & Wei, D. Efficient enzymatic synthesis of ampicillin by mutant Alcaligenes faecalis penicillin G acylase. *J. Biotechnol.* **199**, 62–8 (2015).
78. Hwang, K.-S., Kim, H. U., Charusanti, P., Palsson, B. Ø. & Lee, S. Y. Systems biology and biotechnology of Streptomyces species for the production of secondary metabolites. *Biotechnol. Adv.* **32**, 255–68 (2014).
79. Martínez-García, E. & De Lorenzo, V. Engineering multiple genomic deletions in Gram-negative bacteria: analysis of the multi-resistant antibiotic profile of Pseudomonas putida KT2440e mi_2538 2702..2716. (2011). doi:10.1111/j.1462-2920.2011.02538.x
80. Menaa, F., Menaa, B. & Sharts, O. Development of carbon-fluorine spectroscopy for pharmaceutical and biomedical applications. *Faraday Discuss.* **149**, 269–278 (2011).
81. Shirling, E. B. & Gottlieb, D. Methods for Characterization of Streptomyces Species. *Int. J. Syst. Bacteriol.* **16**, 131–340 (1966).
82. Kieser, T. *et al. Practical Streptomyces genetics*.
83. Schulze, H. G., Foist, R. B., Okuda, K., Ivanov, A. & Turner, R. F. B. A model-free, fully automated baseline-removal method for Raman spectra. *Appl. Spectrosc.* **65**, 75–84 (2011).
84. de Lima Procópio, R. E., da Silva, I. R., Martins, M. K., de Azevedo, J. L. & de Araújo, J. M. Antibiotics produced by Streptomyces. *Brazilian J. Infect. Dis.* **16**, 466–471 (2012).
85. Aparicio, T., de Lorenzo, V. & Martínez-García, E. Broadening the SEVA Plasmid Repertoire to Facilitate Genomic Editing of Gram-Negative Bacteria. in 9–27 (Springer, Berlin, Heidelberg, 2015). doi:10.1007/8623_2015_102
86. O'Hagan, D., Schaffrath, C., Cobb, S. L., Hamilton, J. T. G. & Murphy, C. D. Biochemistry: biosynthesis of an organofluorine molecule. *Nature* **416**, 279 (2002).
87. Perozziello, G. *et al.* Microfluidic device for continuous single cells analysis via Raman spectroscopy enhanced by integrated plasmonic nanodimers. *J. Nanosci. Nanotechnol* **11**, 2057–2063 (2011).
88. He, Y. *et al.* Printing 3D microfluidic chips with a 3D sugar printer. *Microfluid Nanofluid* (2015).
89. Comina, G., Suska, A. & Filippini, D. PDMS lab-on-a-chip fabrication using 3D printed templates. *Lab Chip* **14**, 424–30 (2014).
90. Koepff, J. *et al.* Germination and Growth Analysis of Streptomyces lividans at the Single-Cell Level Under Varying Medium Compositions. *Front. Microbiol.* **9**, 2680 (2018).
91. Lin, C.-F. *et al.* Microfluidic pH-sensing chips integrated with pneumatic fluid-control devices. *Biosens. Bioelectron.* **21**, 1468–75 (2006).
92. Yamada, A. & Suzuki, M. A Microfluidic pH Measurement Device with a Flowing Liquid Junction. *Sensors (Basel).* **17**, (2017).
93. Wu, J., Cao, W., Wen, W., Chang, D. C. & Sheng, P. Polydimethylsiloxane microfluidic chip with integrated microheater and thermal sensor. *Biomicrofluidics* **3**,

12005 (2009).
94. Shehata, T. E. & Marr, A. G. *Effect of Nutrient Concentration on the Growth of Escherichia coli*. *JOURNAL OF BACTERIOLOGY* **107**, (1971).
95. Zumbusch, A., Holtom, G. R. & Xie, X. S. *Three-Dimensional Vibrational Imaging by Coherent Anti-Stokes Raman Scattering*. (1999).
96. Freudiger, C. W. *et al.* Label-free biomedical imaging with high sensitivity by stimulated Raman scattering microscopy. *Science* **322**, 1857–61 (2008).
97. Tsikritsis, D. *et al.* Label-free biomarkers of human embryonic stem cell differentiation to hepatocytes. *Cytom. Part A* **89**, 575–584 (2016).
98. Lee, C. L. D. & Hewitt, K. C. First demonstration of surface enhanced-stimulated Raman spectroscopy (SE-SRS) using low-power CW sources. *Faraday Discuss.* **205**, 227–232 (2017).

Appendices

Permissions for figures:

THE AMERICAN ASSOCIATION FOR THE ADVANCEMENT OF SCIENCE LICENSE
TERMS AND CONDITIONS

Jan 22, 2020

This Agreement between University of Edinburgh -- Alex Warne ("You") and The American Association for the Advancement of Science ("The American Association for the Advancement of Science") consists of your license details and the terms and conditions provided by The American Association for the Advancement of Science and Copyright Clearance Center.
License Number

4744781471606

License date

Jan 09, 2020

Licensed Content Publisher

The American Association for the Advancement of Science

Licensed Content Publication

Science

Licensed Content Title

Long-Term Monitoring of Bacteria Undergoing Programmed Population Control in a Microchemostat

Licensed Content Author

Frederick K. Balagaddé,Lingchong You,Carl L. Hansen,Frances H. Arnold,Stephen R. Quake

Licensed Content Date

Jul 1, 2005

Licensed Content Volume

309

Licensed Content Issue

5731

Volume number

309

Issue number

5731

Type of Use

Thesis / Dissertation

Requestor type

Scientist/individual at a research institution

Format

Print and electronic

Portion

Figure

Number of figures/tables

1

Order reference number

Title of your thesis / dissertation

Evaluating the Way2Production SolFlex350 Digital Light Projection 3D Printer as a Fabrication Technology for Microfluidics

Expected completion date

Jan 2020

Estimated size(pages)

1

Requestor Location

67 Delamere Park Way West
Cuddington

Northwich, Cheshire CW82UL
United Kingdom
Attn: University of Edinburgh

SPRINGER NATURE LICENSE
TERMS AND CONDITIONS

Jan 22, 2020

This Agreement between University of Edinburgh -- Alex Warne ("You") and Springer Nature ("Springer Nature") consists of your license details and the terms and conditions provided by Springer Nature and Copyright Clearance Center.
License Number

4744250352687

License date

Jan 08, 2020

Licensed Content Publisher

Springer Nature

Licensed Content Publication

Nature Methods

Licensed Content Title

A microfluidic chemostat for experiments with bacterial and yeast cells

Licensed Content Author

Alex Groisman et al

Licensed Content Date

Aug 23, 2005

Type of Use

Thesis/Dissertation

Requestor type

academic/university or research institute

Format

print and electronic

Portion

figures/tables/illustrations

Number of figures/tables/illustrations

1

High-res required

no

Will you be translating?

no

Circulation/distribution

1 - 29

Author of this Springer Nature content

no

Title

Evaluating the Way2Production SolFlex350 Digital Light Projection 3D Printer as a Fabrication Technology for Microfluidics

Institution name

University of Edinburgh

Expected presentation date

Jan 2020

Portions

figure 1

Requestor Location

67 Delamere Park Way West
Cuddington

Northwich, Cheshire CW82UL
United Kingdom
Attn: University of Edinburgh

Issue number

2920

Type of Use

Thesis / Dissertation

Requestor type

Scientist/individual at a research institution

Format

Print and electronic

Portion

Figure

Number of figures/tables

1

Order reference number

Title of your thesis / dissertation

Evaluating the Way2Production SolFlex350 Digital Light Projection 3D Printer as a Fabrication Technology for Microfluidics

Expected completion date

Jan 2020

Estimated size(pages)

1

Requestor Location

67 Delamere Park Way West
Cuddington

Northwich, Cheshire CW82UL
United Kingdom
Attn: University of Edinburgh

Order Date	08-Jan-2020	Type of Use	Republish in a thesis/dissertation
Order license ID	1012513-1	Publisher	ROYAL SOCIETY OF CHEMISTRY
ISSN	1473-0189	Portion	Chart/graph/table/figure

LICENSED CONTENT

Publication Title	Lab on a chip	Country	United Kingdom of Great Britain and Northern Ireland
Author/Editor	Royal Society of Chemistry (Great Britain)	Rightsholder	Royal Society of Chemistry
Date	01/01/2001	Publication Type	e-Journal
Language	English	URL	http://www.rsc.org/loc

REQUEST DETAILS

Portion Type	Chart/graph/table/figure	Distribution	U.K. and Commonwealth (excluding Canada)
Number of charts / graphs / tables / figures requested	1	Translation	Original language of publication
Format (select all that apply)	Print	Copies for the disabled?	No
Who will republish the content?	Academic institution	Minor editing privileges?	No
Duration of Use	Life of current edition	Incidental promotional use?	No
Lifetime Unit Quantity	Up to 499	Currency	GBP
Rights Requested	Main product		

NEW WORK DETAILS

Title	Evaluating the Way2Production SolFlex350 Digital Light Projection 3D Printer as a Fabrication Technology for Microfluidics	Institution name	University of Edinburgh
		Expected presentation date	2020-01-23
Instructor name	Alex Warne		

ADDITIONAL DETAILS

Order reference number	N/A	The requesting person / organization to appear on the license	Alex Warne

REUSE CONTENT DETAILS

Title, description or numeric reference of the portion(s)	Fig 1 Schematic illustration of a single small-volume fraction replenishment microchemostat	Title of the article/chapter the portion is from	Microchemostat array with small-volume fraction replenishment for steady-state microbial culture
Editor of portion(s)	N/A	Author of portion(s)	Royal Society of Chemistry (Great Britain)
Volume of serial or monograph	13	Issue, if republishing an article from a serial	N/A
Page or page range of portion	4219	Publication date of portion	2001-01-01

Order Date	08-Jan-2020	Type of Use	Republish in a thesis/dissertation
Order license ID	1012509-1	Publisher	ROYAL SOCIETY OF CHEMISTRY
ISSN	1473-0189	Portion	Chart/graph/table/figure

LICENSED CONTENT

Publication Title	Lab on a chip	Country	United Kingdom of Great Britain and Northern Ireland
Author/Editor	Royal Society of Chemistry (Great Britain)	Rightsholder	Royal Society of Chemistry
Date	01/01/2001	Publication Type	e-Journal
Language	English	URL	http://www.rsc.org/loc

REQUEST DETAILS

Portion Type	Chart/graph/table/figure	Distribution	U.K. and Commonwealth (excluding Canada)
Number of charts / graphs / tables / figures requested	1	Translation	Original language of publication
Format (select all that apply)	Print	Copies for the disabled?	No
Who will republish the content?	Academic institution	Minor editing privileges?	No
Duration of Use	Life of current edition	Incidental promotional use?	No
Lifetime Unit Quantity	Up to 499	Currency	GBP
Rights Requested	Main product		

NEW WORK DETAILS

Title	Evaluating the Way2Production SolFlex350 Digital Light Projection 3D Printer as a Fabrication Technology for Microfluidics.	Institution name	University of Edinburgh
		Expected presentation date	2020-01-23
Instructor name	Alex Warne		

ADDITIONAL DETAILS

Order reference number	N/A	The requesting person / organization to appear on the license	Alex Warne

REUSE CONTENT DETAILS

Title, description or numeric reference of the portion(s)	The microfluidic chemostat	Title of the article/chapter the portion is from	Microfluidic chemostat for measuring single cell dynamics in bacteria
Editor of portion(s)	N/A	Author of portion(s)	Royal Society of Chemistry (Great Britain)
Volume of serial or monograph	13	Issue, if republishing an article from a serial	N/A
Page or page range of portion	949	Publication date of portion	2001-01-01